Departamento de Fisiología Médica y Biofísica
Universidad de Sevilla

Presynaptic calcium dynamics, neuronal excitability and synaptic vesicle cycle in central synapses lacking Cysteine String Protein-α (CSP-α)

José Antonio Martínez López

Advisors
Dr. Rafael Fernández Chacón
Dr. José Luis Nieto González

Dissertation submitted for the degree of Doctor of Philosophy

Seville, 2017

Departamento de Fisiología Médica y Biofísica
Universidad de Sevilla
Avda. Sánchez Pizjuán, 4
41009, Sevilla
España

Dr. Rafael Fernández Chacón, Professor of the Departamento de Fisiología Médica y Biofísica at Universidad de Sevilla and

Dr. José Luis González Nieto, Associate Professor of the Departamento de Fisiología Médica y Biofísica at Universidad de Sevilla

hereby certify that:

José Antonio Martínez López, candidate for the degree of Doctor of Philosophy has carried out under our supervision the dissertation entitled:

Presynaptic calcium dynamics, neuronal excitability and synaptic vesicle cycle in central synapses lacking Cysteine String Protein-α (CSP-α)

Signature:_____
Dr. Rafael Fernández Chacón

Signature:_____
Dr. José Luis Nieto González

Seville, 2017

Presynaptic calcium dynamics, neuronal excitability and synaptic vesicle cycle in central synapsis lacking Cysteine String Protein-α (CSP-α)

Cysteine String Protein-α (CSP-α) is a molecular co-chaperone of the synaptic vesicles that prevents presynaptic degeneration. The role of CSP-α in the machinery of calcium dependent release of neurotransmitter from synaptic vesicles has been studied previously but some functional aspects remain still unknown, such as its role in exo- and endocytosis in central neurons and its role in the regulation of presynaptic calcium. To study this, we have measured the exo- and endocytosis of synaptic vesicles in hippocampal synapses lacking CSP-α using a pH-sensitive green fluorescent protein (GFP) fused to the luminal part of synaptic vesicles (pHluorin) showing no differences between wild type and mutant synapses. In addition, we have measured presynaptic cytosolic calcium changes in hippocampal cultures lacking CSP-α using a genetically encoded calcium indicator (GECI) called syGCaMP3, uncovering different type of responses in glutamatergic synapses: long duration responses (LDRs) and short duration responses (SDRs). These measurements show normal presynaptic calcium dynamics in neurons lacking CSP-α.

On the other hand, highly active GABAergic synapses formed by fast spiking parvalbumin positive interneurons are extremely sensitive to the absence of CSP-α and they degenerate early postnatally in CSP-α KO mice. In contrast, glutamatergic hippocampal synapses do not show obvious signs of early neurodegeneration. Using electrophysiological and imaging techniques, in this thesis we demonstrate the propensity of hippocampal circuits of mice lacking CSP-α to hyperexcitability, probably produced by this excitatory/inhibitory imbalance caused by loss of inhibitory synapses.

Funding

This work has been supported by grants from MINECO (BFU2013-47493-P), Junta de Andalucía (P12-CTS-2232), ISCIII (CIBERNED) and FEDER.

AGRADECIMIENTOS

Ya hace más de un año que dejé atrás el laboratorio de Sevilla para venirme a Estocolmo y por fin se acerca el momento de poner punto final a esta etapa que empecé hace bastante tiempo y que finalmente acaba con la conclusión de esta tesis doctoral.

Para llevar a cabo un trabajo de investigación se necesitan cada vez más conocimientos técnicos y científicos de diversas disciplinas de los que no dispones al comenzar una tesis doctoral. Dedicarse a la ciencia requiere de un aprendizaje continuo ya que cada semana aparecen nuevos artículos científicos describiendo resultados novedosos que pueden cambiar tu visión de como funciona la naturaleza del estudio en cuestión, o incluso la aparición de nuevas técnicas o tecnologías que pueden revolucionar cualquier materia. Por todo ello es indispensable el trabajo en equipo, y rodearse de las personas adecuadas es un aspecto fundamental del que en gran medida dependerá tu aprendizaje y el éxito de tu proyecto. Sentirse feliz en el ámbito personal dentro y fuera del laboratorio es otro aspecto muy importante que hay que tener muy presente. Aquí dedico mi gratitud a todas aquellas personas que han contribuido a todo ello de alguna u otra forma.

En primer lugar quiero mencionar a mi director de tesis. Rafa, gracias por darme la oportunidad de trabajar en tu laboratorio. También por transmitirme todo tu entusiasmo por la ciencia y permitirme sumergirme en el mundo de la Neurobiología, un campo tan intrigante y aún tan desconocido del que prácticamente no conocemos nada y del que veremos grandes avances en los próximos años. También por darme la oportunidad de poder adquirir una perspectiva internacional de la ciencia, permitiéndome visitar los mejores centros de investigación. Para mí fue muy divertido y fascinante aquel fin de semana que me invitaste a pasar contigo y tu familia en el Laboratorio de Biología Marina (MBL) de Woods Hole en Massachusetts, donde pude conocer el centro, su historia y todo el trabajo que se realizaba allí. Por último, gracias por haber sabido elegir adecuadamente al equipo de personas con las que he podido trabajar y aprender, y a las que tengo una gran admiración tras haber compartido tanto tiempo juntos dentro y fuera del laboratorio y que se han convertido en grandes amigos que perdurarán para siempre.

Nada mas llegar al laboratorio del Campus Macarena conocí a la mayoría de personas con las que he podido compartir la mayor parte del tiempo durante estos años. Tengo que decir que aquel lugar se me presentó como algo extremadamente peculiar desde el primer momento que lo pisé.

Cuando empecé a ir por el laboratorio, una de las primeras personas que conocí fue

a José Luis Rozas. José Luis, para mí eres una de las personas más inteligente que he conocido y de la que he recibido una gran influencia. Me gusta mucho tu forma de razonar y sobre todo tu carácter crítico. Fue una gran pérdida para mí el día que te fuiste, pero no te quedaba otra. Nunca olvidaré aquel fin de semana en Aracena que organizamos para tu despedida, donde fue imposible reírnos más con aquellas conversaciones tan absurdas.

Perico, cuando llegué al departamento tú ya estabas acabando tu tesis y eras miembro del núcleo duro del sindicato junto a algunos otros, algo que resultaba bastante chocante para un recién llegado. Cuando empecé a levantarme del escritorio para hacer de biólogo tú me guiaste con los primeros experimentos de imagen. Aquello era un mundo totalmente nuevo para mí. Gracias por tener la suficiente paciencia para enseñar a alguien con tan escasa idea de aquello. No sé que hubiera hecho sin ti.

Pablo, me gusta tu forma de decir las cosas tan claras y directas. A veces me sorprendía por ello pero otras veces me resultaba muy gracioso. Gracias por esa sinceridad y por ser una de las personas más divertidas que conozco. Tengo que reconocer que al final simpre ganabas cerrando cualquier bar. Gloria, a ti me gustaría darte las gracias por ser un encanto y hacer sentir tan bien a cualquiera que esté a tu lado. Es un gusto poder trabajar junto a tí. Así las cosas son mucho más fáciles. Contigo y con Pablo empecé a conocer que era eso de la electrofisiología y el *patch-clamp*. Muchas gracias por vuestra ayuda y consejos. Ángel, aunque no trabajabas en el mismo grupo era como si fueses uno más porque siempre estabas con nosotros en todos sitios. Gracias por ser tan bondadoso y tan buena gente. Mari Carmen, gracias por haber sido el pilar del laboratorio, sin ti no funcionaría nada. Menos mal que te teníamos allí para mantener el orden. Con todo el trabajo que has hecho tendrías para presentar varias tesis. Es admirable que al final conseguías que todo saliese bien y nunca había ningún reto imposible para ti. Ale, gracias a ti también por estar disponible en cualquier momento y por poner tanto ímpetu para que todo funcionase. Sin tu trabajo y el de Mari Carmen, esta tesis no se podría haber hecho.

Leo, nosotros empezamos esto juntos. Nunca olvidaré aquellas tardes tan divertidas en las que nos dedicábamos a fabricar juntos algún aparato nuevo, aunque después muchos de ellos eran totalmente inútiles. Me reí mucho el día que estuvimos trabajando con el trompo de Guillermo, aunque quizás no era la herramienta más apropiada para nuestros propósitos. Y gracias también por todas esas buenas ideas y sugerencias. Era un lujo tenerte cerca para poder preguntarte sobre cualquier cosa. Nunca olvidaremos a Vicente y su amigo en aquel charco perdido en mitad de la Sierra el fin de semana

de tu despedida. Josif, gracias por ser tan sociable y abierto y por ayudar siempre en lo que hiciese falta. Y por supuesto por todas tus bromas, que a veces no sabía si ibas en serio o no. Gracias también a Carmen y Macarena. Quizás sois de las personas más extrovertidas y con más ganas de viajar y conocer sitios nuevos que haya conocido jamás. Me gusta mucho vuestra actitud siempre tan positiva y optimista ante cualquier situación. También destacar la facilidad que teneis para organizar cualquier plan de forma espontánea, incluso para hacer un viaje a cualquier sitio del mundo. Gracias por todo ello. Siempre he querido tener a gente como vosotras a mi lado.

José Luis Nieto, lo que admiro de ti es tu capacidad de trabajo y con la facilidad con la que consigues que funcione cualquier cosa. De ti aprendí que nada es imposible técnicamente. Echaré mucho de menos aquellos días en los que nos poníamos a registrar neuronas. Para mí era muy divertido y aprendía mucho de ti, aunque había veces que los equipos se apagaban de repente misteriosamente ¿Por qué sería? Supongo que son cosas que ocurren en el mundo de la electrofisiología y que no vamos a dar más detalles. Gracias por codirigir esta tesis y contribuir con tus consejos y trabajo. Sin ti, no se hubiera podido acabar.

Fabi, contigo el laboratorio era un sitio más entretenido y divertido. Era imposible aburrirse teniéndote al lado. Te echaba mucho de menos cuando no te tenía cerca. Además me gustaba mucho hacer ingeniería genética contigo. Me resultaba muy divertido quitar y poner microlitros de lo que fuese en tubitos y agitar las bolas dentro de las placas. Gracias por introducirme a la biología molecular, un campo con mucho futuro y que para mí en esos inicios me resultaba fascinante. Gracias por dedicar tu tiempo a los diseños y generación de lentivirus sin los cuales esta tesis no se podría haber hecho. Y también por preocuparte de mí, sobre todo los Lunes por la mañana al llegar al laboratorio.

Emi, casi empezamos la tesis al mismo tiempo y desde entonces hemos estado trabajando siempre bastante cerca, primero en el departamento de la Macarena y luego en el IBiS, aunque es cierto que tu acabaste la tesis mucho antes ¡Cuanto tiempo hace ya de aquel día de barranquismo donde nos lo pasamos tan bien! Gracias por ser tan buena amiga y por todos esos buenos ratos, algunos de ellos donde no podíamos parar de reír. Espero que estés planificando ya la fiesta de tu próximo cumpleaños.

Juanjo Casañas, gracias por hacer del departamento un sitio más agradable. Me gusta mucho tu sentido del humor. No creo que haya mejor imitador de Rafa Chacón en el mundo. Juan Antonio, fue muy divertida aquella noche que fuimos a ver el cielo con tu telescopio. Aprendí mucho sobre Astronomía. Es una suerte tener a alguien cerca con

este tipo de inquietudes. Marisa, gracias a ti también por ser tan amable y estar dispuesta a ayudar en todo lo que hiciese falta.

Ángela, gracias por estar siempre tan atenta y por tener tan buena memoria para todo. Me venía muy bien que me recordases las cosas porque mi memoria muchas veces no da para tanto. Al final nunca llegamos a visitar tu pueblo, pero queda pendiente. Marina, a ti te sigo viendo de vez en cuando por Estocolmo, incluso hasta compartimos la misma oficina. Al tenerte por aquí, parece como si no me hubiese ido aún del laboratorio. No te preocupes que ya queda menos para que salga adelante tu proyecto de *single-cell* y tendrás tu tesis lista en breve. Verás como al final voy a ser yo quién te deba la cena. Selu, a ti ya te conocí en mi última etapa en el laboratorio. Muchas gracias por todas esas buenas discusiones sobre ciencia que solían ser bastante provechosas para mí. Contigo aprendí muchísimo sobre los últimos avances en rutas moleculares. Fue una suerte tenerte sentado justo en la mesa de al lado. Espero que ya hayas dejado de marearte en los taxis.

Rocío, tuve mucha suerte poder tenerte de compañera en Boston porque hiciste mi estancia allí mucho más fácil y también mucho más divertida durante los meses que estuvimos viviendo juntos. Para mí era como estar en casa. Gracias por tener la suficiente paciencia con aquel incidente con la cisterna del váter. Miguel, fue una suerte poder conocerte en Boston y así tener alguien con quien vivir el último mes que nos quedaba allí. No sé que hubiera sido de mí. Al final conseguimos tener un piso en el último momento después de tanta búsqueda. Lo de que no tuviera muebles no fue un problema porque al final pudimos solucionarlo, aunque quizás no de la mejor forma. También, a Txema y Sara por todos esos buenos momentos que pasamos de bares y excursiones. Creo que no nos quedó nada por ver en Massachusetts. Sara, qué alegría que te vinieses a Estocolmo y podamos recordar viejos tiempos. A partir de ahora vamos a compartir mucho tiempo juntos. Assunta, gracias a ti también por todos esos buenos momentos y por toda tu ayuda.

También dar las gracias al Profesor Guillermo Álvarez de Toledo por su devoción y su entusiasmo por la ciencia y por ofrecerme siempre su ayuda para resolver cualquier problema técnico o pregunta científica. A Marga y Mari Ángeles del laboratorio de Guillermo por estar ahí siempre que he necesitado vuestra ayuda. También a los Profesores Lucía Tabares, Mari Luz Montesinos, Francisco Gómez Scholl, Francisco Sánchez Doblado y Antonio Leal por toda vuestra ayuda.

Al Profesor Bernardo Sabatini, por acogerme en su laboratorio durante dos veranos y por dedicarme parte de su tiempo a enseñarme a montar un microscopio de superresolución STED. Fue un lujo haber estado allí y poder aprender tanto sobre las tecnologías más novedosas de microscopía de fluorescencia.

Gracias también a los Profesores José M. Delgado García y Agnès Gruart de la División de Neurociencias de la Universidad Pablo de Olavide (Sevilla, España) por su colaboración en este proyecto.

A Loli, por recibirme cada mañana en la puerta del departamento con tanta simpatía y por ser tan eficiente y resolutiva ayudando con cualquier papeleo. También a Fernando por su ayuda con la gestión de cualquier documento.

A Antonio Guillén, por fabricar y proporcionarnos infinidad de piezas para nuestros equipos, a pesar de que llegó un momento en el que ya no quería ni cogernos el teléfono, pero supongo que sus motivos tendría.

Por otro lado, también dar las gracias a mis amigos de fuera del laboratorio, Carlos, Manolo, Nani, Emma y Sergio por todos esos ratos que me permitían desconectar del laboratorio y que muchas veces eran tan necesarios.

Por último, dar las gracias a mis padres Teresa y José y a mi hermana Laura por haber estado ahí siempre para ayudarme incondicionalmente en todo lo necesario, y también por haberme dado la oportunidad de estudiar y formarme en lo que quise. Por último, y no por ello menos importante, a mi prima Rocío, ya que quizás sin ella no hubiera podido conocer a Rafa y nada de esto hubiera sido posible.

Podría contar muchas anécdotas divertidas, incluso algunas no tan divertidas, que ocurrieron durante este tiempo y de las que tanto nos hemos reído y hemos hablado y que también son de agradecer, pero quizás este no sea el lugar mas apropiado para detallarlas, pero que quedaran para siempre en nuestros recuerdos. Aunque ahora no esté por allí, a la mayoría os sigo viendo de vez en cuando y me da mucha alegría poder compartir nuevos momentos donde siempre acabamos rememorando los viejos recuerdos. Mil gracias a todos vosotros.

TABLE OF CONTENTS

1. INTRODUCTION

1.1. Motivation

Individuality of neurons was firstly predicted by Santiago Ramón y Cajal against the wrong view of reticularists about the nervous system in the late 19th century (Ramón y Cajal, 1888, 1911, 1933). Reticularists saw axonal and dendritic processes as being continuous with the processes of other cells whereas Cajal's neuron doctrine proposed that there is a physical gap between connected neurons. The connection of one nerve cell to another was called synapse and the term was proposed by Charles Sherrington in 1897 (Foster, 1897). Ramón y Cajal received the Nobel Prize in 1906 and today his neuron theory is considered the birth of modern neuroscience.

J. Newport Langley provided the first conclusive evidence that synaptic transmission may occur by chemical means (Cowan et al., 2001; Langley, 1921). In chemical synaptic transmission, the presynaptic electrical signal is converted into a secretory response, leading to the release of chemical signal called neurotransmitter (Kandel et al., 2013). Before release, neurotransmitter is stored within the presynaptic terminal in synaptic vesicles and release occurs when synaptic vesicles fuse with the plasma membrane and expose the neurotransmitter to the synaptic cleft (Südhof, 2004). The chemical message is reconverted into an electrical signal after neurotransmitter binds and activates receptors at the postsynaptic neuron (Kandel et al., 2013). On the other hand, there are also a small minority of synapses that communicate via direct electrical junctions termed gap junctions where synaptic transmission allows bidirectional propagation of the electrical signal without chemical conversion (Bennett and Zukin, 2004).

Molecular machinery of synapses has been extensively studied in last 25 years. J.E. Rothman, R. W. Schekman and T. C. Südhof received the Nobel Prize for their discoveries of machinery regulating vesicle traffic in cells in 2013 (Südhof, 2014), but today the function of many proteins at the synapse still have to be clarified. In the cellular environment, most proteins must fold into defined three-dimensional structures to reach functional activity, but newly synthesized proteins are at great risk of anomalous folding and aggregation. To avoid these dangers, cells invest in a complex network of molecular chaperones, which use ingenious mechanisms to prevent aggregation and promote efficient folding (Hartl et al., 2011). Molecular chaperones are neuroprotective because of their ability to modulate the earliest aberrant protein interactions that trigger pathogenic cascades (Muchowski and Wacker, 2005).

This thesis is focused on the study of the function of Cysteine String Protein-α (CSP-α), a molecular co-chaperone of the synaptic vesicles that prevents presynaptic degeneration

(Fernández-Chacón et al., 2004). A detailed understanding of the molecular basis of chaperone-mediated protection against neurodegeneration might lead to the development of therapies for neurodegenerative disorders that are associated with protein misfolding and aggregation (Muchowski and Wacker, 2005).

1.2. The synaptic vesicle cycle

Chemical synapses are composed of a collection of synaptic vesicles in the presynaptic terminal. Synaptic vesicles are uniformly small and abundant organelles with radius of approximately 20 nm and its function is to take up and release neurotransmitters. Synaptic vesicles have two classes of components: transport proteins, such as the vacuolar-type proton pump that generates the electrochemical gradient across the vesicle membrane to accumulate and store neurotransmitter, and trafficking proteins that participate in synaptic vesicle exo- and endocytosis. Quantitative information on the composition of the whole synaptic vesicle has been described in detail (Takamori et al., 2006; Wilhelm et al., 2014).

In the nervous system, neurotransmitter is released from synaptic vesicles when action potentials arrive to the synaptic terminal (Katz, 1969) and open presynaptic voltage-dependent calcium channels, mainly P/Q-type (Cav2.1) and N-type (Cav2.2) channels, that permit calcium influx (Südhof, 2004). The resulting cytosolic calcium at the presynaptic terminal promotes synaptic vesicles exocytosis, the process through which synaptic vesicles are fused with the plasma membrane to release neurotransmitter into the synaptic cleft. After exocytosis, synaptic vesicles undergo endocytosis, the process through which synaptic terminals retake and reuse membranes that have been fused, to generate new synaptic vesicles for new rounds of exocytosis. The current model of synaptic vesicle cycle can be described into different sequential steps (Figure 1). First, neurotransmitter, glutamate or GABA for example, is loaded in synaptic vesicles through neurotransmitter transporters, VGLUT (vesicular glutamate transporter) in the case of glutamatergic synapses or VGAT (vesicular GABA transporter) in the case of GABAergic synapses. Based on spatial localization with respect to the active zone and functional availability for neurotransmission, synaptic vesicles reside in distinct groups: the readily releasable pool (RRP), the reserve/recycling pool and the resting pool (Rizzoli and Betz, 2005). RRP is a few percent of vesicles docked to the plasma membrane, primed to be released and it is immediately available on stimulation (Rizzoli and Betz, 2005). The reserve/recycling pool is thought to be formed by vesicles that are not docked and once the RRP is depleted new vesicles are supplied from this pool to the RRP. The resting

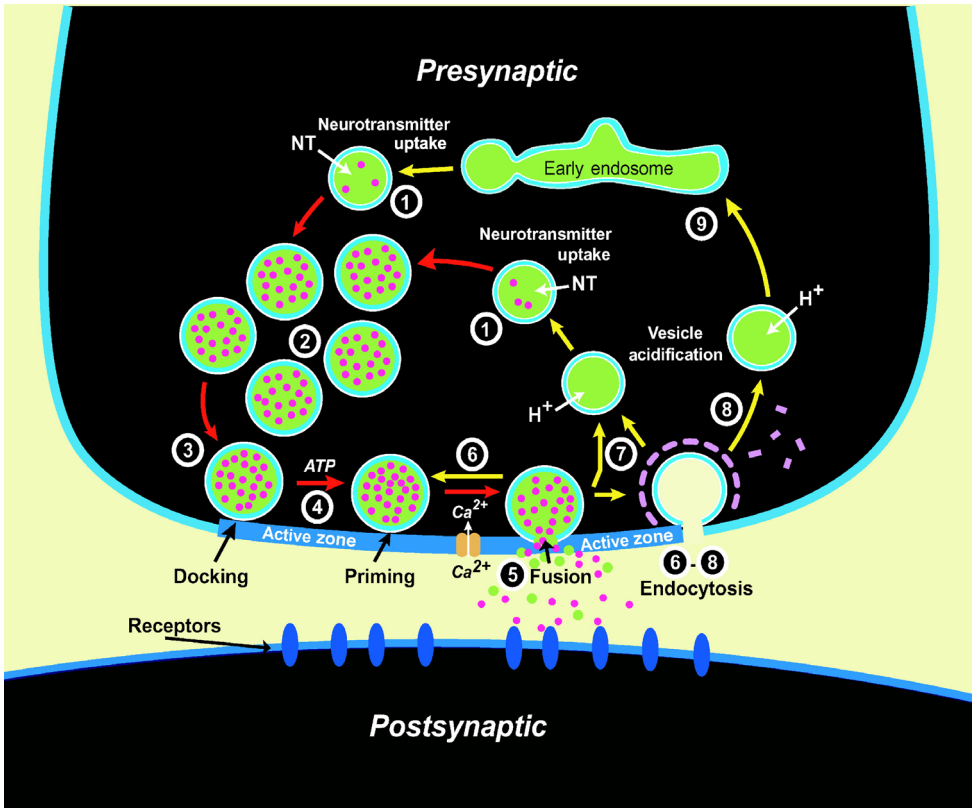

Figure 1: The synaptic vesicle cycle

Synaptic vesicles are filled with neurotransmitters by active transport (step 1) and form the vesicle cluster that may represent the reserve pool (step 2). Filled vesicles dock at the active zone (step 3) where they undergo a priming reaction (step 4) that makes them competent for calcium triggered fusion-pore opening (step 5). After fusion-pore opening, synaptic vesicles undergo endocytosis and recycle via several routes: local reuse (step 6), fast recycling without an endosomal intermediate (step 7), or clathrin-mediated endocytosis (step 8) with recycling via endosomes (step 9). Steps in exocytosis are indicated by red arrows and steps in endocytosis and recycling by yellow arrows (Südhof, 2004).

pool is constituted by the majority of synaptic vesicles at the synapses and is defined as the pool that does not participate in release under physiological conditions of stimulation (Rizzoli and Betz, 2005).

Synaptic vesicles group and dock in the active zone, a small section of the presynaptic plasma membrane containing electron-dense material (Südhof, 2012), where they are primed to convert them into a state of competence for fusion-pore opening triggered by calcium (Südhof, 2004, 2014). Calcium binding to synaptotagmin 1, a protein of synaptic vesicles, determines calcium triggering of exocytosis (Fernández-Chacón et al.,

2001). Exocytosis generally involves SNARE proteins characterized by a homologous 70-residue sequence called the SNARE motif. Synaptic exocytosis is mediated by three SNARE proteins: synaptobrevin, also known as vesicle-associated membrane protein (VAMP) on synaptic vesicles, and syntaxin 1 and SNAP-25 on the presynaptic plasma membrane. After exocytosis, synaptic vesicles endocytosis recycling occurs via different pathways:

i) Vesicles are reacidified and refilled with neurotransmitters without undocking, remaining in the readily releasable pool (RRP) (Südhof, 2004).

ii) Vesicles that do not undergo complete fusion with the plasma membrane and they are undocked and refilled with neurotransmitter locally, without endosome fusion, called kiss-and-run (Álvarez de Toledo et al., 1993). This process takes place within 1 s (Südhof, 2004) but recently it has been proposed another kind of endocytosis faster than kiss-and-run called ultrafast endocytosis that occurs within 50 to 100 ms (Watanabe et al., 2013).

iii) Vesicles are endocytosed via clathrin coated pits (clathrin is a protein involved in the formation of vesicles during endocytosis) and reacidified and refilled with neurotransmitters either directly or after passing through endosome, called clathrin mediated endocytosis (CME) (Brodin et al., 2000; Saheki and De Camilli, 2012). In this kind of endocytosis, invaginated clathrin-coated bud with a narrow neck is formed and the fission of this neck requires the GTPase dynamin leading to a free vesicle that rapidly uncoats (Brodin et al., 2000; Ferguson and De Camilli, 2012). CME takes place approximately 20 s after exocytosis (Südhof, 2004). Also it is known that clathrin may not be absolutely essential for synaptic vesicles reformation because in response to a very strong exocytic burst there is a different endocytic mechanism called bulk endocytosis that leads to the generation of endocytic vacuoles, subsequently converted into synaptic vesicles (Saheki and De Camilli, 2012).

1.3. Short-term presynaptic plasticity

All types of synapses are regulated by a variety of processes some leading to a decrease in synaptic strength and others to synaptic enhancement. The magnitude depends on the recent history of activity, frequency of stimulation, stage of development, the surrounding environment and other factors. Presynaptic plasticity lasting tens of milliseconds to minutes can be divided into three categories: short-term synaptic depression, facilitation and augmentation/posttetanic potentiation (PTP) (Regehr, 2012). In principle, all of

these forms of plasticity might be caused by changes in the probability of release at a synapse that can be quantitatively defined by the product of the number of available vesicles in the RRP and the probability of release for each of the available vesicles.

1.3.1. Depression

At many synapses, transient decrease in synaptic efficacy as a result of repetitive stimulation is termed short-term depression (STD). STD lasts from several milliseconds to minutes and is produced by different mechanisms:

i) RRP depletion and decrease of the probability of release per vesicle (Fioravante and Regehr, 2011).

ii) Calcium channels inactivation at presynaptic terminals can contribute to synaptic depression (Catterall and Few, 2008). Studies at the calyx of held have shown a decreased release probability caused by a calcium-induced inhibition of presynaptic P/Q-type calcium channels (Xu and Wu, 2005). On the other hand, studies of synaptic transmission in cultured superior cervical ganglion neurons suggest that regulation of presynaptic Cav2.1 channels by calcium sensor proteins mediates short-term synaptic plasticity (Mochida et al., 2008).

iii) Spatial arrangement of synaptic vesicles and calcium channels at active zones (Zucker and Regehr, 2002).

iv) Another form of synaptic depression is mediated by metabotropic receptors. Many presynaptic terminals have metabotropic receptors that can be activated by chemical messenger such as GABA and synaptic strength is controlled by these receptors. GABA binds to the $GABA_B$ receptors, a G protein-coupled receptor for GABA, and activates a signaling cascade that inhibits voltage-gated calcium channels (VGCCs) and hence inhibits evoked calcium dependent neurotransmitter release at presynaptic terminals (Gassmann and Bettler, 2012). In some cases, tonic levels are sufficient to partially activate the receptors; v) Inactivation of release sites can also mediate STD. Fusion of a vesicle at an active zone can inhibit subsequent fusion of available vesicles for several seconds (Neher and Sakaba, 2008).

v) Action potential conduction failures at axonal branches has been proposed as a mechanism that contribute to STD in autapses of cultured hippocampal neurons (Brody and Yue, 2000). It is considered as a presynaptic release-independent STD because synaptic transmission is reduced at presynaptic steps that occur before vesicle release.

vi) Finally, postsynaptic mechanism can also mediate STD through desensitization of postsynaptic receptors. Exposure of ligand-gated channels to an agonist can lead to channel opening and it can also put some of the channels into a nonresponsive state (Zucker and Regehr, 2002).

1.3.2. Enhancement mechanisms

When a train of action potentials is generated, the second action potential elicits more neurotransmitter release than the first one producing a synaptic enhancement called facilitation. The initial presynaptic action potential evokes a local calcium signal that triggers release and then the calcium persists at a lower level in the presynaptic bouton (Regehr, 2012). This residual calcium produces the synaptic enhancement for the second action potential.

Other possibility for facilitation is that calcium acts at different presynaptic calcium sensor from synaptotagmin. Synaptotagmin is a low affinity calcium sensor, responding quickly to a brief high calcium signal. In contrast, a high-affinity calcium-binding site with slow kinetics might be quite sensitive to the residual calcium signal (Regehr, 2012). Recently, it has been demonstrated that synaptotagmin 7 (Syt7) is a calcium sensor that is required for facilitation at different central synapses (Jackman et al., 2016).

Facilitation might be also produced by high-affinity calcium buffers in the presynaptic terminal. They can bind calcium after it enters through voltage-gated calcium channels and before it reaches release sites (Neher, 1998).

Another mechanism of facilitation is the activity dependent enhancement of calcium influx at presynaptic terminal that can increase the probability of release via enhancement of calcium currents (Catterall and Few, 2008; Inchauspe et al., 2004).

Posttetanic potentiation (PTP) refers to a transient increase in synaptic strength lasting tens of seconds to minutes that sustained high-frequency stimulation. At many synapses a closely related form of transient enhancement known as augmentation is present, which has a shorter duration than PTP (Regehr, 2012). Different synapses show considerable variability in the number and frequency of stimuli needed to induce PTP and augmentation, being the distinction between PTP and augmentation often unclear (Regehr, 2012). Enhancement mechanisms can be divided in different groups depending on the time course of recovery to baseline. Facilitation is on the order of milliseconds, 5-10 seconds for augmentation and minutes for PTP (Zucker and Regehr, 2002).

1.4. Cysteine string protein-α (CSP-α)

CSP-α has been characterized in different species (*Drosophila*, *Xenopus*, *Caenorhabditis elegans*, *Torpedo californica* and mammals) being a very preserved protein during evolution. The first identification of CSP-α was in retina and brain of *Drosophila* (Zinsmaier et al., 1990). Two years later, it was identified in *Torpedo californica* and was closely related with a subunit of the calcium channels that regulate transmitter release at nerve endings (Gundersen and Umbach, 1992). *C. elegans* and *Drosophila* have a single CSP gene, whereas mammals have three CSP genes: CSP-α, CSP-β and CSP-γ. CSP-α is the main isoform in the brain (Fernández-Chacón et al., 2004). Knockout mice lacking CSP-α gene (Dnajc5) survive less than 3 months (Fernández-Chacón et al., 2004) and during early postnatal development, CSP-α is not essential for neurotransmitter release at the calyx of Held, but at later ages, the absence of CSP-α leads to deficits in neurotransmitter release because of neurodegeneration of presynaptic terminals (Fernández-Chacón et al., 2004). The fastest synaptic degeneration occurs in photoreceptor ribbon synapses suggesting that requirement for CSP-α might be greater at synapses undergoing heavy membrane trafficking because of intense synaptic vesicle cycling, such as in photoreceptors (Schmitz et al., 2006). Furthermore, highly active neurons appear to be affected by neurodegeneration in CSP-α KO mice, suggesting that neurodegeneration is activity dependent (García-Junco-Clemente et al., 2010).

1.4.1. Localization

CSP-α is localized to the membrane of synaptic vesicles in the brain and is also found outside the brain in endocrine, neuroendocrine and exocrine tissues (Chamberlain and Burgoyne, 1996). In exocrine and endocrine glands, CSP-α has been localized to various secretory granules: the chromaffin granules in chromaffin cells (Chamberlain et al., 1996; Graham and Burgoyne, 2000), zymogen granules in exocrine pancreatic cells (Braun and Scheller, 1995), insulin-containing secretory granules of neuroendocrine beta-cells (Brown et al., 1998), hormone-containing secretory granules in secretory epithelia (Gleave et al., 2001). CSP-α has been also found in some nonsecretory tissues: heart, kidney, spleen, testis and adipose tissue (Chamberlain and Burgoyne, 1996; Eberle et al., 1998).

1.4.2. Molecular structure

The structure of CSPs are characterized by distinct domains:

i) A DNAJ domain typical of cochaperones from the Hsp40 family (Buchner and

Gundersen, 1997; Johnson et al., 2010). J domains comprise a stretch of approximately 70 amino-acids highly conserved from bacteria to humans (Caplan et al., 1993; Silver and Way, 1993).

ii) A central string of multiple cysteine residues. In mouse 13 cysteine residues are found within a 22 amino-acid stretch present in the central portion of the protein. These residues are highly palmitoylated, essential for membrane targeting (Chamberlain and Burgoyne, 1998b).

iii) The linker region (L region) between the J domain and the cysteine string region, highly conserved in evolution.

iv) A variable C-terminus. The C-terminus is subject to differential splicing and generates C-terminally truncated proteins in Drosophila and mammals.

1.4.3. The trimeric complex CSPα-Hsc70-SGT

CSP-α forms a chaperone complex with heat shock cognate protein Hsc70 and the small glutamine-rich tetratricopeptide repeat protein SGT (Tobaben et al., 2001). The trimeric complex consisting of CSP-α, Hsp70 and SGT is formed *in vivo* on the surface of synaptic vesicles and is able to refold denatured luciferase *in vitro* (Tobaben et al., 2001). It has been demonstrated in mice that CSPα-Hsc70-SGT complex binds directly to monomeric SNAP-25 to prevent its degradation, enabling SNARE-complex formation (Figure 2) (Sharma et al., 2012; Sharma et al., 2011). There is a decrease of approximately 50 % in SNAP-25 levels in mice lacking CSP-α, and a corresponding decrease in SNARE-complex assembly (Chandra et al., 2005). Remarkably, the overexpression of α-synuclein partially restores SNARE complex stability, indicating that CSP-α and α-synuclein cooperate to chaperone the SNARE complex (Chandra et al., 2005).

1.4.4. Interaction of CSP-α with voltage-dependent calcium channels (VDCC)

Several studies suggested that regulation of calcium influx through voltage-dependent presynatpic calcium channels are main targets of CSP-α. Early studies on CSP-α function described that the expression of Torpedo N-type VDCCs in oocytes was inhibited on injection of CSP-α antisense RNA (Gundersen and Umbach, 1992). Later, the connection between CSP-α and VDCCs was supported by imaging studies of exocytosis in nerve terminals of *Drosophila* CSP-α mutants (Umbach and Gundersen, 1997) suggesting that CSP-α links synaptic vesicles to calcium secretion coupling (Ranjan et al., 1998).

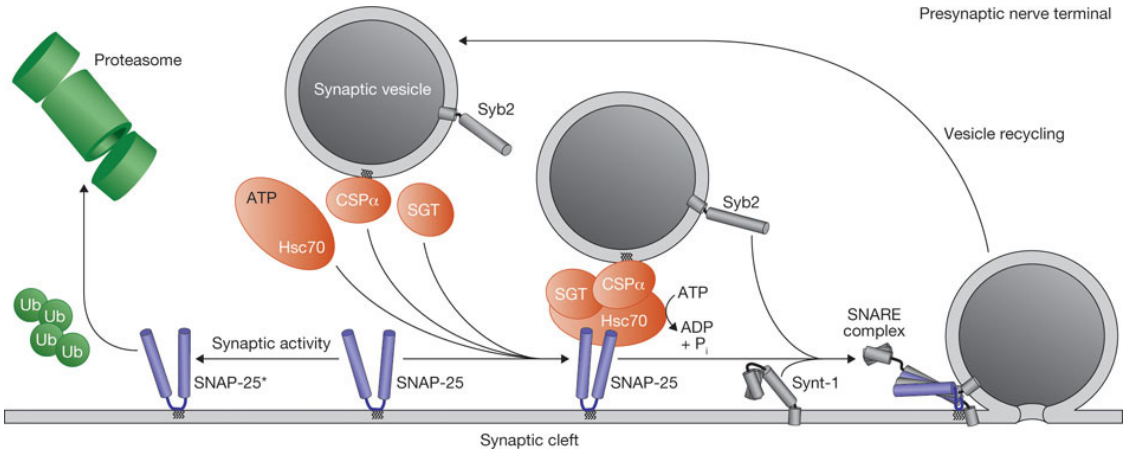

Figure 2: Model of the function of the CSPα-Hsc70-SGT chaperone complex

The CSPα-Hsc70-SGT complex refolds SNAP-25* into SNARE-complex competent SNAP-25, preventing its degradation to the proteasome and boosting SNARE-complexes (Sharma et al., 2011).

Increased calcium signals coupled with reduced release suggested a direct function of CSP-α in exocytosis downstream from calcium entry at neuromuscular junctions of *Drosophila*. Because of the reduction of evoked release in CSP-α mutants was counteracted by increased calcium levels, it was suggested that CSP primarily increases the calcium sensitivity of the exocytotic machinery (Dawson-Scully et al., 2000). On the other hand, biochemical studies have shown the interaction of CSP-α, receptor-coupled trimeric GTP binding proteins (G proteins) and N-type calcium channels (Magga et al., 2000; Miller et al., 2003). Interaction of CSP with the alpha1A subunit of the P/Q-type calcium channel was also reported (Leveque et al., 1998).

Other observations rule out the hypothesis of the interaction between CSP-α and calcium channels. Direct measurements of cytosolic calcium levels in synapses of Drosophila CSP mutants revealed that calcium influx elicited by depolarization was even higher than normal, ruling out that a deficit in calcium influx through VDCC causes the impairment in neurotransmitter release (Dawson-Scully et al., 2000). This notion was supported by experiments of CSP overexpression in neuroendocrine cells that showed altered exocytosis without effect on calcium channel activity, arguing against a major importance of CSP-α in regulating VDCCs (Chamberlain and Burgoyne, 1998a). Electrophysiological recordings of presynaptic calcium currents in CSP peptidergic

terminals in Drosophila are entirely normal (Morales et al., 1999). Furthermore, measurements of presynaptic P/Q-type and N-type calcium currents in Caliceal terminals from CSP-α KO mice failed to uncover any detectable impairment. Neither the amplitude nor the regulation of calcium currents was altered (Fernández-Chacón et al., 2004). Similarly, L- and T-type VDCCs in ribbon synapses of the inner ear were found to be normal in CSP-α KO mice (Schmitz et al., 2006).

On the other hand, it has been proposed that endogenous SNAP-25 regulates native voltage-gated calcium channels in glutamatergic neurons from rat hippocampal cultures by shifting the voltage-dependence of inactivation of predominant P/Q-type channel current in these cells (Condliffe et al., 2010). Silencing SNAP-25 in glutamatergic neurons significantly slowed the inactivation rate of P/Q-type VGCC current whereas alterations in SNAP-25 expression did not alter inactivation rates in GABAergic neurons (Condliffe and Matteoli, 2011). These observations are very interesting in the context of CSP-α. Since CSP-α deletion leads to a dramatic decreased in SNAP-25 levels, a significant increase in the levels of cytosolic Ca^{2+} would be expected in terminals lacking CSP-α.

1.4.5. Implication of CSP-α in synaptic exo- and endocytosis

CSP-α has been also implicated in endocytosis of synaptic vesicles. It has been proposed that motorneurons of neuromuscular junctions (NMJ) of transgenic mice expressing synaptopHluorin, a pH sensitive GFP (pHluorin) fused to the luminal part of synaptic vescicles to monitor synaptic exo- and endocytosis, require CSP-α to maintain the readily releasable vesicular pool and synaptic vesicle recycling (Rozas et al., 2012). On the other hand, it has been shown in the nervous system of mice the implication of CSP-α in the regulation of polymerization of dynamin 1, a protein necessary for vesicle endocytosis (Zhang et al., 2012).

1.4.6. CSP-α and GABAergic synapses

The vesicular gamma-aminobutyric acid (GABA) transporter (VGAT) has been found in a complex with CSP-α, Hsc70 and glutamate decarboxylase (GAD), the enzyme in charge of GABA synthesis. This interaction suggests an involvement of CSP-α in neurotransmitter synthesis and filling of synaptic vesicles with the neurotransmitter GABA (Jin et al., 2003).

On the other hand, highly active synaptotagmin 2 (Syt2)-expressing GABAergic synapses formed by fast spiking parvalbumin positive interneurons are extremely

sensitive to the absence of CSP-α and they degenerate early postnatally in CSP-α KO mice, but not glutamatergic hippocampal synapses, demonstrating that CSP-α is essential to maintain presynaptic function under elevated neural activity (García-Junco-Clemente et al., 2010).

1.4.7. Interaction of CSP-α with other proteins

Further studies proposed the interaction of CSP with proteins implicated in synaptic vesicle fusion. Synaptotagmin I was identified as a potential interacting protein for CSP in rat brain homogenates (Evans and Morgan, 2002). Also, an interaction between CSP and sintaxin in *Drosophila* has been reported (Nie et al., 1999). Furthermore, higher expression of large-conductance, calcium-activated potassium (BK) channels involved in the regulation of action potential duration and firing frequency has been demonstrated (Ahrendt et al., 2014; Kyle et al., 2013).

1.4.8. CSP-α in human disease

CSP-α has been implicated in the pathogenesis of neurodegenerative diseases in humans. Heterozygous mutations in the CSP-α gene in humans cause autosomal-dominant adult-onset neuronal ceroid lipofuscinosis (ANCL), a neurodegenerative disorder characterized by lysosomal accumulation of misfolded proteins. These mutations (causing a deletion, p.Leu116del, and an amino acid exchange, p.Leu115Arg) are located within the cysteine-string domain of the protein and affect both palmitoylation-dependent sorting and the amount of CSP-α in neuronal cells. Common characteristics of affected individuals included generalized seizures, movement disorders, cognitive deterioration, and progressive dementia (Benitez et al., 2011; Noskova et al., 2011).

1.5. The hippocampus

The hippocampal formation is a group of brain areas consisting of the dentate gyrus, hippocampus, subiculum, presubiculum, parasubiculum and entorhinal cortex. The hippocampus proper has three subdivisions: CA3, CA2 and CA1 (CA comes from cornu ammonis) originally described by Lorente de Nó (Figure 3) (Andersen et al., 2007; Lorente de Nó, 1934). The unidirectionally projections from the entorhinal cortex to the dentate gyrus, CA3 and CA1 form part of the major hippocampal input pathway called the perforant path. There are two glutamatergic principal cells at the dentate gyrus, the granule cells and the mossy cells (Scharfman and Myers, 2012). The granule cells, give rise to axons called mossy fibers that connect unidirectionally with pyramidal cells of the CA3 and the pyramidal cells of CA3 are the source of the major input to the CA1,

the Schaffer collateral axons. The CA1 also projects unidirectionally to the subiculum and entorhinal cortex. Neurobiological principles such as identification of excitatory and inhibitory synapses, discovery of long-term potentiation (LTP) (Bliss and Lømo, 1973) and long-term depression (LTD), role of oscillations in neuronal circuits and underlying mechanisms associated to epileptogenesis have been discovered in this brain area (Andersen et al., 2007).

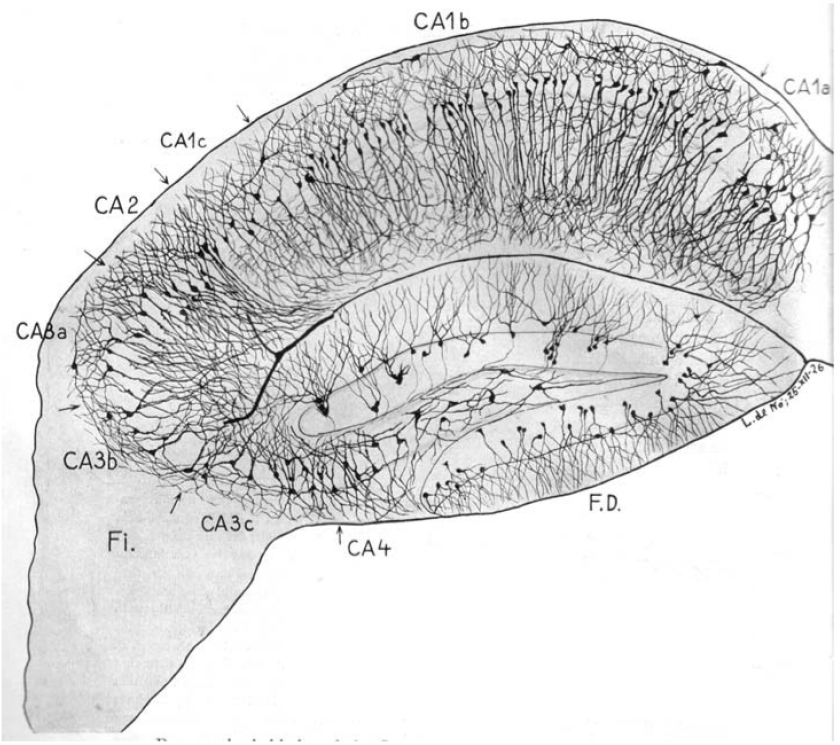

Figure 3: Drawing of the hippocampus by Lorente de Nó

Drawing of the hippocampus by Lorente de Nó showing cell types and the divisions of the hippocampus with the terminology in general use today: fascia or gyrus dentate, CA1 to 4, subiculum, pre- and parasubiculum and the entorhinal area (Andersen et al., 2007; Lorente de Nó, 1934).

A turning point in the knowledge of the hippocampal function was the clinical case of patient H. M. in the 1950s. After this, the interest for the hippocampus increased quickly. Patient H. M. had a relatively pure memory deficit after surgical excision of the medial temporal lobe for the relief of epilepsy (Milner, 1958). This case had a profound effect on the study of memory and through that, had a profound improvement in our understanding of the involvement of the hippocampus in memory (Andersen et al., 2007).

Basically, hippocampal neurons are divided into two major classes: principal or

excitatory neurons and inhibitory interneurons. Within excitatory neurons it is possible to distinguish pyramidal neurons, localized in the CA1, CA2 and CA3 regions of the hippocampus and as we have mentioned before, the excitatory neurons of the dentate gyrus, the granule cells and the mossy cells. Pyramidal neurons are by far the most numerous neurons in the hippocampus. Interneurons represent a heterogeneous group attending to different classifications and are around 10 % of total number of neurons in the hippocampus. Attending to morphological classification, interneurons can be divided in:

i) Chandelier or axo-axonic cells where its major distinguishing feature is the termination of their axon, which forms rows of boutons aligned parallel to the axon initial segments of pyramidal and granule cells.

ii) Basket cells, originally described by Ramón y Cajal in the cerebellar cortex, where the Purkinje cells are surrounded by a basket of axons and terminals. In the hippocampus these cells identify a population of interneurons with hetorogenous afferent connections.

iii) Interneurons innervating principal cell dendrites.

iv) Interneurons specialized to innervate other interneurons (Freund and Buzsáki, 1996).

Attending to neurochemical classification, interneurons can be classified attending to the expression of calcium binding protein such as parvalbumin (PV), calbindin (CB) or calretinin (CR) or the expression of neuropeptides such as somatostatin (ST), Neuropeptide Y (NPY) or cholecystokinin (CCK). In figure 4, we can observe the neural diversity at CA1 region of the hippocampus. The functional classification is based on the firing pattern of neurons. Some GABAergic interneurons have a higher firing rate than principal neurons and can be classified in fast spiking interneuron such as PV or non fast spiking interneuron such as CR.

On the other hand, recent developed single-cell RNA-sequencing (RNA-seq) methods enables systematic categorization of individual cells into groups with similar molecular properties (Poulin et al., 2016). This technology has been used to unravel cell diversity in the somatosensory cortex and the hippocampal CA1 region of the brain, discovering 47 molecularly distinct subclasses of cells (Zeisel et al., 2015).

Within the dentate gyrus, granule cells may function as elements in circuits generating feedforward and feedback inhibition. In feedforward inhibition, remote excitatory

inputs recruit local inhibitory networks that control the strength of the efferent signal. In feedback inhibition, local activation of inhibitory neurons controls local recurrent excitatory activity (Paz and Huguenard, 2015). Glutamatergic hilar mossy cells of the dentate gyrus can either excite or inhibit distant granule cells, depending on whether their direct excitatory projections to granule cells or their projections to local inhibitory interneurons dominate (Jinde et al., 2013). These GABAergic interneurons such as basket cells direct their efferent output toward the somata and proximal dendrites of granule cells. Dysfunctions in feed-forward inhibition and feed-back inhibition microcircuits have been identified in epilepsy in diverse regions of the brain (Paz and Huguenard, 2015).

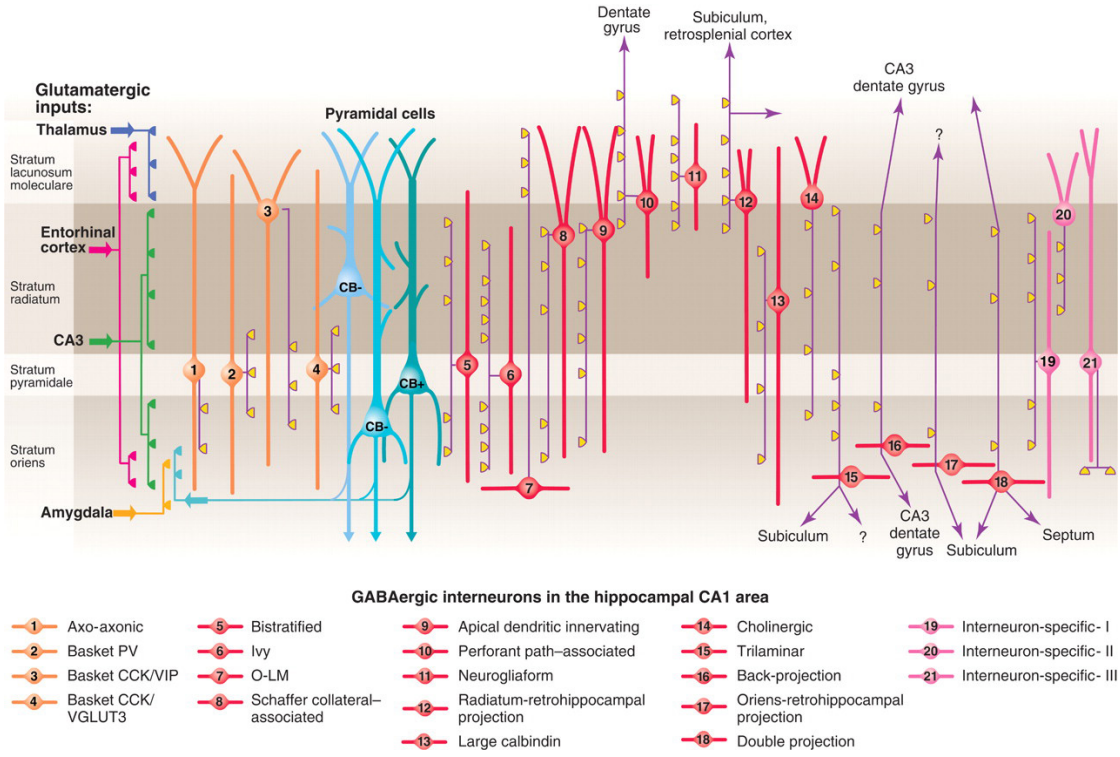

Figure 4: Neural diversity at hippocampus

Three types of pyramidal cell are accompanied by at least 21 classes of interneuron in the hippocampal CA1 area. The main terminations of five glutamatergic inputs are indicated on the left. The somata and dendrites of interneurons innervating pyramidal cells (blue) are orange, and those innervating mainly other interneurons are pink. Axons are purple; the main synaptic terminations are yellow. VIP, vasoactive intestinal polypeptide; VGLUT, vesicular glutamate transporter; O-LM, oriens lacunosum moleculare (Klausberger and Somogyi, 2008).

2. OBJECTIVES

This thesis has two major goals:

1. Investigate the properties of central synapses in hippocampal cultures from CSP-α knock-out mice and littermates using imaging approaches. This objective has two goals: the study of the synaptic vesicle cycle, specially endocytosis, and the study of presynaptic calcium dynamics.

2. Investigate the changes in neuronal excitability that might be caused by the genetic elimination of CSP-α in central neurons.

3. MATERIALS AND METHODS

3.1. Cell culture

3.1.1. Coverslips preparation

Coverslips of 18 mm and 25 mm of diameter were used for neuronal cultures. Before plating the neurons, coverslips were cleaned and sterilized. For that, they were immersed in nitric acid overnight and cleaned with distilled water several times. They were left in ethanol until the day that the culture was prepared.

Coverslips were rinsed with distilled water and they were put in the plates in order to dry them. An aliquot in proportion 3:1:1 with 600 µl of acetic acid 17 mM, 200 µl of collagen and 200 µl of Poly-D-Lysine was prepared to cover the surface of the coverslips using cotton. The plates were left in the hood to dry them completely at least for 3 hours. Other option was to leave them into the hood overnight and sterilize with UV for 20 minutes. After drying them, the coverslips were washed with distilled water.

3.1.2. Culture of astrocytes

Firstly, 3 ml of enzymatic solution 10 ml of Dulbecco's Minimum Essential Medium (DMEM), 2 mg of Cystein, 0.1 ml of 100 mM $CaCl_2$, 0.1 ml of 50 mM EDTA and 20-25 units/ml of Papain was prepared and bubbled with carbogen (95 % O_2, 5 % CO_2) for 10-20 minutes at 37 ºC. Then, the solution was filtered and left in the bath at 37 ºC until its use. For each culture, the hippocampi of two newborn rats (P0-P1) were taken out from the brain. For this, each brain was left in a Petri dish of 5 cm of diameter with 5 ml of Hank's Balanced Salt Solution 1x (HBSS) at 4 ºC. The cerebellum, the brain stem and the olfactory bulb were discarded upon removing them with a scalpel. The meninges were removed using tweezers and the brain was divided in two hemispheres with a sagittal cut. Finally, the hippocampi from each hemisphere were removed with the tweezers.

The hippocampi were left in a 15 ml tube with 3 ml of enzymatic solution and incubated for 45 minutes at 37 ºC in a shaking bath. After this enzymatic digestion, the tube was centrifuged for 5 minutes at 1000 rpm. The supernatant was discarded and 2 ml of inactivation solution containing 25 mg of Albumin, 25 mg of Trypsin inhibitor and 10 ml of neuronal solution was added for 5 minutes in order to stop the reaction of papain. The solution was centrifuged again at 1000 rpm for 5 minutes, the supernatant was discarded and the pellet was suspended in 1 ml of astrocytes medium that contains 180 ml of Dulbecco's Minimum Essential Medium (DMEM), 20 ml of Fetal Bovine Serum (FBS) and 1 ml of Penicillin/Streptomycin.

The pellet was transferred in an eppendorf tube and the tissue was pipetted to get a good suspension. The content was transferred to a Roux recipient and filled with medium until completing 15 ml. The Roux recipient was left in the incubator (37 ºC, 5 % CO_2) for 5 days and when cells reached the confluence, they were transferred to another recipient in order to purify the culture. They were left in the incubator until achieving the confluence again (4 days approximately).

For each plate containing coverslips, each well was filled with astrocytes medium where astrocytes were plated. Antimytotic treatment that contains 25 mg of 5-Fluoro-2'-Deoxyuridine, 62.5 mg of Uridine and 12.5 ml of DMEM was applied for 24 hours at 4-5 days in vitro in order to stop the growth of astrocytes.

3.1.3. Culture of neurons

Once the astrocytes were plated we started with the culture of neurons. The protocol to culture neurons is very similar to the protocol to culture astrocytes. Hippocampi from P0-P1 wild type and CSP-α KO mice were left in a 15 ml tube with 1.5 ml of enzymatic solution. They were left in a shaking bath for 45 minutes at 37 ºC and centrifuged at 1000 rpm for 5 minutes. The supernatant was removed and the pellet was suspended in 500 µl of neuronal medium 192 ml of Neurobasal A, 4 ml of B27, 2 ml of GlutaMAX 200 mM 100x and 1 ml of Penicillin/Streptomycin. The content of the tube was moved to an eppendorf tube for the mechanic digestion (3 or 4 consecutive steps of tissue dispersion). After this step, neurons were counted using the hemocytometer, cultured on plates with astrocytes and left in the incubator under standard conditions, 37 ºC and 5 % CO_2. 2-3 hours before plating the neurons, astrocytes medium was removed from the plates and neuronal medium was added. Neuronal medium was renovated each 3-4 days, at least a fourth of each well.

3.2. Lentiviral generation and production

A dual-promoter lentiviral vector was used to express exogenous proteins in cultured neurons (Gascón et al., 2008). This plasmid has two copies of a human synapsin promoter/WPRE cassette in a single lentiviral vector (Lenlox Syn-WPRE-Syn-GFP-WPRE). SynaptopHluorin lentivirus was generated by insertion of the sequence for synaptopHluorin obtained from pCiNeo-synaptopHluorin plasmid (gift of Dr. Gero Miessenböck) into the dual-promoter lentiviral vector in the place where one synapsin promoter and the sequence for GFP was removed. Similarly, GCaMP3 lentivirus was generated by the insertion of the sequence for GCaMP3 obtained from GCaMP3 plasmid

(Addgene, plasmid #22692) into the dual-promoter lentiviral vector in the place where one synapsin promoter and the sequence for GFP was removed.

For syGCaMP3 generation, GCaMP2 was removed from CMV::ratSyGCaMP2 plasmid (Addgene, plasmid #26124) and in its place the sequence for GCaMP3 was inserted. SyGCaMP3 lentivirus was generated by the insertion of the sequence for syGCaMP3 into the dual-promoter lentiviral vector in the place where one synapsin promoter and the sequence for GFP was removed.

For lentiviral production, HEK293T cells were transfected using the calcium phosphate method with the lentiviral expression vector and two packaging vectors: pCAG-VSVg, a plasmid expressing the VSV-G envelope gene, and pCMVΔR8.91, a plasmid expressing the gag/pol genes (Gascón et al., 2008). After 72 h of transfection, supernatants containing viral particles were collected and viruses were concentrated following a centrifugation protocol. Viral titers were determined by viral serial dilution on SH-SY5Y human cell line and the ratio of infection (number of cells expressing GFP divided by the total number of cells detected) was calculated by flow cytometry after 48 h of infection. For viral titer calculation (equation 1), viral amounts for ratios of infection under 0.12 were only chosen to rule out saturated infections. To calculate the viral amount needed to infect cultured hippocampal neurons (equation 2), multiplicity of infection (MOI) was established to 10.

$$\text{Viral titer} = \frac{\text{Number of plated cells} \cdot \text{Ratio of infection}}{\text{Viral amount}} \qquad \text{(Equation 1)}$$

$$\text{Viral amount per well} = \frac{\text{Number of cells to infect} \cdot \text{MOI}}{\text{Viral titer}} \qquad \text{(Equation 2)}$$

3.3. Imaging

A PCO Sensicam QE CCD camera connected to a Nikon Eclipse TE-2000-U inverted microscope was used to acquire sequences of fluorescence images of live primary neuronal cultures. The microscope was mounted inside a Faraday's cage on an anti vibration table (Newport). A shutter (Uniblitz, model VCM-D1) was used to control the exposure time of acquisition. For stimulation with fluorescence a mercury lamp (Ushio 103D) and a set of dichroic mirrors, excitation and emission filters were used depending of the fluorophore. Sequences of images were acquired using a 20x Nikon Plan Fluor objective (NA: 0.75, WD: 0.35 mm, oil) or 40x Nikon S-Fluor objective (NA: 1.3, WD: 0.22 mm, oil). Electrical field stimulations of hippocampal cultures were carried out

using a stimulus isolation unit (Warner Instruments, model SIU-102) and the electrical stimulator A-M Systems, model 2100. Electrical field stimulation protocols and imaging acquisition were synchronized using the acquisition card of the patch-clamp EPC10 amplifier (Heka).

Perfusion was delivered to the chamber at 1 ml/minute approx. and the solution was composed of 119 mM NaCl, 2.5 mM KCl, 2 mM $CaCl_2$, 2 mM $MgCl_2$, 25 mM HEPES, 30 mM glucose and the pH of the solution was adjusted to 7.4 with NaOH. All experiments were realized at room temperature.

3.3.1. Fluo4-AM calcium dye

Intracellular calcium was monitorized using Fluo4-AM (Invitrogen), a molecule that exhibit an increase in fluorescence upon binding Ca^{2+}. Fluo4-AM was diluted in dimethyl sulfoxide (DMSO) and cells were loaded with the AM ester forms of this calcium indicator by adding the dissolved indicator at 4 µM directly to dishes containing cultured cells during 25 min at room temperature before imaging experiments. The dissociation constant of Fluo4-AM was 335 nM and the excitation and emission wavelength were 494 and 506 nm. Coverslips with primary neuronal cultures were mounted on the bottom of a closed bath imaging chamber incorporating field stimulation platinum electrodes, Warner Instruments model RC-21BRFS. The bath volume of the completed assembly is 260 µl and the distance between the platinum wires is 6.3 mm. Images were acquired using the software Camware (5 frames/s, exposure time 100 ms and binning 2x2). Stimulated sequences of images were acquired applying biphasic pulses of current, amplitude 10 mA and width 5 ms (2.5 ms each phase) at different frequencies and duration using the electrical stimulator A-M Systems, model 2100.

3.3.2. Genetically encoded optical probes

The genetically encoded optical probe synaptopHluorin, a fusion protein of the synaptic vesicle protein synaptobrevin and a pH-sensitive GFP was used to study the synaptic vesicle cycle in cultured neurons. SynaptopHluorin was expressed in neuronal cultures via viral gene transduction. Neuronal cultures infections were done at 2-7 DIV and imaging experiments were realized from 15 DIV on. Images were acquired using the software Camware (1 frames/s, exposure time 100 ms and 2x2 binning). Ammonium Chloride solution was used to basify the internal compartment of neurons in order to see the maximum fluorescence of pH-sensitive proteins. This solution was composed of 50 NH_4Cl, 69 mM NaCl, 2.5 mM KCl, 2 mM $CaCl_2$, 2 mM $MgCl_2$, 25 mM HEPES, 30 mM

glucose and the pH of the solution was adjusted to 7.4 with NaOH.

Calcium is a very important second messenger in cell biology and it is has an important role in the molecular machinery of neurotransmitter release. Genetically encoded calcium indicators (GECIs), such as green fluorescent protein (GFP)-based G-CaMPs, are very useful reporters to monitor the calcium dynamics in defined cell populations or specific subcellular locations such as synapses. G-CaMP is composed of the calcium responsive element calmodulin and a calmodulin binding peptide (M13) attached to a circularly permutated GFP (Nakai et al., 2001). When calcium binds G-CaMP, calmodulin executes a conformational change, interacting with the M13 peptide and altering the protonation state of the chromophore, thus increasing the fluorescence intensity of the protein (McCombs and Palmer, 2008).

In this thesis, the genetically encoded calcium indicators (GECIs) GCaMP3 an improved version of the G-CaMP calcium indicator with affinity for Ca^{2+} of 660 nM (Tian et al., 2009) and synaptophysin-GCaMP3 (syGCaMP3) were used to image neuronal calcium activity and synaptic calcium activity in neural networks respectively. Previous characterization of syGCaMP3 using the ionophore ionomycin showed a dynamic range of 6.5-fold from 0 Ca^{2+} and 10 mM EGTA to 2 mM Ca^{2+} in the absence of EGTA with a peak fluorescence during 40 Hz 30 s stimulation approximately half maximal, within the dynamic range of the indicator (Li et al., 2011). GCaMP3 and syGCaMP3 were expressed in neuronal cultures via viral gene transduction. Neuronal cultures infections were done at 2-7 DIV and imaging experiments were realized from 15 DIV on. Images were acquired using the software Camware (5 frames/s, exposure time 100 ms and 2x2 binning). In syGCaMP3 experiments, high potassium solution was used to increase neuronal activity for luminal Vgat antibody uptake. This solution was composed of 51.5 mM NaCl, 70 mM KCl, 2 mM $CaCl_2$, 2 mM $MgCl_2$, 25 mM HEPES, 30 mM glucose and the pH of the solution was adjusted to 7.4 with NaOH.

For all experiments with genetically encoded optical probes, 18 mm coverslips with primary neuronal cultures were mounted on the bottom of a bath open imaging chamber incorporating field stimulation platinum electrodes (Warner Instruments model RC-49MFS). The distance between the platinum wires is 10 mm. Stimulated sequences of images were acquired applying biphasic pulses of current, amplitude 50 mA and width 1 ms (0.5 ms each phase) at 20 Hz for 10 seconds through the stimulus isolation unit (Warner Instruments, model SIU-102) receiving the timing pulses from the electrical stimulator A-M Systems, model 2100.

3.4. Electrophysiology

Whole cell recordings in current-clamp configuration were performed using an EPC10 amplifier (Heka). Data were filtered with a Bessel filter at 2.9 KHz and acquired at 20 KHz using PatchMaster software (Heka). Cells were voltage clamped at -70 mV and after opening the configuration was changed to current clamp. Patch electrodes (Science Products GmbH, GB150F-8P) were pulled with a P-97 puller (Sutter Instruments) and had a resistance of 2-4 MΩ.

Recordings of cultured neurons were performed with the external solution 119 mM NaCl, 2.5 mM KCl, 2 mM $CaCl_2$, 2 mM $MgCl_2$, 25 mM HEPES, 30 mM glucose and the pH of the solution was adjusted to 7.4 with NaOH. The composition of internal solution was 120 mM K-gluconate, 10 mM NaCl, 4.6 mM $MgCl_2$, 4 mM Na_2ATP, 15 mM creatine phosphate, 20 U/ml phosphocreatine kinase, 1 mM K-EGTA, 10 mM HEPES and pH was adjusted to 7.4 using KOH.

Hippocampal granule cells at dentate gyrus recordings in brain slices were performed from P10-P31 mice. Before sacrifice, mice were anesthetized with Tribromoethanol (TBE) 2 % in PBS. Brain was extracted and cut in 350 µm slices with a vibrating blade microtome (Leica VT1200). The external solution was 126 mM NaCl, 2.5 mM KCl, 1.25 mM NaH_2PO_4, 2 mM $CaCl_2$, 2 mM $MgCl_2$, 10 mM glucose, 26 mM $NaHCO_3$. During slicing, storage (30-60 min before recording) and recording, extracellular solution was gassed with 95 % O_2, 5 % CO_2 to a pH of 7.4. 0.2 mM pyruvic acid (28 µl from 2 M stock in 500 ml of external solution) and 0.2 mM ascorbic acid (17.5 mg in 500 ml of external solution) were added to improve slice quality. For current-clamp recordings, internal solution was 120 mM K-gluconate, 10 mM KCl, 10 mM phosphocreatine disodium salt, 2 mM MgATP, 0.3 mM NaGTP, 0.1 mM ethyleneglycolbis (2-aminoethylether)-N,N,N',N'-tetra acetic acid (EGTA), 10 mM 4-(2-hydroxyethyl)-1-piperazineethanesulfonic acid (HEPES), pH 7.2 adjusted with KOH and osmolality 280-290 mosmol/kg, adjusted with sucrose. Under voltage-clamp conditions, the patch-pipettes for inhibitory postsynaptic currents recording (IPSCs) contained (mM): 140 CsCl, 2 $MgCl_2$, 0.05 EGTA, and 10 HEPES, adjusted to pH 7.2 with CsOH (280-290 mosmol/kg).

3.5. Immunofluorescence

Cultured neurons were fixed for 20 minutes at room temperature in PBS containing 4 % paraformaldehyde. Following three washes with PBS, the fixed neurons were

	Antibody	Description	Dilution	Reference
Primary antibodies	Synaptobrevin 2 VAMP 2	Mouse monoclonal	1/500	Synaptic Systems Cat. No. 104 211
	Vglut 1	Mouse monoclonal	1/100	Synaptic Systems Cat. No. 135 311
	Vgat	Rabbit polyclonal	1/500	Gift of Reinhard Jahn (Takamori et al., 2000)
	GFP	Chicken	1/1000	Aves Labs Cat. No. GFP-1010
Secundary antibodies	Alexa Fluor® 488	Anti-chiken	1/500	Jackson ImmunoResearch Code number: 703-545-155
	Cy™3	Anti-rabbit	1/500	Jackson ImmunoResearch Code number: 711-165-152
	Alexa Fluor® 647	Anti-mouse	1/500	Jackson ImmunoResearch Code number: 115-605-146
Antibody for functional experiments	Vgat (luminal)	Rabbit polyclonal Fluorescence-labeled with Oyster® 550	2-5 µg/ml	Synaptic Systems Cat. No. 131 103C3

Table 1: List of antibodies

permeabilized for 10 minutes in blocking solution (PBS containing 1 % FBS) supplemented with 0.05 % Triton X-100. Primary antibodies were incubated either for 2 hours at room temperature or overnight at 4 ºC. For hippocampal neurons expressing a GFP-based genetically encoded optical probe, an anti-GPF antibody was used to detect expression. Following three washes with PBS, secondary antibodies were applied for 2 hours at room temperature, followed by three new washes in PBS. Coverslips were mounted with Dako fluorescent mounting medium and stored at 4 ºC. Coverslips were examined with the laser scanning confocal microscopy Zeiss LSM 7 DUO. Lists of antibodies used in this thesis are shown in table 1.

3.6. Data analysis

3.6.1. Synaptic quantification

Fluorescence time courses of synaptic spots expressing synaptopHluorin or syGCaMP3 were isolated using square ROIs of 4 x 4 pixels (1.66 µm^2) selected manually with ImageJ after background subtraction. Each synaptic spot's time trace was obtained calculating the mean gray value of each ROI in every image using Multi Measure tool of ROI manager. In set measurements, mean gray value has to be selected. Statistics of synaptic spots' time traces was performed using custom software written in MATLAB

(The MathWorks). Statistical significance was calculated using SPSS software.

3.6.2. Sequence alignment

Sequence alignment based on spatial correlation was performed to correct movements during image acquisition using custom ImageJ plug-in written in Java (file with code is attached to this dissertation). For that, normalized correlation coefficient c(x,y) (equation 3) of a selected mask w(x,y) of size m x n with each image f(x,y) of the sequence was used.

Mask w(x,y), also called template, must be a ROI (Region of Interest) as constant as possible and normally was taken from the first image of the sequence. $\overline{w}$ is the average value of the mask and $\bar{f}$ is the average value of f in the region coincident with w. Spatial correlation consists on template matching in every image of the sequence. The best possible match (correlation coefficient c(x,y) is equal to 1) is achieved when template and the corresponding region of image are identical. To correct the movement, each image of the sequence was shifted in x-coordinate and y-coordinate as many pixels as given by the difference between the coordinates at maximum normalized correlation coefficient and the original coordinates of the mask w(x,y).

$$c(x,y) = \frac{\sum_s \sum_t [w(s,t) - \overline{w}] \sum_s \sum_t \left[f(x+s, y+t) - \bar{f}(x+s, y+t)\right]}{\sqrt{\sum_s \sum_t [w(s,t) - \overline{w}]^2 \sum_s \sum_t \left[f(x+s, y+t) - \bar{f}(x+s, y+t)\right]^2}} \qquad \text{(equation 3)}$$

3.6.3. Activity correlation analysis

Imaging correlation analysis was performed to separate patterns of synaptic activity of neurons infected with syGCaMP3 using custom ImageJ plug-in written in Java (file with code is attached to this dissertation). In order to look for a specific pattern of activity in the area of interest, correlation coefficient r_{xy} (equation 4) between the time course of a selected reference signal x and each pixel's time trace y was calculated to obtain a correlation map. After applying a threshold, a binary map highlights pixels with correlation coefficient over this threshold, indicating high similarity. In contrast, traces with correlation coefficient under the threshold appear white in this map, indicating low similarity.

$$r_{xy} = \frac{\sum_{t=1}^{n}(x_t - \bar{x})(y_t - \bar{y})}{\sqrt{\sum_{t=1}^{n}(x_t - \bar{x})^2 \sum_{t=1}^{n}(y_t - \bar{y})^2}} \quad \text{(equation 4)}$$

3.6.4. Electrophysiological patch-clamp recordings analysis

Detection of action potentials of cultured hippocampal neurons and the measurements of duration between consecutives action potentials were performed using Stimfit Software (Guzman et al., 2014). Data analysis was performed using custom software written in MATLAB (The MathWorks) and statistical significance was calculated using SPSS software. The analysis of dentate granule cells recordings was also performed using Stimfit Software and statistical significance was calculated using SPSS software.

4. RESULTS

4.1. Studying the function of CSP-α in synaptic exo- and endocytosis of hippocampal central neurons using synaptopHluorin

In this chapter, we describe the experiments carried out in hippocampal cultures to study the role of CSP-α in the machinery of synaptic exo- and endocytosis. For this purpose, we have used a pH-sensitive green fluorescent protein (GFP) fused to the luminal part of synaptic vesicles (pHluorin). The pHluorins targeted to the synaptic vesicle lumen (synaptopHluorin) enabled measurements of dynamics changes in pH of vesicles lumen resulting from exocytosis and endocytosis of synaptic vesicles during presynaptic activity (Miesenbock et al., 1998). The pHluorin molecule is attached to the luminal part of Synaptobrevin/VAMP2 (Syb2) and the expression in neurons is driven by the specific human promoter synapsin using viral transduction (Figure 5.A).

During firing of action potentials, synaptic vesicles undergo fusion with the plasma membrane leading to the externalization of pHluorin to pH of 7.4, removing the proton-dependent quenching and increasing the fluorescence. After reacidification of vesicles, fluorescence signal recovers following endocytosis (Figure 5.B-C) (Sankaranarayanan et al., 2000).

Hippocampal neurons from newborn CSP-α KO mice and their wild type littermates were cultured on rat astrocytes. The pH-dependent fluorescence changes associated to exo- and endocytosis were recorded under electrical field stimulation at 20 Hz for 10 seconds (200 electrical pulses in total) to evoke action potentials (Figure 6.A). A pseudocolour line scan of the fluorescence changes along a selected line (in red) and the time course of fluorescence changes at the regions of interest (ROIs) indicated by yellow rectangles are shown in Figure 6.A. Fluorescence changes are represented such as the difference between the fluorescence F of the synaptic spots and its fluorescence in resting conditions F_0 ($\Delta F=F-F_0$), in arbitrary units (a.u.). 2D and 3D view of synaptic spots are also shown for region 1 (CSP-α WT) and region 3 (CSP-α KO). White rectangles indicate the region of interest used for quantification of fluorescence changes of each synaptic spot (1.66 μm^2).

Comparing the amplitude (ΔF) of the total number of synaptic spots quantified for CSP-α WT and CSP-α KO hippocampal cultures, no significant differences were detected. Histogram and cumulative distribution showing the amplitudes of synaptopHluorin responses are represented (Figure 6.B) as well as the whisker and box plot of amplitudes (Figure 6.C). n=11 imaging experiments and 677 synaptic spots for CSP-α WT and n=9 experiments and 604 synaptic spots for CSP-α KO.

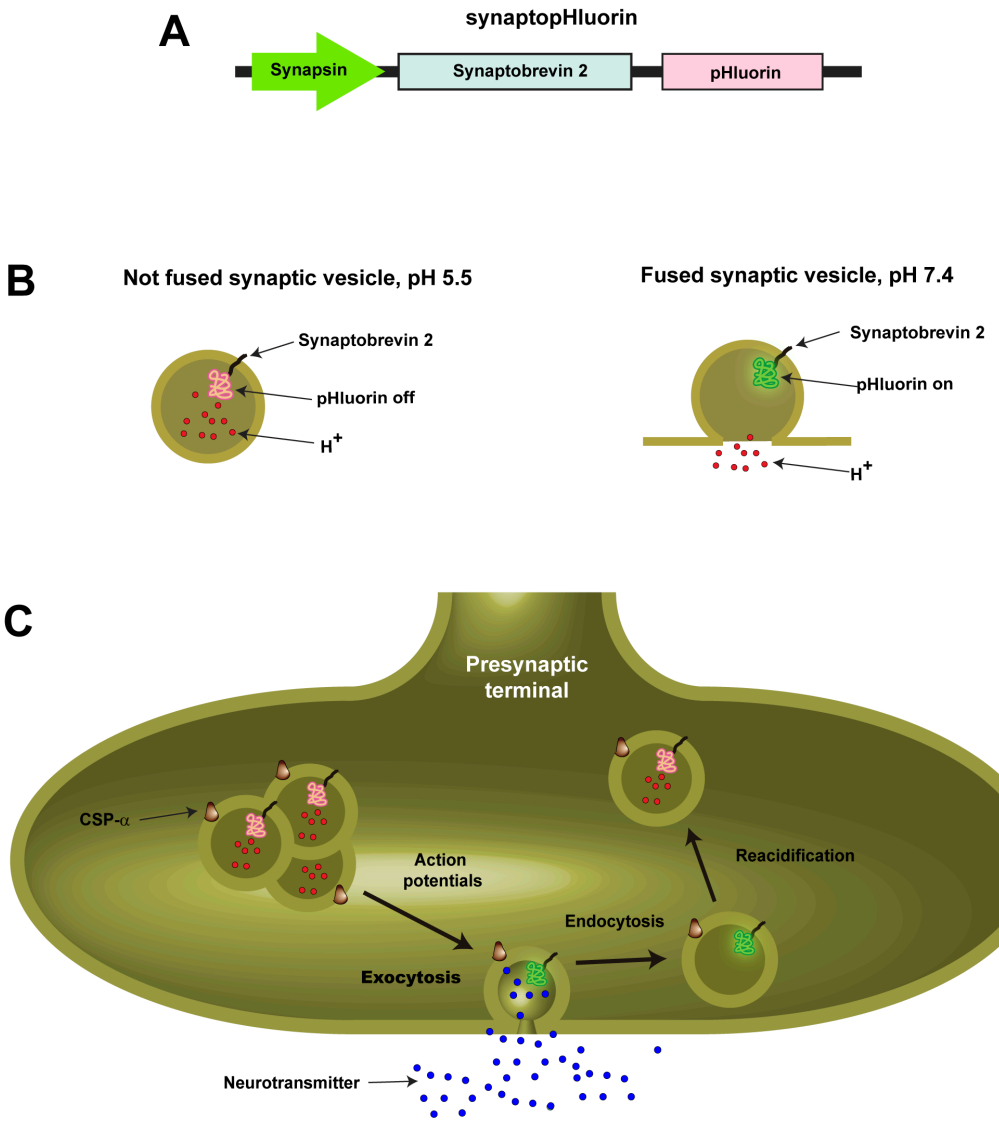

Figure 5: synaptopHluorin is a pH sensitive GFP (pHluorin) fused to the luminal part of synaptic vesicles to monitor synaptic exo- and endocytosis

A: pHluorin is fused to the luminal end of synaptobrevin 2 and the specific human promoter synapsin drives the expression in neurons.

B: The emission spectra of pHluorin is pH-dependent. pHluorin is turned off at pH 5.5 and has its maximum spectra at pH 7.4 when the synaptic vesicles is fused with the plasma membrane and the pHluorin is exposed to the extracellular medium. Absorption of pHluorin is at 488 nm light and its maximum emission light is at 510 nm.

C: pH-dependent emission allows monitoring pH changes associated to exo- and endocytosis in the synaptic vesicle cycle.

Half decay of synaptic spots was also quantified for CSP-α WT and CSP-α KO hippocampal cultures. Half decay is the time that amplitude falls 50 % from the maximum. No significant differences were detected in the half decay between CSP-α KO and WT indicating normal vesicle recycling in CSP-α KO synapses. Histogram and cumulative distribution showing the half decay of synaptopHluorin responses are represented (Figure 6.D) as well as the whisker and box plot (Figure 6.E). n=11 imaging experiments and 677 synaptic spots for CSP-α WT and n=9 experiments and 604 synaptic spots for CSP-α KO.

CSP-α KO terminals at neuromuscular junction show a reduced number of synaptic release sites (Rozas et al., 2012) and decreased levels of SNAP-25 (Chandra et al., 2005; Rozas et al., 2012; Sharma et al., 2012). In this situation, we might expect reduced amplitude in fluorescence signals of mutant synapses compared to control indicating an alteration in the exocytic machinery, but in contrast, we do not see significant differences (Figure 6.B-C). This could be explained whether the total pool of vesicles is different between mutant and control. We can know the total pool of vesicles measuring the total amount of synaptopHluorin expressed in the synaptic terminals. For that, hippocampal cultures were alkalinizated with a solution containing 50 mM of ammonium chloride (NH_4Cl) after application of the electrical stimulus necessary to see exo- and endocytosis (Figure 7.A-B). The total fluorescence values in ammonium chloride solution were very similar in terminals lacking CSP-α compared to controls, indicating similar total pool of vesicles. Mean time course of fluorescence changes of synaptic spots expressing synaptopHluorin during exo- and endocytosis and during exposition to ammonium chloride are represented in Figure 7.C as ΔF (a.u.) ± sem. n=11 experiments for CSP-α WT and n=9 experiments for CSP-α KO. Also, mean time course of exo- and endocytosis responses normalized to the responses in the presence of NH_4Cl are represented as $\Delta F/\Delta NH_4Cl$ ± sem (Figure 7.D). No significant differences were found in the amplitude of synaptopHluorin responses either, under normalization with ammonium chloride. This is shown in the histogram and cumulative distribution of Figure 7.E and the whisker and box plot of Figure 7.F.

These results go against the initial hypothesis, where a decreased levels of SNAP-25 in mutants would lead to a decreased amplitude in synaptopHluorin fluorescence and where the regulation of CSP-α in the polymerization of dynamin-1 (Zhang et al., 2012), a protein necessary for endocytosis, would lead to an increased half decay. An explanation for this could be that during analysis only functional synaptic spots were chosen for quantification, that is, only synaptic spots that showed fluorescence changes, because it is

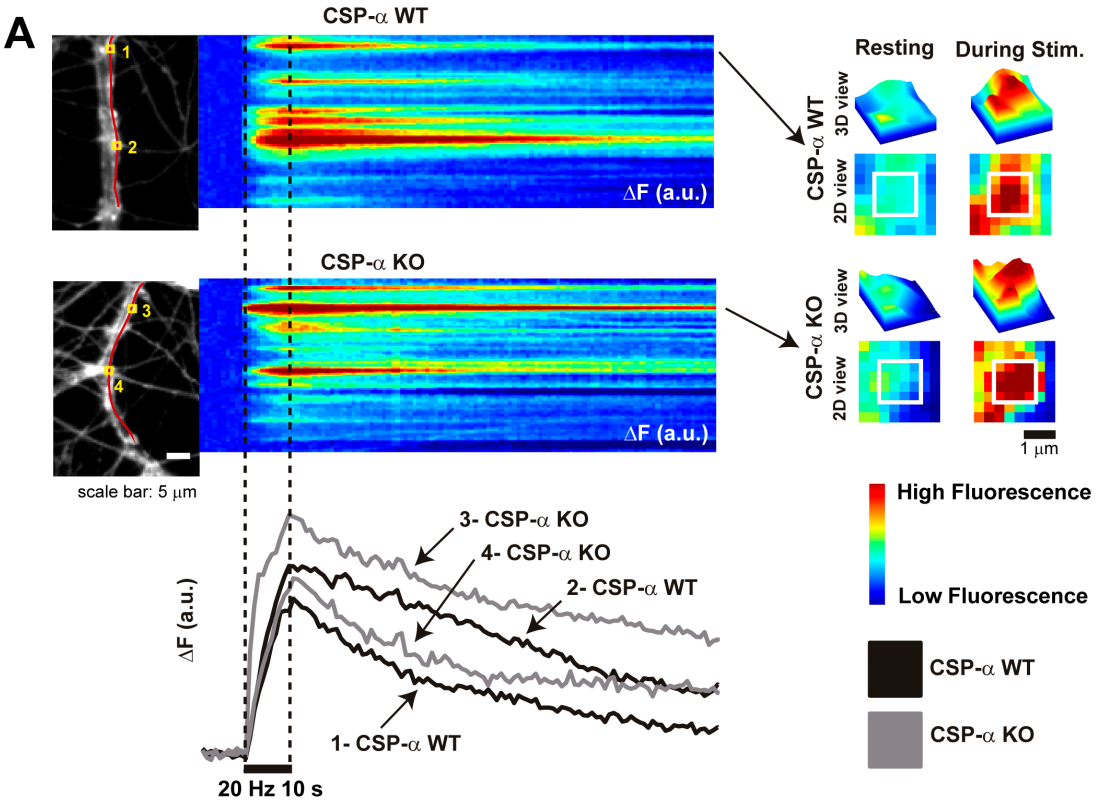
A
CSP-α WT
ΔF (a.u.)
CSP-α KO
ΔF (a.u.)
scale bar: 5 μm
Resting
During Stim.
CSP-α WT
3D view
2D view
CSP-α KO
3D view
2D view
1 μm
High Fluorescence
Low Fluorescence
CSP-α WT
CSP-α KO
3- CSP-α KO
4- CSP-α KO
2- CSP-α WT
1- CSP-α WT
ΔF (a.u.)
20 Hz 10 s

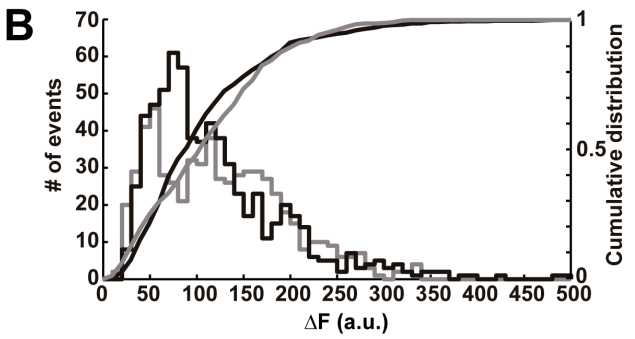
B
# of events
Cumulative distribution
ΔF (a.u.)

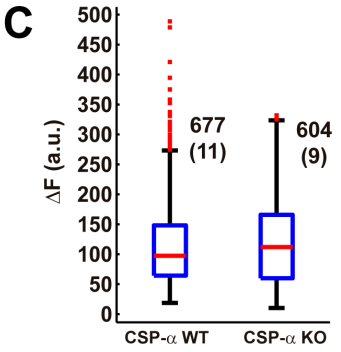
C
ΔF (a.u.)
677
(11)
604
(9)
CSP-α WT
CSP-α KO

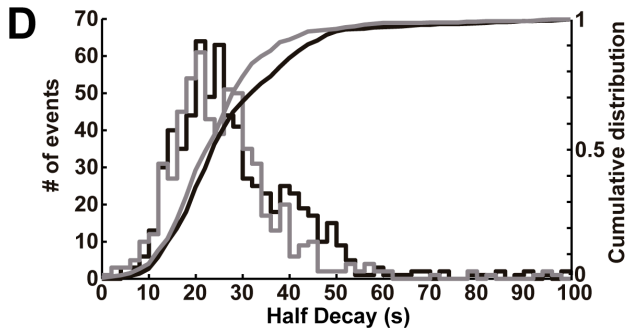
D
# of events
Cumulative distribution
Half Decay (s)

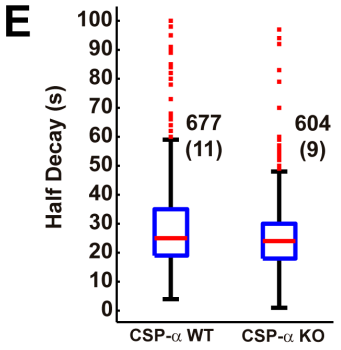
E
Half Decay (s)
677
(11)
604
(9)
CSP-α WT
CSP-α KO

Figure 6: Imaging of synaptic exo- and endocytosis using synaptopHluorin shows that synapses lacking CSP-α present exo- and endocytosis responses similar to the responses found in hippocampal cultures from wild type littermates

A: Fluorescence changes of synapses expressing synaptopHluorin when a field electrical stimulation at 20 Hz for 10 seconds is applied to wild type and CSP-α KO hippocampal cultures. A pseudocolour line scan of the fluorescence changes along a selected line (in red) and the time course of fluorescence changes at the regions of interest (ROIs) indicated by yellow rectangles are shown. 2D and 3D view of synaptic spots are also shown. White rectangles indicate the regions of interest (regions 1 and 3).

B: Histogram and cumulative distribution showing the amplitudes (ΔF) of synaptopHluorin responses. n=11 experiments and 677 synaptic spots for CSP-α WT and n=9 experiments and 604 synaptic spots for CSP-α KO.

C: Box plot of data shown in B.

D: Histogram and cumulative distribution showing the half decay of synaptopHluorin responses. n=11 experiments and 677 synaptic spots for CSP-α WT and n=9 experiments and 604 synaptic spots for CSP-α KO.

E: Box plot of data shown in D.

Experiments were performed in the presence of the NMDA receptor antagonist APV (50 μM) and the AMPA receptor antagonist CNQX (25 μM) at 17-24 DIV from three different hippocampal cultures.

not possible to distinguish between background expression and non functional synapses. If it would have a population of synapses with a total defect in the exocytic machinery, it could not be detected with this method. Even other conditions such as prolonger network activity could be needed to see a synaptic defect in the exo- and endocytic machinery.

4.2. Imaging calcium dynamics in cultured hippocampal neurons lacking CSP-α

4.2.1. Presynaptic genetically encoded calcium indicator syGCaMP3 in hippocampal cultures

To image synaptic activity, GCaMP3 was fused to the cytosolic part of the synaptic vesicle protein synaptophysin in order to target the calcium indicator specifically to synaptic terminals (Dreosti et al., 2009). In this thesis, this presynaptic cytosolic calcium reporter (syGCaMP3) has been used under the specific human promoter synapsin to direct the expression in cultured hippocampal neurons (Figure 8.A-B), in order to study the role of CSP-α in the regulation of presynaptic calcium dynamics.

The arrival of action potentials to the presynaptic terminals leads to a calcium influx through the presynaptic voltage-gated calcium channels (VGCCs) and syGCaMP3 should allow monitoring fluorescence changes associated to calcium concentrations

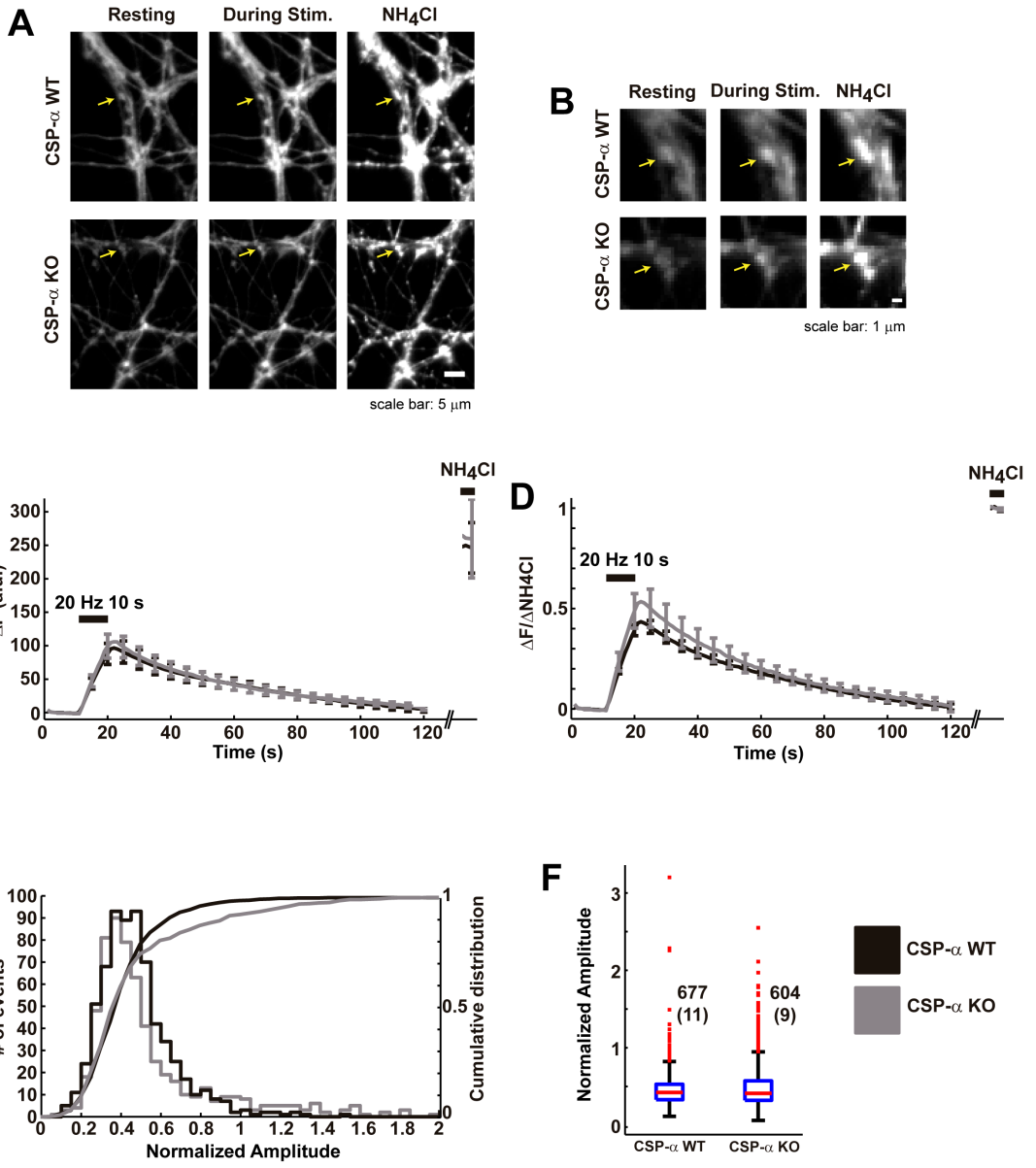
A
Resting
During Stim.
NH4Cl
CSP-α WT
CSP-α KO
scale bar: 5 μm
B
Resting
During Stim.
NH4Cl
CSP-α WT
CSP-α KO
scale bar: 1 μm
C
NH4Cl
20 Hz 10 s
ΔF (a.u.)
Time (s)
D
NH4Cl
20 Hz 10 s
ΔF/ΔNH4Cl
Time (s)
E
# of events
Cumulative distribution
Normalized Amplitude
F
Normalized Amplitude
677
(11)
604
(9)
CSP-α WT
CSP-α KO
CSP-α WT
CSP-α KO

Figure 7: Imaging of synaptic exo- and endocytosis using synaptopHluorin shows that normalized responses to the total pool of vesicles observed by adding NH_4Cl are similar in hippocampal cultures from mice lacking CSP-α and wild type littermates

A: Images of hippocampal cultures expressing synaptopHluorin during resting, electrical stimulation (20 Hz, 10 s) and in the presence of external solution containing NH_4Cl. Yellow arrows indicate synaptic spots in those conditions.

B: Zoom of images shown in A. Yellow arrows indicate synaptic spots shown in A.

C: Mean time course of synaptic spots expressing synaptopHluorin, ΔF (a.u.) ± sem. n=11 experiments for CSP-α WT and n=9 experiments for CSP-α KO.

D: Mean time course of synaptopHluorin responses normalized to the responses in the presence of NH_4Cl, $\Delta F/\Delta NH_4Cl$ ± sem. n=11 experiments for CSP-α WT and n=9 experiments for CSP-α KO.

E: Histogram and cumulative distribution showing the normalized amplitudes of synaptopHluorin responses $\Delta F/\Delta NH_4Cl$. n=11 experiments and 677 synaptic spots for CSP-α WT and n=9 experiments and 604 synaptic spots for CSP-α KO.

F: Box plot of data shown in E.

Experiments were performed in the presence of the NMDA receptor antagonist APV (50 μM) and the AMPA receptor antagonist CNQX (25 μM) at 17-24 DIV from three different hippocampal cultures.

(Figure 8.C). Hippocampal neurons from newborn CSP-α KO mice and their wild type littermates were cultured on rat astrocytes and syGCaMP3 expression was achieved at synapses via viral vector transduction. In figure 8.D we show the colocalization of syGCaMP3 with the presynaptic marker synaptobrevin 2 (Syb2) by immunofluorescence-based labeling (yellow puncta indicated by white arrows), indicating that expression was successfully driven to synapses. Furthermore, immunolabeling against glutamatergic and GABAergic synaptic markers of hippocampal cultures expressing syGCaMP3 were performed to know the type of synapses that were targeted (Figure 9). In figure 9.A we can observe three different regions where syGCaMP3 (green) and VGLUT 1 (magenta) colocalize (white puncta indicated by yellow arrows), but however, there is not colocalization between syGCaMP3 (green) and the GABAergic marker VGAT (red), indicating that expression of syGCaMP3 is not driven in GABAergic synapses. In figure 9.B we show the whisker and box plot of Pearson's correlation coefficients between syGCaMP3, VGLUT 1 and VGAT patterns. Correlation coefficients between syGCaMP3 and VGLUT 1 images were higher than correlation coefficients between syGCaMP3 and VGAT images, indicating that syGCaMP3 localization fits better with glutamatergic patterns. Furthermore, VGLUT 1 and VGAT are markers of different synapses and low correlation coefficients are expected for these patterns. In figure 9.B we can observe no

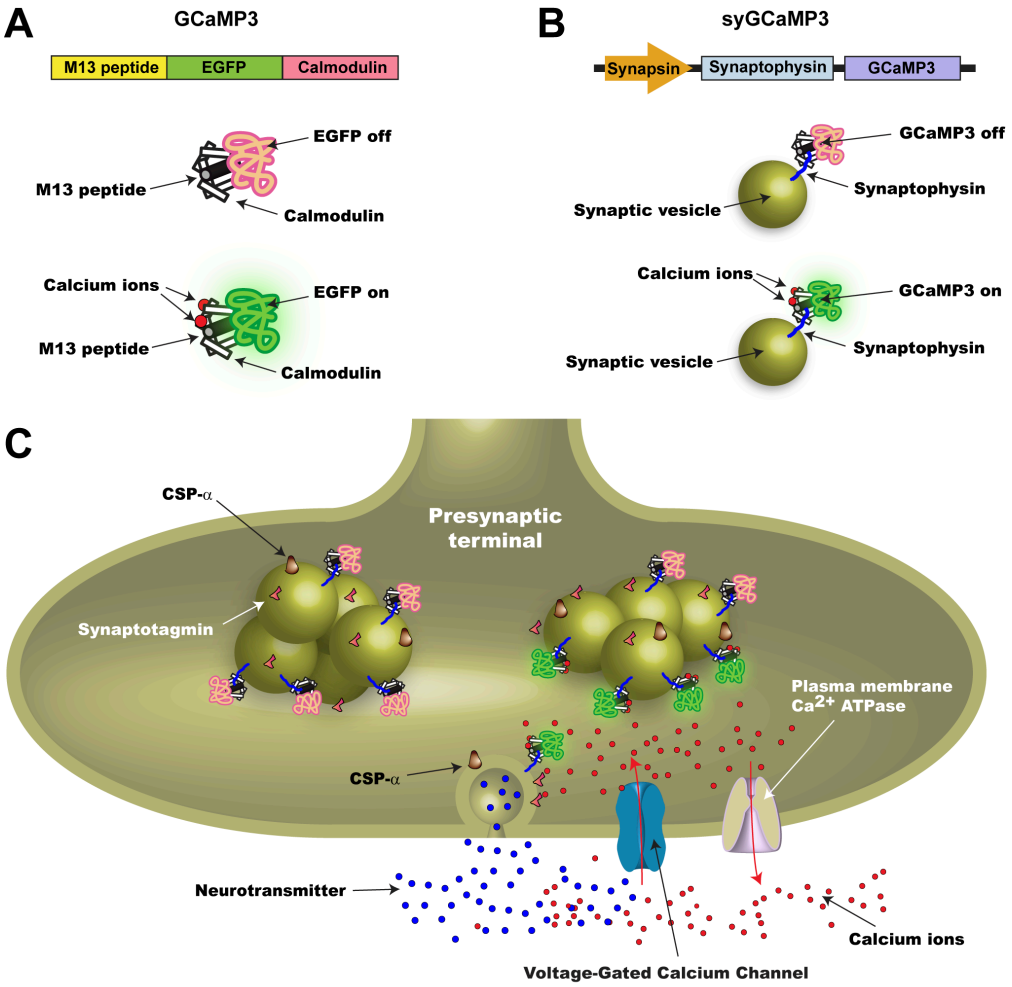
A
GCaMP3
M13 peptide
EGFP
Calmodulin
EGFP off
M13 peptide
Calmodulin
Calcium ions
EGFP on
M13 peptide
Calmodulin
B
syGCaMP3
Synapsin
Synaptophysin
GCaMP3
GCaMP3 off
Synaptophysin
Synaptic vesicle
Calcium ions
GCaMP3 on
Synaptophysin
Synaptic vesicle
C
CSP-α
Presynaptic terminal
Synaptotagmin
Plasma membrane Ca2+ ATPase
CSP-α
Neurotransmitter
Calcium ions
Voltage-Gated Calcium Channel

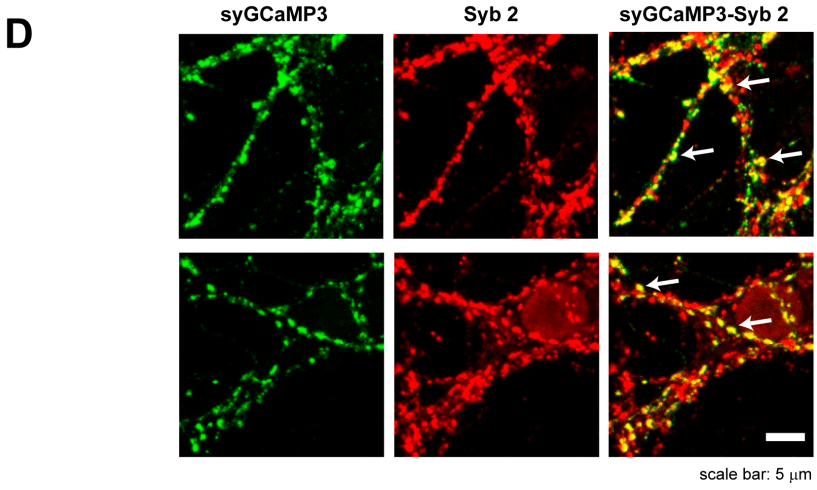
D
syGCaMP3
Syb 2
syGCaMP3-Syb 2
scale bar: 5 μm

Figure 8: The calcium indicator syGCaMP3 is located at presynaptic terminals

A: Structure of the genetically encoded calcium indicator GCaMP3. When calcium binds to GCaMP3, calmodulin executes a conformational change, interacting with the M13 peptide and altering the protonation state of the chromophore, thus changing the fluorescence intensity of the protein.

B: Structure of the genetically encoded calcium indicator syGCaMP3. syGCaMP3 is the calcium indicator GCaMP3 fused to the cytosolic part of the synaptic vesicle protein synaptophysin.

C: syGCaMP3 allows monitoring fluorescence changes associated to the levels of presynaptic calcium concentrations.

D: Immunofluorescence of hippocampal cultures expressing syGCaMP3. Colocalization of syGCaMP3 with the presynaptic marker Synaptobrevin 2 (Syb 2) indicates that expression was successfully driven to synapses. White arrows indicate examples of synapses expressing syGCaMP3 (in yellow).

significant differences between syGCaMP3-VGAT and VGLUT 1-VGAT correlation coefficients providing a quantitative measurement of low similarity between the spatial distribution of synapses expressing syGCaMP3 and GABAergic synapses. In figure 9.B, statistical significance was calculated using the Student's t-test.

On the other hand, the identification of active GABAergic synapses was possible using a fluorescence-labeled antibody against the luminal region of the vesicular GABA transporter VGAT (Martens et al., 2008). To confirm previous results, functional imaging recordings of synapses expressing syGCaMP3 loaded with the luminal VGAT antibody was performed to visualize GABAergic synapses. Synapses were loaded using a 70 mM KCl solution containing the luminal VGAT antibody, necessary to depolarize neurons and to trigger the recycling of synaptic vesicles, allowing the internalization of the antibody into synaptic vesicles (Figure 10.A). In Figure 10.B we can observe images of synapses expressing syGCaMP3 (green), images of synapses loaded with the luminal VGAT antibody (red) and merged images. Accordingly with immunolabeling of fixed cultures, no colocalization between syGCaMP3 and GABAergic synapses was detected. These results indicate that syGCaMP3 is an appropriate genetically encoded calcium indicator to study presynaptic calcium dynamics in glutamatergic synapses of hippocampal cultures.

In figure 11, we can observe typical presynaptic calcium signals from 15 synaptic spots expressing syGCaMP3 (Figure 11.B) obtained under application of the electrical field stimulation protocol at 20 Hz for 10 s where fluorescence elevations are concomitant with stimulus application. Fluorescence changes are represented as $\Delta F/F_0$, that is the difference between the fluorescence F and its fluorescence in resting conditions F_0,

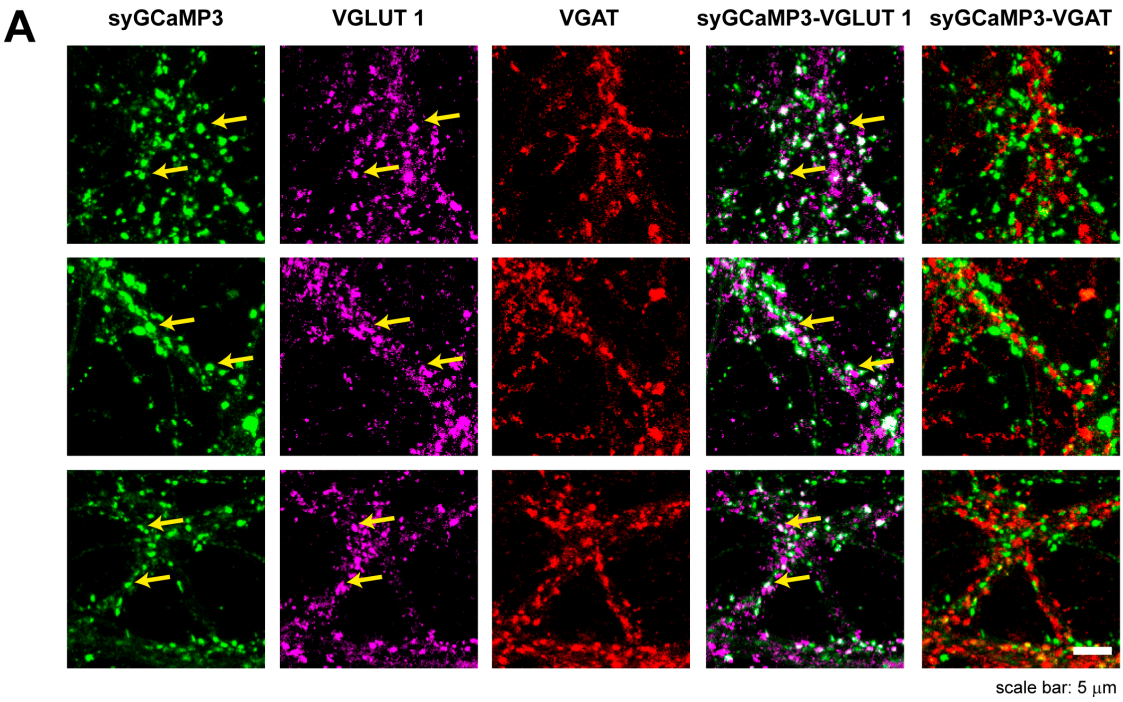
A
syGCaMP3
VGLUT 1
VGAT
syGCaMP3-VGLUT 1
syGCaMP3-VGAT
scale bar: 5 μm

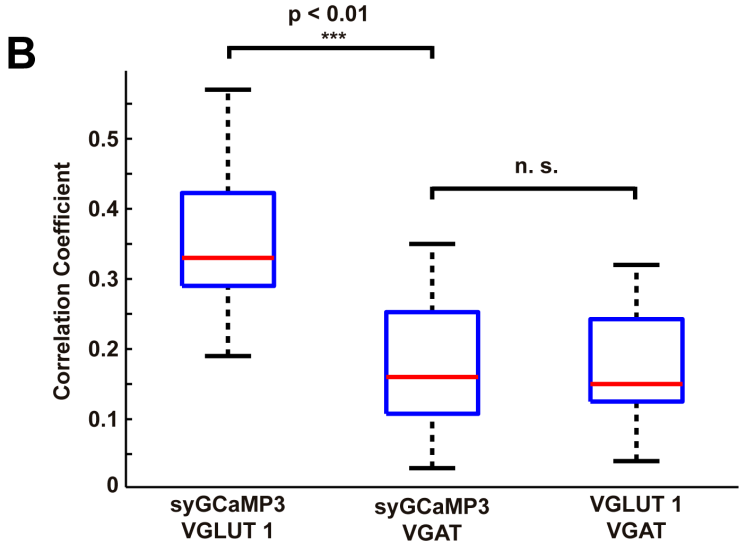
B
p < 0.01
***
n. s.
Correlation Coefficient
0
0.1
0.2
0.3
0.4
0.5
syGCaMP3
VGLUT 1
syGCaMP3
VGAT
VGLUT 1
VGAT

Figure 9: syGCaMP3 localized at glutamatergic but not at GABAergic synapses

A: Immunolabelings of hippocampal cultures expressing syGCaMP3 (green) against the vesicular glutamate transporter (VGLUT 1) and the vesicular GABA transporter (VGAT) show that synapses expressing syGCaMP3 colocalize with glutamatergic synapses (magenta) but, however, they do not colocalize with GABAergic synapses (red).

B: Measurement of colocalization between synapses expressing syGCaMP3 and synapses labeled with VGLUT 1 and VGAT antibodies using the Pearson's correlation coefficient. n=21 regions of size 25 µm x 25 µm from 3 different cultures were used for the quantification. Background subtractions were previously performed using the rolling ball method with a rolling ball radius of 3 pixels. Correlation coefficients between syGCaMP3 and VGLUT 1 images were higher than correlation coefficients between syGCaMP3 and VGAT images, indicating that syGCaMP3 localization fits better with glutamatergic patterns. No significant differences were found between syGCaMP3-VGAT and VGLUT 1-VGAT correlation coefficients. Statistical significance was calculated using the Student's t-test.

and divided by the fluorescence in resting conditions F_0: $\Delta F/F_0=(F-F_0)/F_0$, expressed in arbitrary units (a.u.). The experiments were carried out in the presence of the NMDA receptor antagonist APV (50 µM) and the AMPA receptor antagonist CNQX (25 µM) to inhibit the activity of the neuronal network by blocking excitatory transmission, in order to record presynaptic calcium signal produced exclusively by the intrinsic activity of individual neurons. These signals were recorded under three different conditions: before adding, in the presence and after washing the Na^+ channels blocker TTX (1 µM), demonstrating that under electrical field stimulation at 20 Hz for 10 s, presynaptic calcium transients of neurons expressing the presynaptic calcium indicator syGCaMP3 are driven by action potentials because they were inhibited during the application of TTX (1 µM) and recovered after TTX washing (Figure 11.A-B).

In this section we have described the experiments carried out to characterize the genetically encoded reporter syGCaMP3 in hippocampal cultures. Viral transduction of syGCaMP3 in hippocampal cultures represents an appropriate strategy to study the functional properties of the presynaptic glutamatergic calcium machinery using field electrical stimulation protocols.

4.2.2. Studying the role of CSP-α in the regulation of presynaptic calcium dynamics using syGCaMP3

Fluorescence changes associated to presynaptic calcium dynamics were recorded under electrical field stimulation at 20 Hz for 10 seconds (200 electrical pulses in total) to evoke action potentials. Figure 12 shows different grayscale images of wild type

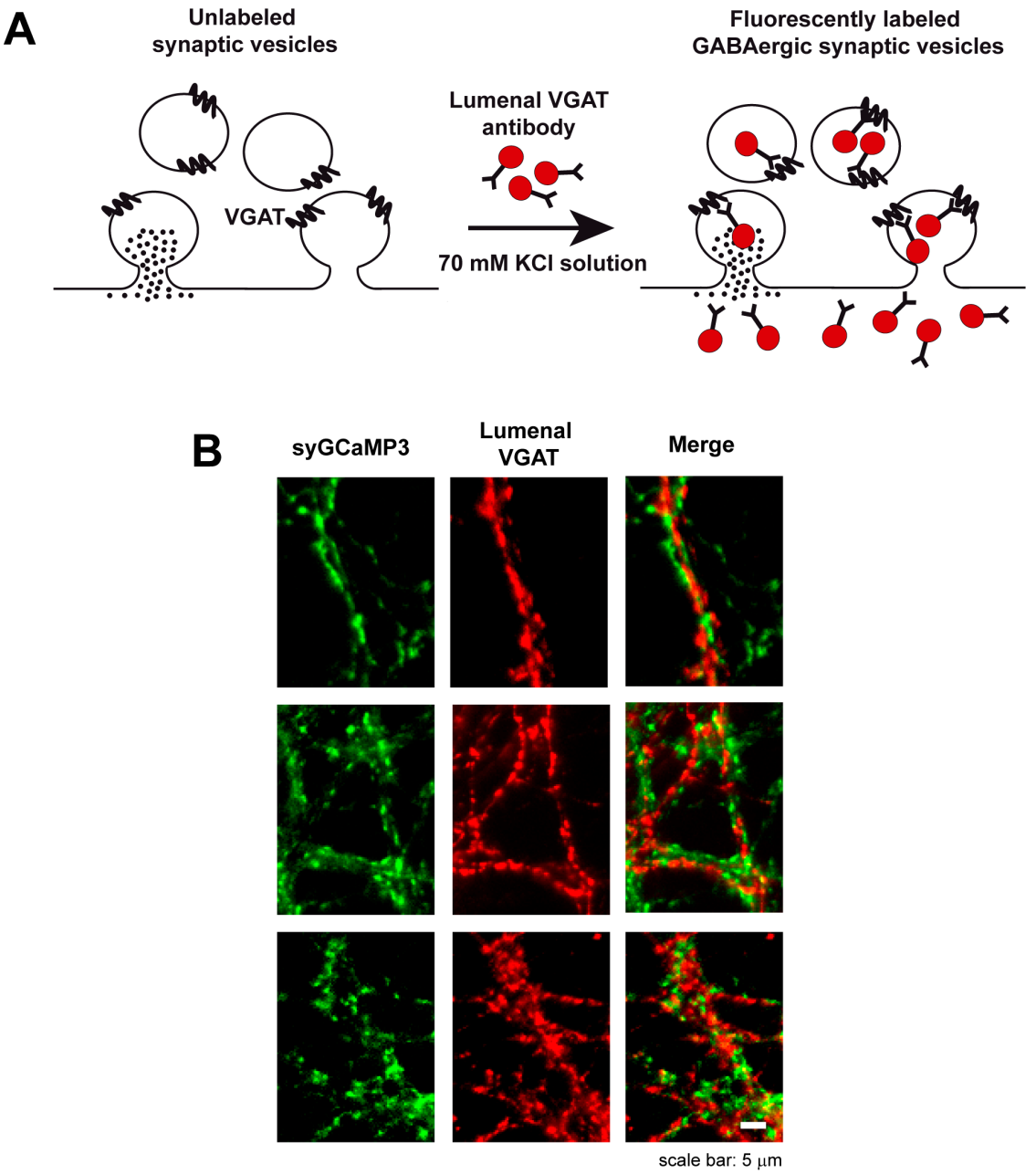
A
Unlabeled
synaptic vesicles
VGAT
Lumenal VGAT
antibody
70 mM KCl solution
Fluorescently labeled
GABAergic synaptic vesicles
B
syGCaMP3
Lumenal
VGAT
Merge
scale bar: 5 μm

Figure 10: Monitoring the recycling of GABAergic synaptic vesicles with an antibody against the luminal region of vesicular GABA transporter VGAT reveals low colocalization between synapses expressing syGCaMP3 and GABAergic synapses

A: Model explaining the protocol to load the luminal antibody VGAT into synaptic vesicles. Hippocampal cultures were incubated with an external solution containing 70 mM of KCl for 5 minutes to depolarize the neurons, increasing the activity of hippocampal neurons and the recycling of synaptic vesicles to internalize the antibody. This external solution also contained the luminal VGAT antibody fluorescence-labeled with Oyster 550 (2-5 µg/ml). After loading, neurons were washed with physiological external solution.

B: Images showing synapses expressing syGCaMP3 (green) and synapses loaded with the luminal VGAT antibody (red). Merged images show low colocalization between synapses expressing syGCaMP3 and GABAergic synapses.

Experiments were performed in the presence of the NMDA receptor antagonist APV (50 µM) and the AMPA receptor antagonist CNQX (25 µM) at 17-20 DIV from three different cultures (n=5 experiments).

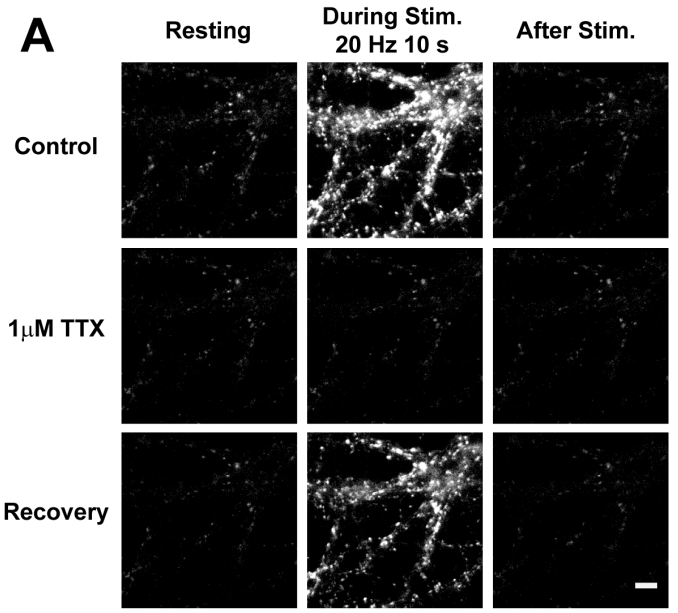
A
Resting
During Stim.
20 Hz 10 s
After Stim.
Control
1μM TTX
Recovery
scale bar: 10 μm

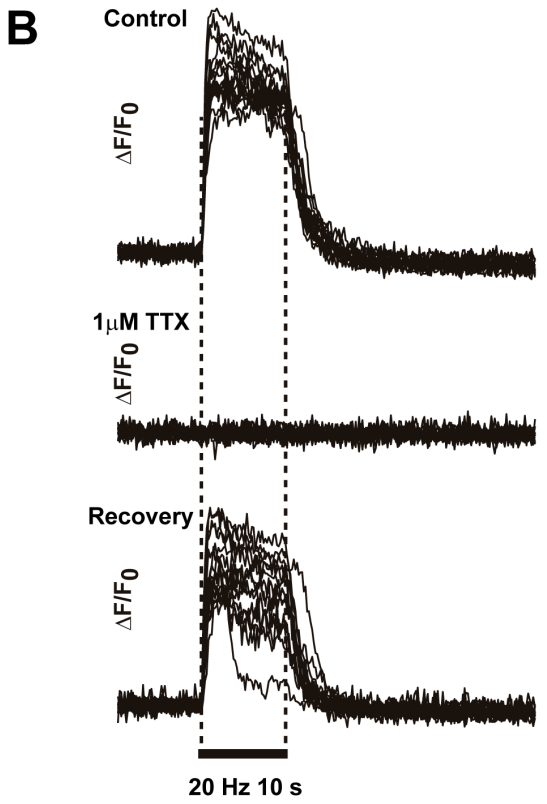
B
Control
ΔF/F0
1μM TTX
ΔF/F0
Recovery
ΔF/F0
20 Hz 10 s

Figure 11: Action potentials drive presynaptic calcium signals uncovered by syGCaMP3 fluorescence changes

A: Images showing that hippocampal synapses expressing syGCaMP3 do not show fluorescence changes in the presence of the Na^+ channel blocker TTX (1 μM) under electrical field stimulation (20 Hz 10 s). After washing of TTX synapses recover fluorescence emission.

B: Examples of presynaptic calcium fluorescence signals of 15 synaptic spots under electrical field stimulation (20 Hz 10 s): 1st train of stimulus was applied without TTX application (control), 2nd train of stimulus was applied in the presence of TTX and the 3rd train of stimulus was applied after washing of TTX (recovery).

All experiments were done in the presence of the NMDA receptor antagonist APV (50 μM) and the AMPA receptor antagonist CNQX (25 μM).

and CSP-α KO hippocampal synapses expressing syGCaMP3, where white pixels indicate high expression and black pixels low expression. A pseudocolour line scan of the fluorescence changes, represented as $\Delta F/F_{0,}$ along a selected line (in red) and the time course of fluorescence changes at the regions of interest (ROIs) indicated by yellow rectangles are also shown.

In figure 12.A, 2D and 3D view of one control synaptic spot and one mutant synaptic spot are also shown. White rectangles indicate the region of interest used for quantification of fluorescence changes of each synaptic spot (1.66 μm^2).

Attending to the duration of calcium transients, different types of responses were observed: long duration responses (LDRs), characterized by a persistent elevation of calcium levels concomitant with the stimulus application, and short duration responses (SDRs), characterized by a transient elevation of calcium levels of similar amplitude to LDRs but, however, shorter duration followed by a shoulder of lower amplitude persisting during the stimulation train (Figure 12.A). Both types of responses were found in wild type and CSP-α KO hippocampal cultures. Furthermore, another type of responses characterized by a non persistent elevations, showing more than one calcium transients during the duration of the stimulus were recorded in wild type and CSP-α KO hippocampal cultures (Figure 12.B). These responses have been called intermediate responses (IRs).

Mean time course of fluorescence changes of synaptic spots comparing wild type and CSP-α KO hippocampal cultures are shown in figure 13.A for LDRs and in figure 13.B for SDRs. The fluorescence peaks of these signals showed approximately a 2.5-fold changes during stimulation, accordingly with previous description within the dynamic range of the indicator (Li et al., 2011). For LDRs, n=22 experiments for CSP-α WT

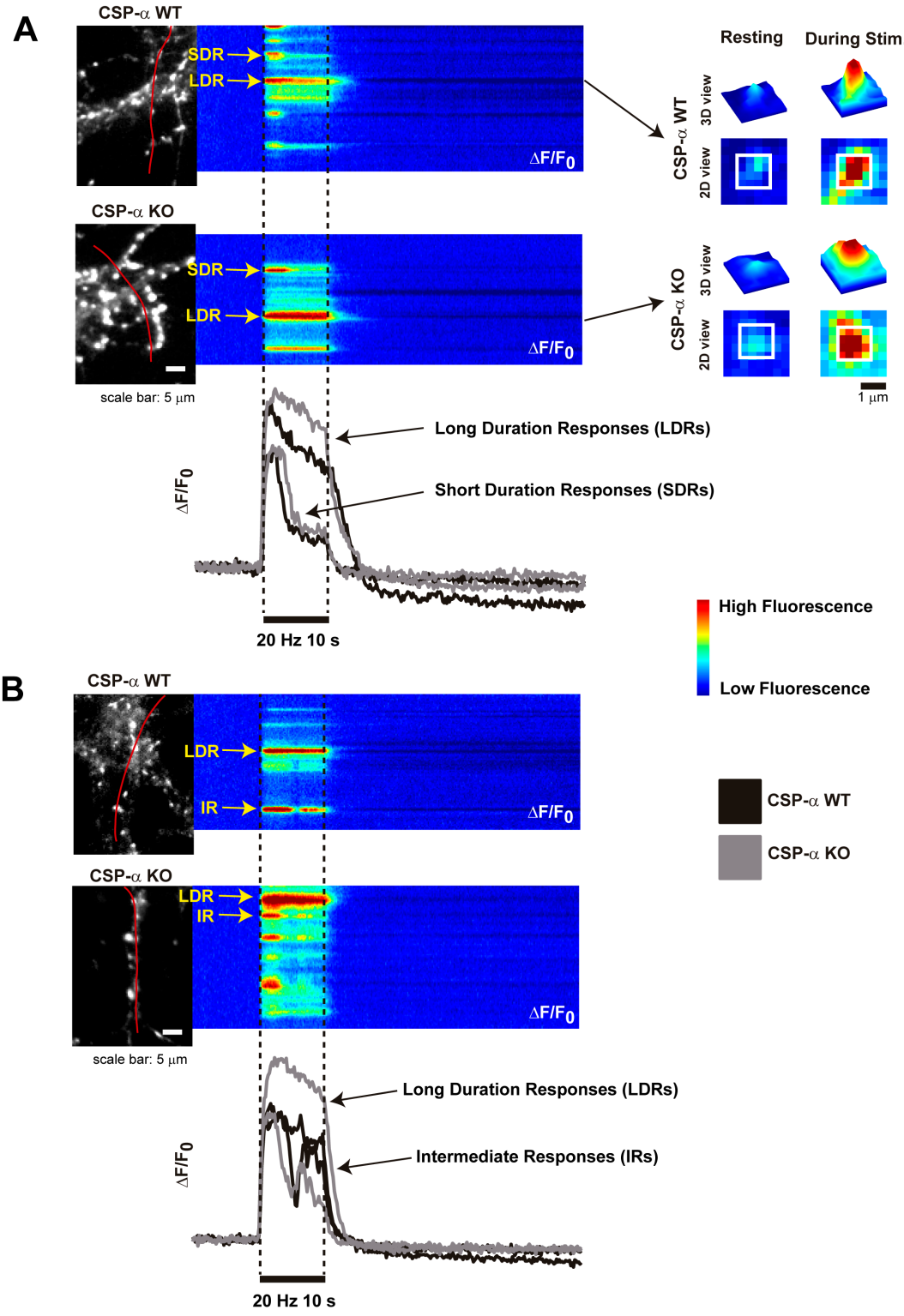
A
CSP-α WT
SDR
LDR
ΔF/F0
Resting
During Stim.
CSP-α WT
3D view
2D view
CSP-α KO
3D view
2D view
1 μm
CSP-α KO
SDR
LDR
ΔF/F0
scale bar: 5 μm
Long Duration Responses (LDRs)
Short Duration Responses (SDRs)
ΔF/F0
20 Hz 10 s
High Fluorescence
Low Fluorescence
B
CSP-α WT
LDR
IR
ΔF/F0
CSP-α KO
LDR
IR
ΔF/F0
scale bar: 5 μm
CSP-α WT
CSP-α KO
Long Duration Responses (LDRs)
Intermediate Responses (IRs)
ΔF/F0
20 Hz 10 s

hippocampal cultures and n=18 for CSP-α KO. For SDRs, n=11 experiments for CSP-α WT hippocampal cultures and n=8 for CSP-α KO. Data is shown as $\Delta F/F_0 \pm$ sem. Also, normalized histogram and cumulative distribution showing the amplitudes ($\Delta F/F_0$) of LDRs responses, n=4342 synaptic spots from 22 experiments for CSP-α WT hippocampal cultures and n=2788 synaptic spots from 18 experiments for CSP-α KO are shown (Figure 13.C). Histogram and cumulative distribution of amplitudes ($\Delta F/F_0$) of SDRs are shown in figure 13.D, n=282 synaptic spots from 11 experiments for CSP-α WT hippocampal cultures and n=176 synaptic spots from 8 experiments for CSP-α KO. These values are represented as a whisker and box plot in figure 13.E. Amplitudes shown as 1st quartile: 2nd quartile: 3rd quartile were 2.23:2.78:3.34 for wild type LDRs, 2.06:2.58:3.17 for CSP-α KO LDRs, 2.11:2.65:3.17 for wild type SDRs and 1.97:2.36:2.80 for CSP-α KO SDRs. No significant differences were observed between amplitudes of wild type and CSP-α KO.

Normalized histogram and cumulative distribution showing the half width of calcium transients of wild type and CSP-α KO LDRs and SDRs are shown in figure 13.F. For LDRs, n=4342 synaptic spots from 22 experiments for CSP-α WT hippocampal cultures and n=2788 synaptic spots from 18 experiments for CSP-α KO. For SDRs, n=282 synaptic spots from 11 experiments for CSP-α WT hippocampal cultures and n=176 synaptic spots from 8 experiments for CSP-α KO. These values are represented as a whisker and box plot in figure 13.G. Half widths shown as 1st quartile: 2nd quartile: 3rd quartile were 10:10.2:10.6 s for wild type LDRs, 9.8:10:10.4 s for CSP-α KO LDRs, 3:3.6:4.6 for wild type SDRs and 2.4:3:3.8 s for CSP-α KO SDRs. No significant

Figure 12: Kinetically different presynaptic calcium signals uncovered with syGCaMP3 in wild type and CSP-α KO

Fluorescence changes of synapses expressing syGCaMP3 when a field electrical stimulation at 20 Hz for 10 seconds is applied to wild type and CSP-α KO hippocampal cultures. A pseudocolour line scan of the fluorescence changes along a selected line (in red) and the time course of fluorescence changes of synaptic spots indicated by yellow arrows are shown.

A: Synaptic spots showing long duration responses (LDRs) and short duration responses (SDRs) in CSP-α KO and wild type synapses. 2D and 3D view of synaptic spots indicated by the black arrows are also shown. White rectangles indicate the region of interest to isolate synaptic spots.

B: Synaptic spots showing long duration responses (LDRs) and intermediate responses (IRs) in CSP-α KO and wild type synapses.

Experiments were done in the presence of the NMDA receptor antagonist APV (50 µM) and the AMPA receptor antagonist CNQX (25 µM).

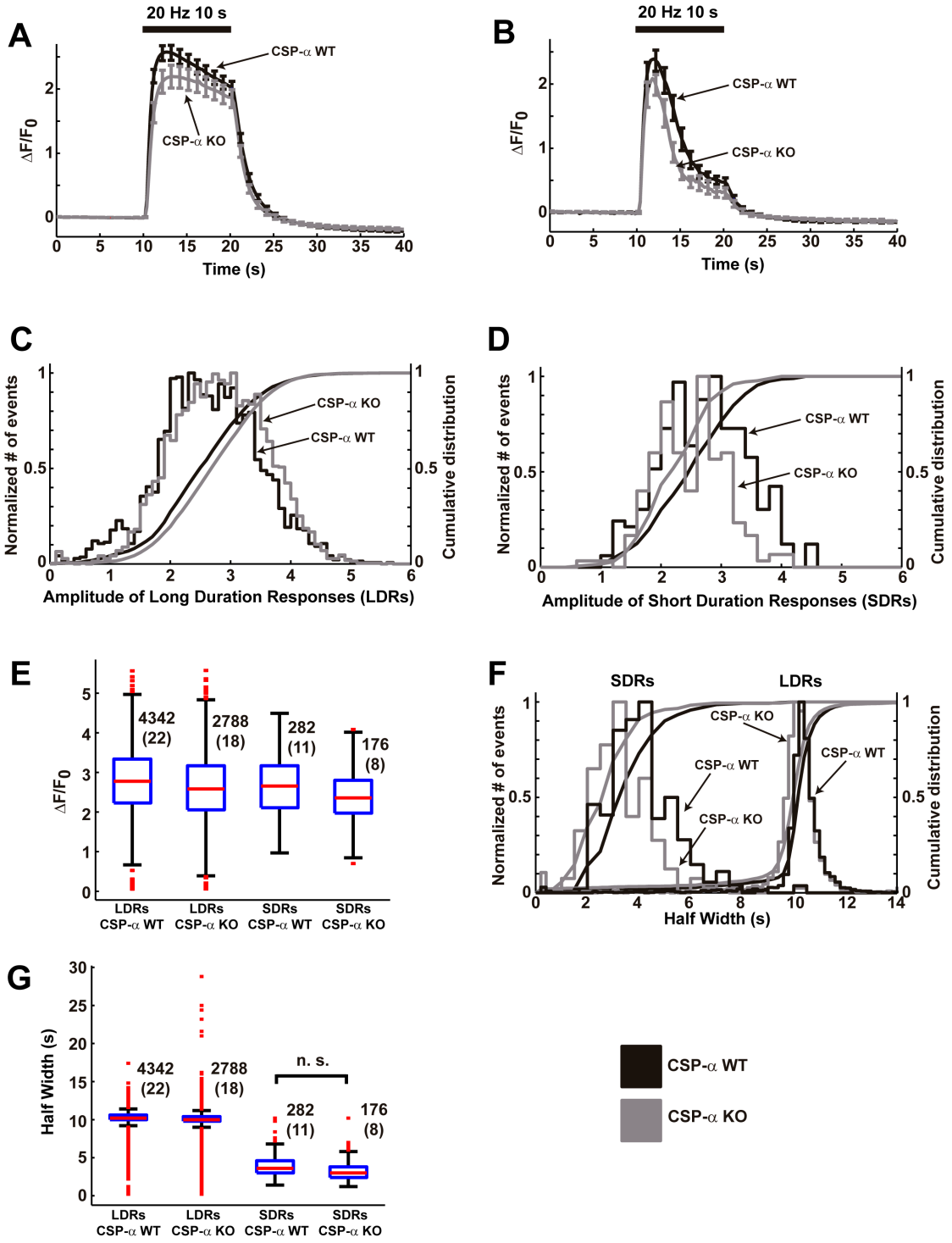
A
20 Hz 10 s
CSP-α WT
CSP-α KO
ΔF/F0
Time (s)
B
20 Hz 10 s
CSP-α WT
CSP-α KO
ΔF/F0
Time (s)
C
Normalized # of events
Cumulative distribution
CSP-α KO
CSP-α WT
Amplitude of Long Duration Responses (LDRs)
D
Normalized # of events
Cumulative distribution
CSP-α WT
CSP-α KO
Amplitude of Short Duration Responses (SDRs)
E
ΔF/F0
4342 (22)
2788 (18)
282 (11)
176 (8)
LDRs CSP-α WT
LDRs CSP-α KO
SDRs CSP-α WT
SDRs CSP-α KO
F
SDRs
LDRs
Normalized # of events
Cumulative distribution
CSP-α KO
CSP-α WT
CSP-α KO
CSP-α WT
Half Width (s)
G
Half Width (s)
4342 (22)
2788 (18)
n. s.
282 (11)
176 (8)
LDRs CSP-α WT
LDRs CSP-α KO
SDRs CSP-α WT
SDRs CSP-α KO
CSP-α WT
CSP-α KO

Figure 13: Evoked presynaptic calcium signals uncovered with syGCaMP3 are similar in hippocampal cultures from mice lacking CSP-α and wild type littermates

A: Mean time course of long duration responses (LDRs) of wild type and CSP-α KO synapses expressing syGCaMP3. n=22 experiments for CSP-α WT hippocampal cultures and n=18 for CSP-α KO. Data is shown as $\Delta F/F_0 \pm$ sem.

B: Mean time course of short duration responses (SDRs) of wild type and CSP-α KO synapses expressing syGCaMP3. n=11 experiments for CSP-α WT hippocampal cultures and n=8 for CSP-α KO. Data is shown as $\Delta F/F_0 \pm$ sem.

C: Normalized histogram and cumulative distribution showing the amplitudes ($\Delta F/F_0$) of LDRs responses. n=22 experiments and 4342 synaptic spots for CSP-α WT and n=18 experiments and 2788 synaptic spots for CSP-α KO.

D: Normalized histogram and cumulative distribution showing the amplitudes ($\Delta F/F_0$) of SDRs responses. n=11 experiments and 282 synaptic spots for CSP-α WT and n=8 experiments and 176 synaptic spots for CSP-α KO.

E: Box plot of data shown in C and D.

F: Normalized histogram and cumulative distribution showing the half width of LDRs and SDRs responses.

G: Box plot of data shown in F.

Experiments were performed in the presence of the NMDA receptor antagonist APV (50 μM) and the AMPA receptor antagonist CNQX (25 μM) at 15-23 DIV from at least three different cultures.

differences were observed between half width of wild type and CSP-α KO calcium transients for LDRs and SDRs.

We have seen that fluorescence signals associated to presynaptic calcium dynamics comes back to resting levels after finishing the application of the electrical stimulus. However, in figure 14 we report that some synaptic spots show spontaneous calcium elevations after stimulus application. A pseudocolour line scan representations ($\Delta F/F_0$) of the fluorescence changes of the total synaptic spots showing spontaneous calcium activity are shown in figure 14.A from wild type and CSP-α KO hippocampal cultures, since its time courses. A total of n=45 synaptic spots from 21 CSP-α WT imaging experiments, representing approximately 1 % of the total wild type synaptic spots analyzed previously and n=145 synaptic spots from 17 CSP-α KO imaging experiments, representing approximately 4 % of the total mutant synaptic spots analyzed previously, were found (Figure 14.A). The number of synaptic spots with spontaneous calcium activity after stimulus application is shown for each experiment in figure 14.B where bars represent the mean value. For these data, statistical significance was detected between wild type and CSP-α KO synapses ($p<0.05$) using the Mann-Whitney U test.

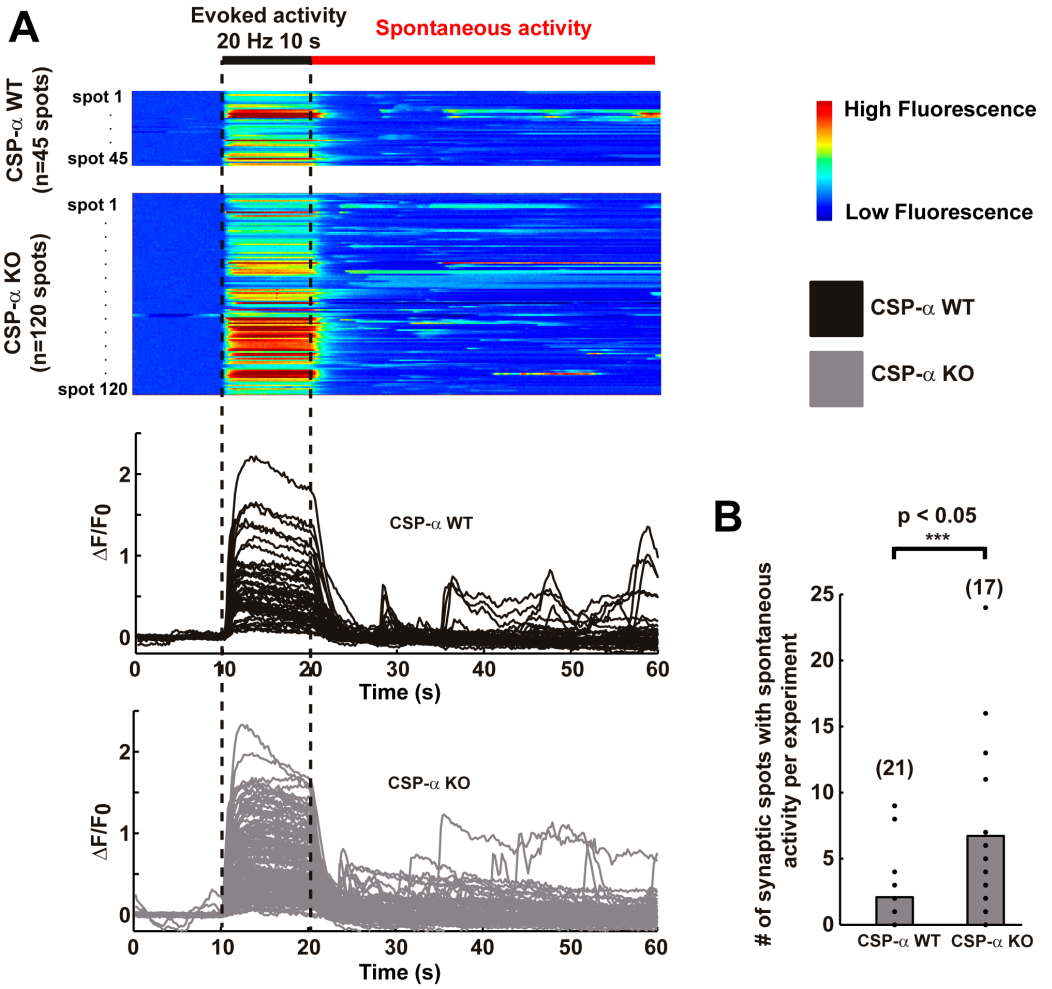

Figure 14: CSP-α KO synapses show higher number of synaptic spots with spontaneous presynaptic calcium signals than wild type synapses

A: Total fluorescence signals of synapses expressing syGCaMP3 showing spontaneous activity. A pseudocolour line scan and the time course of fluorescence signal of each synaptic spot are shown. In n=21 experiments of CSP-α WT hippocampal cultures a total of 45 synaptic spots showed spontaneous activity that represent approximately 1 % of the total synaptic spots analyzed. In n=17 experiments of CSP-α KO hippocampal cultures a total of 120 synaptic spots showed spontaneous activity that represent approximately 4 % of the total synaptic spots analyzed.

B: Bars representing the number of synaptic spots with spontaneous activity per experiment and its mean value. n=21 experiments for CSP-α WT and n=17 experiments for CSP-α KO. Statistical significance was calculated using the Mann-Whitney U test.

Experiments were performed in the presence of the NMDA receptor antagonist APV (50 µM) and the AMPA receptor antagonist CNQX (25 µM) at 15-23 DIV from at least three different cultures.

4.2.3. Studying the presynaptic depression mechanism underlying short duration responses (SDRs)

Our previous results show no significant differences in the amplitude and the duration of presynaptic calcium transients between wild type and CSP-α KO synapses but a new question arise from these results regarding SDRs: what is the underlying mechanism behind this kind of presynaptic depression?

As LDRs and SDRs might represent different types of synapses, we wanted to know the distribution of both kind of synapses and whether they follow a specific pattern of localization. Activity correlation imaging is an excellent method to get structural information of a neural network from functional information of neurons (Junek et al., 2009). Here, we applied this idea to get structural information of LDR and SDR synapses from their patterns of activity. In order to find the localization of synapses with a specific pattern of activity, correlation coefficient between the time course of a selected reference signal, SDR or LDR, and each pixel's time trace of a region of interest was calculated to obtain the synaptic activity correlation map. This map represents the value of the correlation coefficient between each pixel and the reference signal giving us the level of similarity between both signals. Blue represents low similarity and red represents high similarity. After applying a threshold, a binary map highlights pixels with correlation coefficient over this threshold, indicating the distribution pattern of synapses with SDRs or LDRs (Figure 15.A). After overlapping both pattern of activity, SDRs and LDRs, we can observe the localization of both types of responses separated by different colors, LDR synapses in red and SDR synapses in blue. In figure 15.B we show several examples of LDRs and SDRs patterns of localization for wild type and CSP-α KO hippocampal cultures. We can observe that spatial distributions of LDRs are absolutely irregular, but however, distributions of SDRs suggest a linear organization comparable to synapses along axons (Figure 15.B). These results might suggest that the reason of presynaptic depression of SDRs is not an intrinsic mechanism of individual synapses, but a general mechanism of depression of entire neurons or even a mechanism working along complete axons related with the firing patterns of neurons where somehow, action potentials could fail to sustain electrical field stimulus. Patterns of activity at presynaptic terminals might vary thus changing the calcium dynamics at presynaptic terminals. To know whether synaptic strength, manifested as LDRs or SDRs, is maintained in time, the experimental protocol indicated in the figure 16.A was followed. After the application of a first train of electrical stimulus at 20 Hz for 10 seconds, passed 10 min a subsequent train stimulus was applied at the same frequency and duration. In the

scatter plot of figure 16.B we can observe the half width durations of synaptic spots during two consecutive electrical train stimuli separated 10 minutes in time (n=1200 synaptic spots from six different experiments). Comparing durations between first and second trains, most of synaptic spots show LDRs with permanent duration but however, a small population of synaptic spots with SDRs becomes in LDRs and also another small population of LDRs becomes in SDRs. In figure 16.B, red line indicates synaptic spots with similar half width. Changes in presynaptic calcium dynamics are consistent with changes in the firing patterns of neurons that modulate presynaptic strength in time. Furthermore, in figure 16.C we can observe the amplitudes of synaptic spots during two consecutive electrical stimuli. Points under red line represent depressed synapses and points over red line represent potentiated synapses (n=1200 synaptic spots from six different experiments). We can observe that most of synapses are found under the red line.

To check whether the presynaptic depression mechanism underlying to SDRs occurs beyond the synapses, that is, it is produced by a general mechanism affecting the whole neuron, we performed experiments with the soluble calcium indicator GCaMP3 using the same protocol of stimulation at 20 Hz for 10 seconds. In figure 17.A we can observe that calcium transients of neurons expressing GCaMP3 are driven by action potentials because calcium signals uncovered with this reporter were inhibited using the Na^+ channels blocker TTX (1 μM). Figure 17.B shows the image of a pair of neurites of wild type hippocampal neurons expressing GCaMP3 and its pseudocolor line scan representing fluorescence changes along time. We observe that long duration responses (LDRs) and even short duration responses (SDRs) occur along complete

Figure 15: Separation of synaptic activity patterns using imaging correlation analysis. Distribution patterns of SDRs are comparable to synapses along axons

A: Synaptic activity correlation analysis was performed to separate patterns of synaptic activity of neurons infected with syGCaMP3 using custom ImageJ plug-in written in Java. In order to look for a specific pattern of activity in the area of interest, correlation coefficient between the time course of a selected reference signal, SDR or LDR, and each pixel's time trace was calculated to obtain the synaptic activity correlation map. After applying a threshold, a binary map highlights pixels with correlation coefficient over this threshold, indicating high similarity. In contrast, traces with correlation coefficient under the threshold appear white in this map, indicating low similarity.

B: Three different examples showing distribution patterns of SDRs and LDRs for CSP-α WT and CSP-α KO hippocampal cultures.

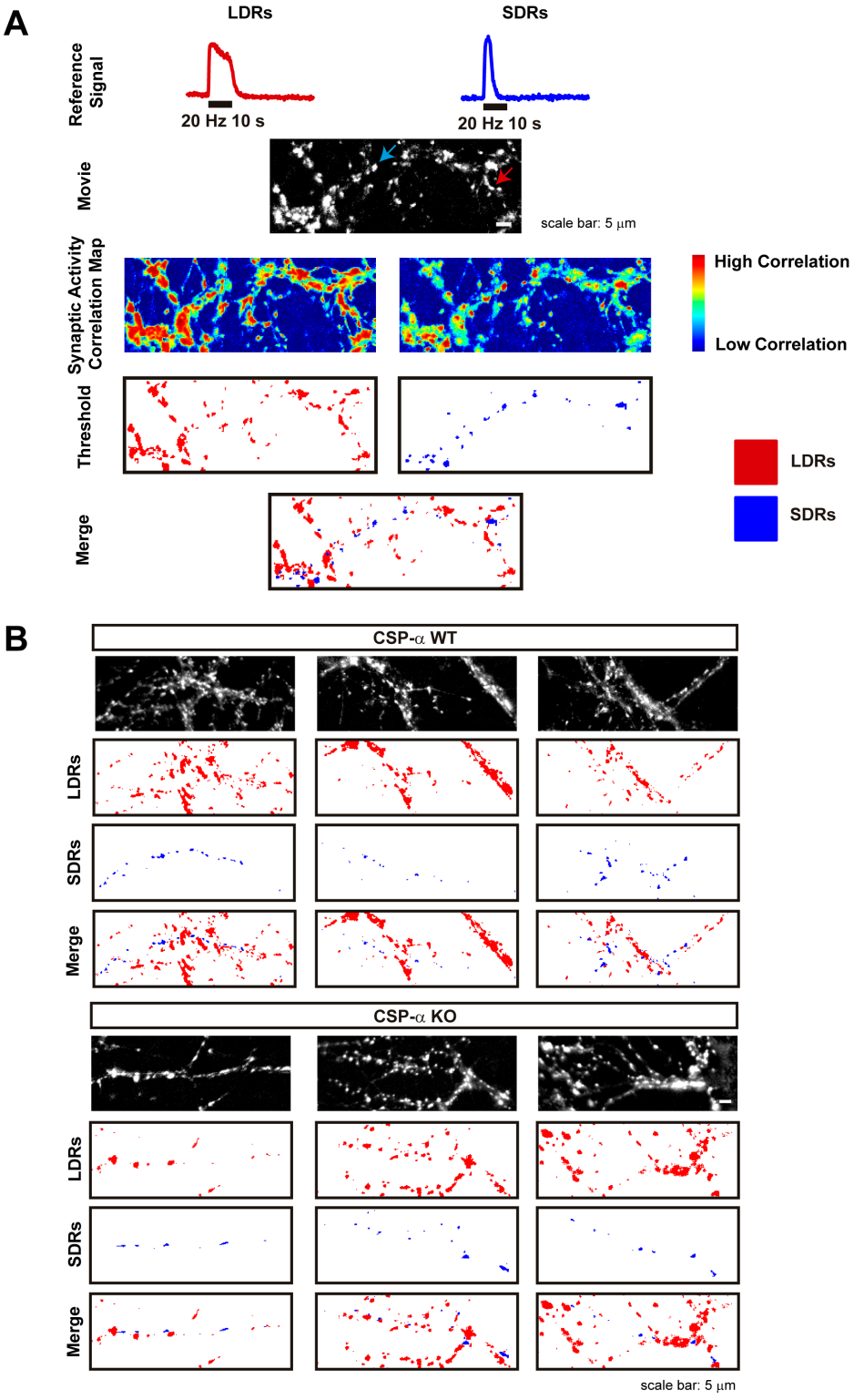
A
LDRs
SDRs
Reference Signal
20 Hz 10 s
20 Hz 10 s
Movie
scale bar: 5 μm
Synaptic Activity Correlation Map
High Correlation
Low Correlation
Threshold
LDRs
SDRs
Merge
B
CSP-α WT
LDRs
SDRs
Merge
CSP-α KO
LDRs
SDRs
Merge
scale bar: 5 μm

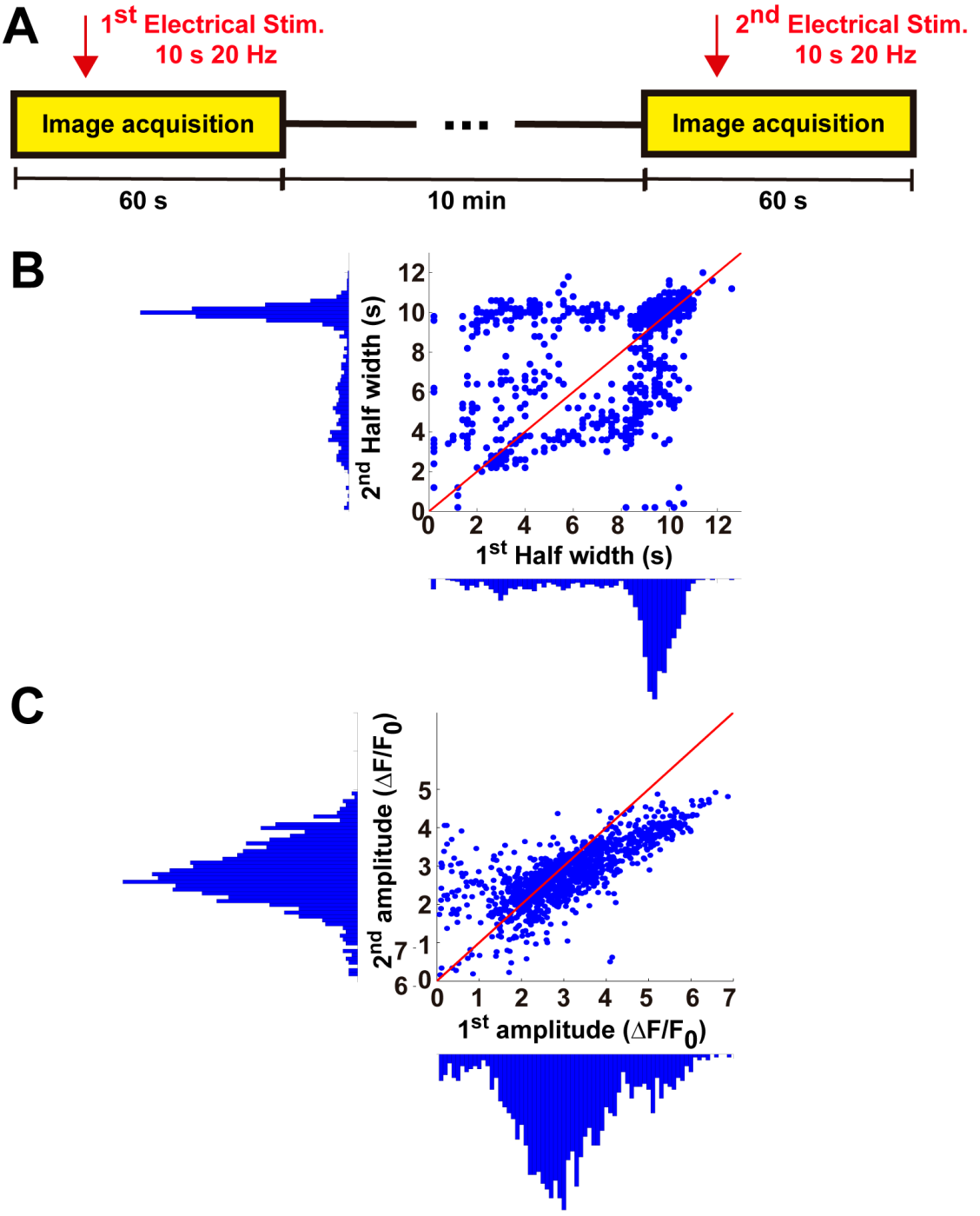
A
1st Electrical Stim.
10 s 20 Hz
2nd Electrical Stim.
10 s 20 Hz
Image acquisition
Image acquisition
60 s
10 min
60 s
B
2nd Half width (s)
1st Half width (s)
C
2nd amplitude (ΔF/F0)
1st amplitude (ΔF/F0)

Figure 16: Presynaptic calcium kinetics under application of a subsequent stimulation train using syGCaMP3

A: Protocol followed. After application the first train of electrical stimulus at 20 Hz for 10 seconds, passed 10 min a subsequent train stimulus was applied at the same frequency and duration.

B: Scatter plot and histograms showing half widths during the first and the subsequent recording. Red line indicates the values where first half-width is equal to the second (n=1200 synaptic spots from six different experiments).

C: Scatter plot and histograms showing amplitudes during the first and the subsequent recording. Red line indicates the values where first amplitude is equal to the second (n=1200 synaptic spots from six different experiments).

Experiments were performed in the presence of the NMDA receptor antagonist APV (50 μM) and the AMPA receptor antagonist CNQX (25 μM) at 15-16 DIV.

neurites (Figure 17.B). Whisker and box plot representing the half width of fluorescence signals in neurites with LDRs and SDRs are shown in figure 16.C, 9:9.6:10 s for LDRs and 2.65:3.6:4.55 s for SDRs (1st quartile: 2nd quartile: 3rd quartile), n=38 neurites for LDRs (38 experiments from 12 different coverslips) and n=11 neurites for SDRs (11 experiments from 6 different coverslips). These results support the idea that presynaptic depression uncovered with the presynaptic reporter syGCaMP3 is probably produced by a general mechanism affecting the whole neuron and this mechanism could be related with the firing patterns of neurons.

In addition to both different neurites responses found, calcium waves were uncovered in neurons expressing the soluble calcium reporter GCaMP3 under electrical field stimulation at 20 Hz for 10 s, n=7 neurons showing calcium waves of a total number of 56 neurons (Figure 18). In neurons in which calcium waves appear, calcium transients start at synaptic contacts (red signal) when electrical stimulation begins and propagate from the dendrites to the soma (green signal). Calcium waves are produced by a mechanism where elevated cytoplasmatic calcium induces further calcium releases from endoplasmic reticulum through a nonlinear cooperative process that involved either reticular IP_3 receptors (IP_3Rs) or reticular Ryanodine receptors (RyRs) (Ross, 2012).

On the other hand, voltage gated calcium channels (VGCCs) play an important role in presynaptic plasticity and metabotropic $GABA_B$ receptors at presynaptic terminals activated by the chemical messenger GABA can inhibit VGCCs (Gassmann and Bettler, 2012) (Figure 19.A). To investigate whether SDRs are mediated by inhibition of VGCCs through $GABA_B$ receptors, we incubated hippocampal cultures expressing syGCaMP3 with the $GABA_B$ receptor antagonist CGP-55845 (1 μM). If this hypothesis was correct,

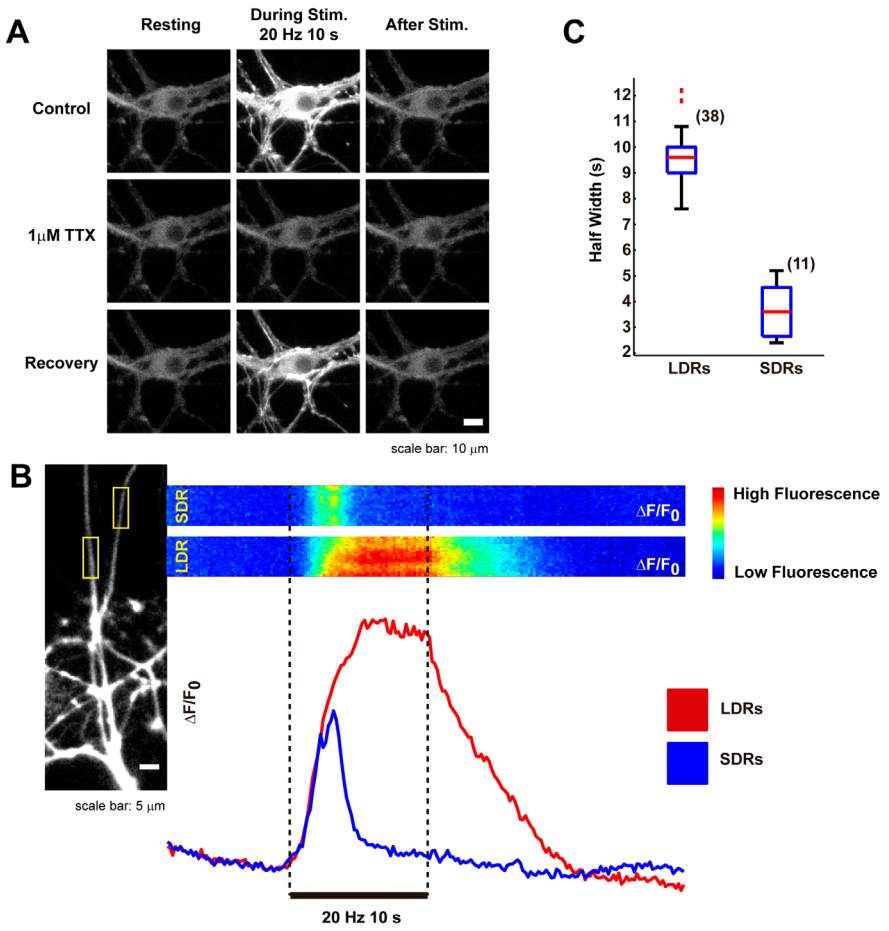

Figure 17: Imaging of neuronal cytosolic calcium signals using GCaMP3 shows neurites with long duration responses (LDRs) and short duration responses (SDRs)

A: Hippocampal neurons expressing GCaMP3 do not show fluorescence changes in the presence of the Na^+ channel blocker TTX (1 µM) under electrical stimulation (20 Hz for 10 s) indicating that calcium signals are driven by action potentials. After TTX washing neurons recover fluorescence emission. (n=3 experiments).

B: Fluorescence changes of neurites expressing GCaMP3 when a field electrical stimulation (20 Hz for 10 s) was applied to wild type hippocampal cultures. A pseudocolour line scan of the fluorescence changes along two different neurites (yellow rectangles) with LDR and SDR are shown including its time courses.

C: Box plot representing the half width of fluorescence signals in neurites with LDRs and SDRs. n=38 axons for LDRs (38 experiments from 12 different coverslips) and n=11 neurites for SDRs (11 experiments from 6 different coverslips) from three different cultures.

Experiments were performed in the presence of the NMDA receptor antagonist APV (50 µM) and the AMPA receptor antagonist CNQX (25 µM) at 15-20 DIV.

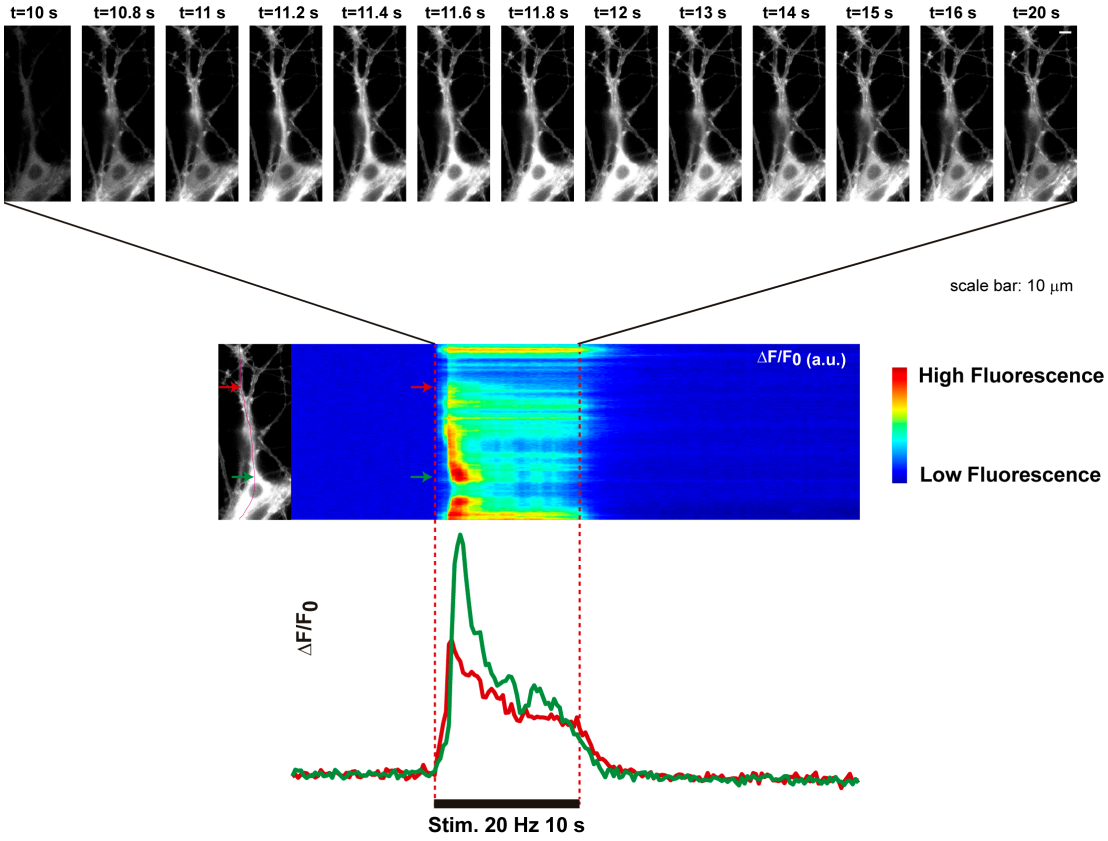

Figure 18: Imaging of neuronal cytosolic calcium signals using GCaMP3 uncovers neuronal calcium waves under sustained electrical field stimulation

Hippocampal neurons expressing GCaMP3 show neuronal calcium waves. n=7 of 56 neurons show calcium waves (41 experiments from 13 coverslips). Red arrow indicates the place where the calcium wave initiates at dendrite (red signal) and green arrow indicates the place where the calcium wave ends, the soma of the neuron (green signal).

Experiments were done in the presence of the NMDA receptor antagonist APV (50 µM) and the AMPA receptor antagonist CNQX (25 µM) at 15-20 DIV from three different cultures.

blockage of $GABA_B$ receptors should abolish SDRs but however, we uncovered SDRs in the presence of the $GABA_B$ receptor antagonist CGP-55845 (Figure 19.B), indicating that SDRs are not mediated by presynaptic metabotropic $GABA_B$ receptors and supporting the non synaptic hypothesis for SDRs mechanism. Half widths quantifications of presynaptic calcium transients were 10.4:10.6:11 s for LDRs and 2.8:4.6:5.2 s for SDRs (shown as 1st quartile: 2nd quartile: 3rd quartile), n=89 synaptic spots from 6 different experiments for SDRs and n=568 synaptic spots from 6 different experiments for LDRs (Figure 19.C).

These results suggest that the most probable mechanism of presynaptic depression underlying to SDRs are produced by action potential failures, but however we cannot rule out the possibility that intrinsic presynaptic mechanisms such as calcium channels inactivation or even a mechanism involving intracellular calcium channels of the endoplasmic reticulum could be participating in the presynaptic depression underlying SDRs.

Figure 19: Blocking of $GABA_B$ receptors using CGP-55845 antagonist shows that SDRs are not mediated by presynaptic metabotropic $GABA_B$ receptors

A: Picture showing that metabotropic $GABA_B$ receptors at presynaptic terminals activated by the chemical messenger GABA can inhibit presynaptic VGCCs.

B: Fluorescence changes of synapses expressing syGCaMP3 when a field electrical stimulation at 20 Hz for 10 s is applied to wild type hippocampal cultures in the presence of CGP-55845. A pseudocolour line scan of the fluorescence changes along a selected line (in red) shows the time course of two synaptic spots (one with LDR and one with SDR).

C: Box plot showing the half widths of LDRs (n=568 synaptic spots from 6 different experiments) and SDRs (n=89 synaptic spots from 6 different experiments) of wild type hippocampal cultures incubated with CGP-55845 (1 μM).

Experiments were done in the presence of the NMDA receptor antagonist APV (50 μM) and the AMPA receptor antagonist CNQX (25 μM).

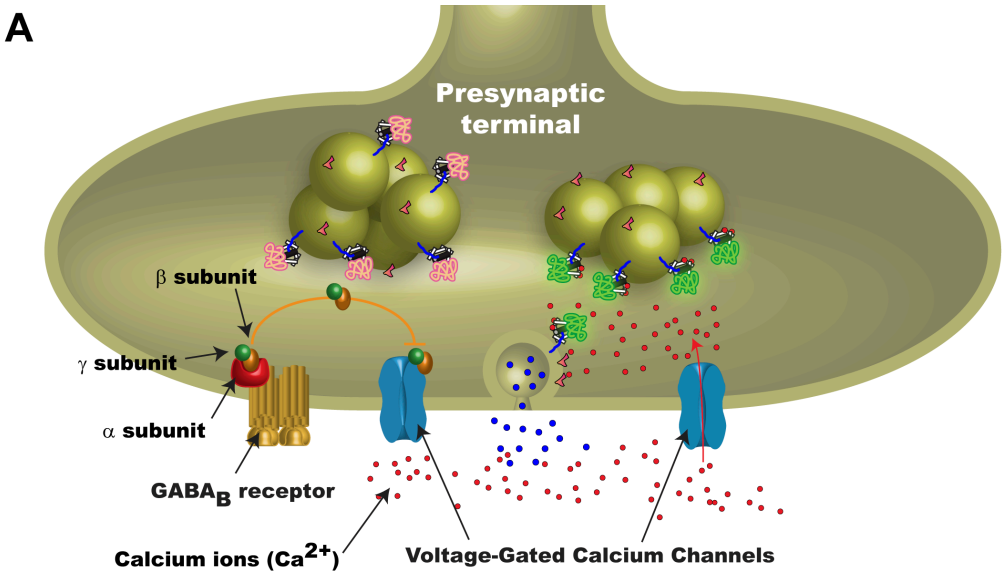
A
Presynaptic terminal
β subunit
γ subunit
α subunit
GABA$_B$ receptor
Calcium ions (Ca^{2+})
Voltage-Gated Calcium Channels

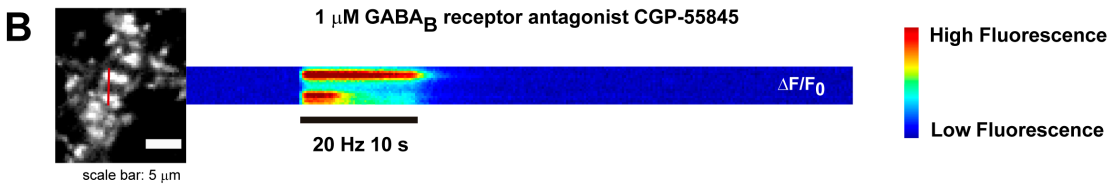
B
1 μM GABA$_B$ receptor antagonist CGP-55845
ΔF/F$_0$
20 Hz 10 s
scale bar: 5 μm
High Fluorescence
Low Fluorescence

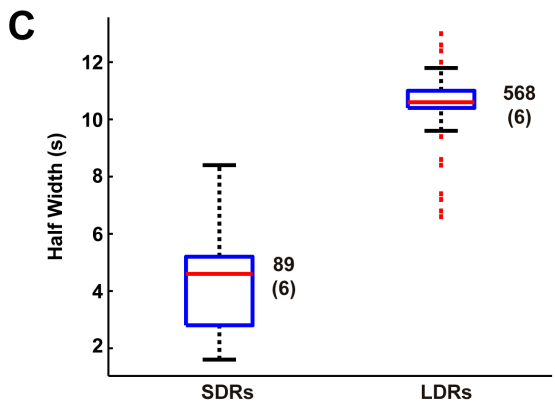
C
Half Width (s)
12
10
8
6
4
2
89
(6)
568
(6)
SDRs
LDRs

4.3. Exploring the excitability of hippocampal circuits lacking CSP-α

Most of studies of CSP-α have been carried out at the synapses but little is known about the functional role of CSP-α beyond the presynaptic terminal, in the context of neural networks. As we have seen in the introduction, fast spiking PV positive GABAergic interneurons are extremely sensitive to the absence of CSP-α and they degenerate in the hippocampus of mice lacking CSP-α but in contrast, glutamatergic synapses do not show obvious sign of neurodegeneration. Our objective is to figure out whether this excitatory/inhibitory imbalance might contribute to the hyperexcitability of hippocampal circuits lacking CSP-α.

4.3.1. Studying neuronal excitability of hippocampal cultures lacking CSP-α

To investigate the properties of the neuronal networks lacking CSP-α, we cultured hippocampal neurons at high density in order to have spontaneous neural activity observed by patch-clamp recordings in current-clamp configuration. As example, in figure 20 we can see 5 recordings from different CSP-α KO neurons and 5 recordings from different wild type neurons representing the heterogeneity of spontaneous patterns of activity found at 15-30 DIV hippocampal cultures. Patterns of activity found in control and mutant neurons include excitatory postsynaptic potentials (EPSPs), individual action potentials and bursts of action potentials at different frequencies.

Durations between two consecutives action potentials (inter-event intervals) of recordings were represented in the histogram and the normalized cumulative distribution of figure 21.A (n=2782 intervals from 12 CSP-α WT neurons and n=1511 intervals from 16 CSP-α KO neurons). Comparing the distributions, we can underline the higher number of inter-event intervals with shorter duration in mutant neurons. To quantify bursts firing frequencies, action potentials were grouped into bursts looking for a pattern of periodicity. We consider that action potentials of two consecutives inter-event intervals belongs to the same burst if the duration of one interval is either higher than the half of the previous interval or shorter than two times the previous interval. Histogram and normalized cumulative distribution of bursts firing frequencies are shown in figure 21.B (n=506 bursts from 12 CSP-α WT neurons and n=289 bursts from 16 CSP-α KO neurons) indicating that bursts firing frequencies of CSP-α KO neurons are higher than wild type neurons.

CSP-α KO neurons exhibit a distinctive pattern of seizure activity with abnormal prolonged depolarization and repetitive spiking known as Paroxysmal Depolarization

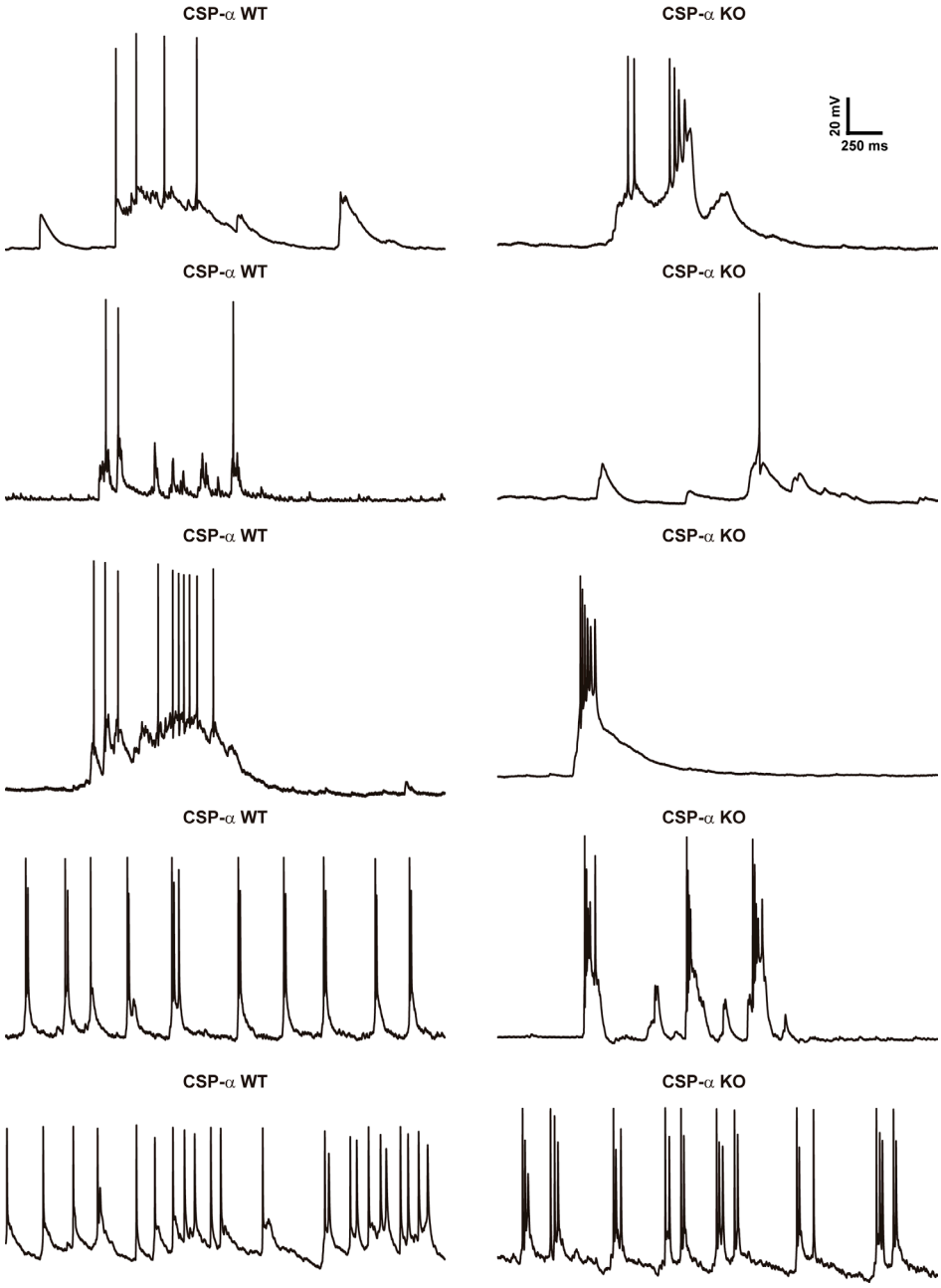

Figure 20: Action potentials recordings using patch clamp electrophysiology show different patterns of spontaneous activity in neurons of hippocampal cultures

Heterogeneous patterns of spontaneous activity were found in 15-30 DIV neurons of hippocampal cultures from mice lacking CSP-α and its wild type littermates using patch clamp electrophysiology in current clamp configuration.

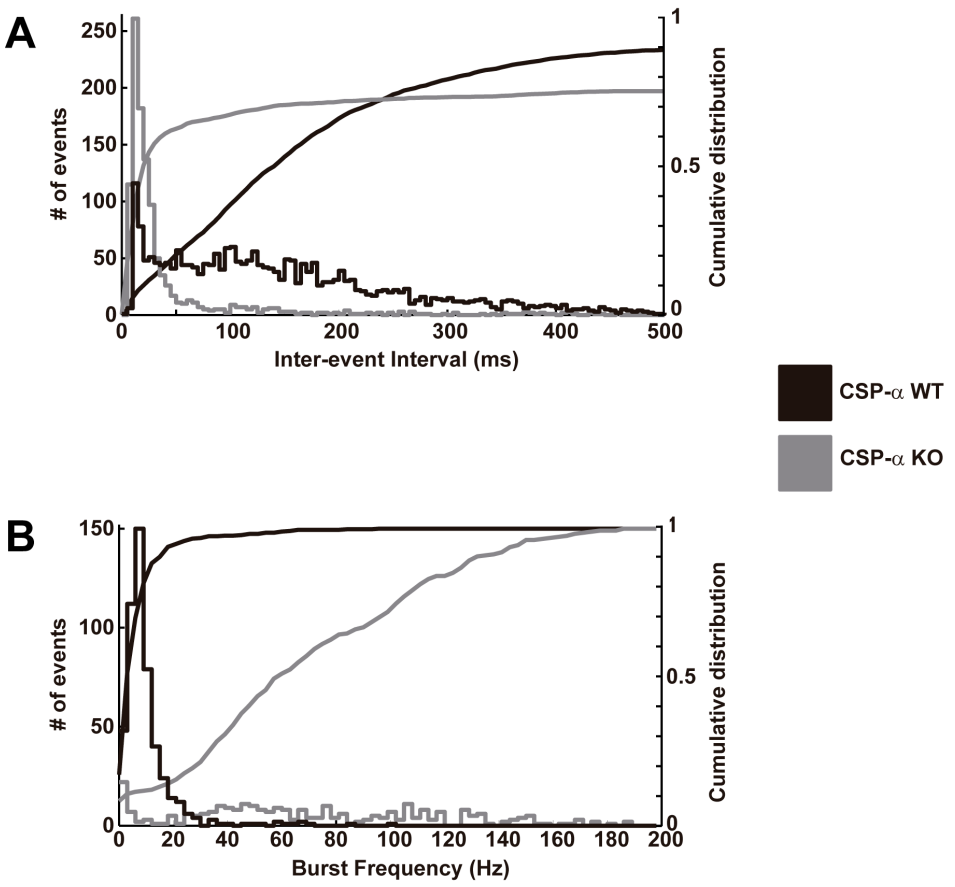

Figure 21: Action potential bursts firing of neurons lacking CSP-α show higher frequency than burst firing of wild type neurons

A: Histogram and cumulative distribution showing that the duration of inter-event intervals (duration between two consecutives action potentials) of CSP-α KO neurons are shorter than wild type neurons. n=2782 intervals from 12 CSP-α WT neurons and n=1511 intervals from 16 CSP-α KO neurons.

B: Histogram and cumulative distribution showing that bursts firing frequency of CSP-α KO neurons is higher than in wild type neurons. n=506 bursts from 12 CSP-α WT neurons and n=289 bursts from 16 CSP-α KO neurons. Action potentials are grouped into bursts looking for a pattern of periodicity. We consider that action potentials of two consecutives inter-event intervals belongs to the same burst if the duration of one interval is either higher than the half of the previous interval or shorter than two times the previous interval.

Neurons are from at least three different cultures. Recordings were performed at 15-30 DIV.

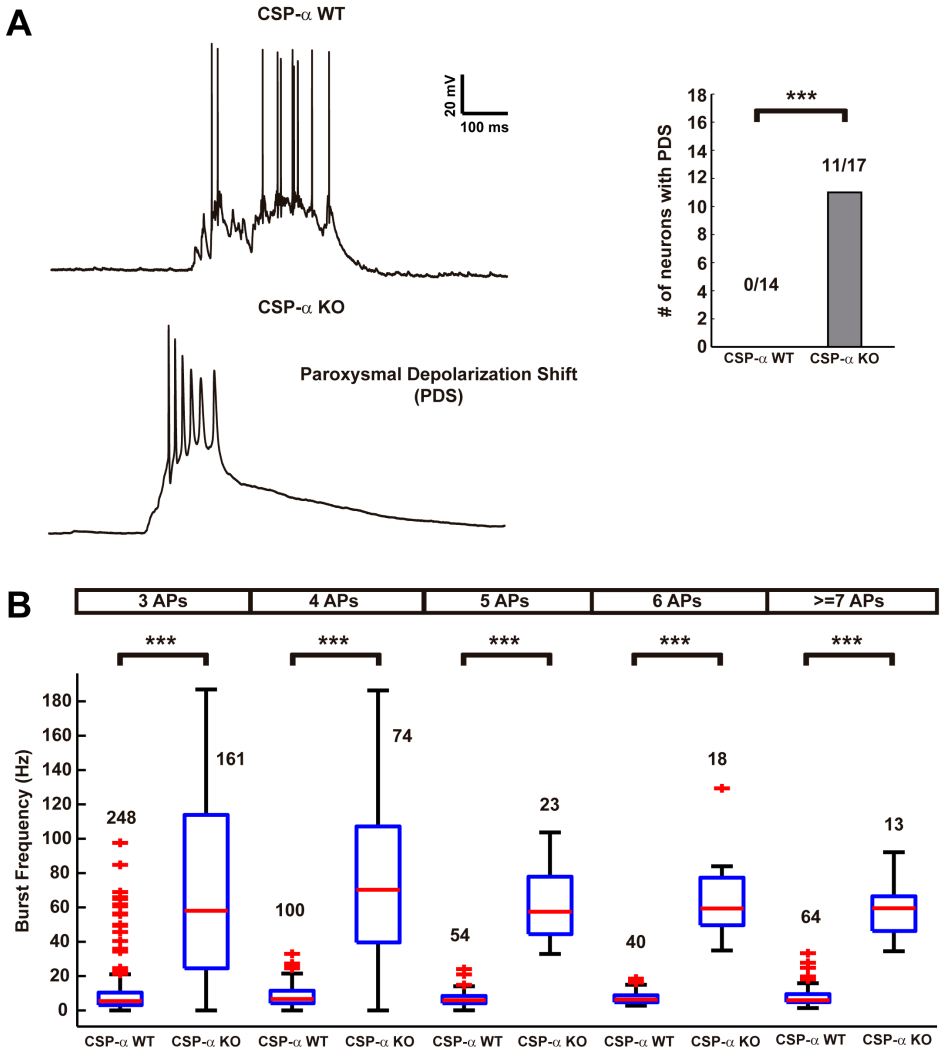

Figure 22: Neurons lacking CSP-α show Paroxysmal Depolarization Shift (PDS), a distinctive pattern of seizure activity with abnormal prolonged depolarization and repetitive spiking

A: Examples of burst firing in neurons from CSP-α KO and wild type hippocampal cultures. Paroxysmal Depolarization Shift (PDS) was observed in 11 of 17 CSP- KO neurons. PDS was not observed in wild type neurons.

B: Box plot showing that action potential burst firing frequency of CSP-α KO neurons is higher than in wild type neurons. Action potential bursts firing are classified by number of action potentials. Numbers of bursts used in the statistic are indicated in the graph for each box plot. Statistical significance was calculated using the Mann-Whitney U test ($p<0.05$).

Recordings were performed in n=14 CSP-α WT neurons and 17 CSP-α KO neurons at 15-30 DIV from at least three different hippocampal cultures.

Shift (PDS) that explain increased bursts firing frequencies in mutants. 11 of 17 mutant neurons show PDS but in contrast, PDS have not been found in wild type neurons (Figure 22.A). Attending to the number of action potentials, bursts firing frequencies are represented in a whisker and box plots (Figure 22.B). Indicating bursts frequencies data sets as 1st quartile; 2nd quartile; 3rd quartile in Hz, for 3 APs bursts, frequencies are 3.09; 5.40; 10.35 Hz for wild type (n=248 bursts) and 24.51; 58.05; 113.88 Hz for mutant (n=161 bursts). For 4 APs bursts, frequencies are 4.13; 6.65; 11.45 Hz for wild type (n=100 bursts) and 39.55; 70.26; 107.14 Hz for mutant (n=74). For 5 APs bursts, frequencies are 4.14; 5.94; 8.43 Hz for wild type (n=54 bursts) and 44.46; 57.47; 77.90 Hz for mutant (n= 23 bursts). For 6 APs bursts, frequencies are 4.71; 6.34; 8.83 Hz for wild type (n=40) and 49.65; 59.35; 77.28 for mutant (n=18). For 7 APs or more, frequencies are 4.78; 5.95; 9.54 Hz for wild type (n=64 bursts) and 46.27; 59.52; 66.50 Hz for mutant (n=13 bursts). For all cases, significant differences were found between CSP-α KO and wild type bursts firing rates (the Mann-Whitney U test, $p<0.05$).

PDS has been proposed as a synchronous network depolarization driven primarily by giant synaptic potentials in a penicillin model of epilepsy (Johnston and Brown, 1981). Models of epilepsy can also be obtained using other pharmacological approaches such as blockage of $GABA_A$ receptors with bicuculline. In Figure 23, we show that the excitatory/inhibitory imbalance caused by blocking inhibitory synapses with the $GABA_A$ antagonist bicuculline leads to PDS and plateau potentials in wild type cultured hippocampal neurons, supporting that PDS in CSP-α mutant cultured neurons are produced by loss of inhibition.

4.3.2. Exploration of neuronal excitability of hippocampal cultures lacking CSP-α with the calcium sensitive dye Fluo4-AM

To confirm hyperexcitability of neurons reported by patch-clamp recordings, we incubated hippocampal cultures with the calcium sensitive dye Fluo4-AM to record calcium activity in neurons. Hippocampal cultures were stimulated using an electrical field stimulation protocol (7 electrical pulses separated by 10 s) to evoke calcium transients. In figure 24.A we can see fluorescence calcium elevations coupled to the stimulus uncovered in wild type and CSP-α KO neurons using measurements from region of interests (ROIs) located onto neuronal somata. In addition two other signals not coupled to the stimulus were found: calcium transients in neurons that reflect spontaneous neural activity and spontaneous astrocytic calcium waves (data not shown). Only neurons that show at least 2 of 7 spikes coupled to the stimulus were taken for analysis and the mean

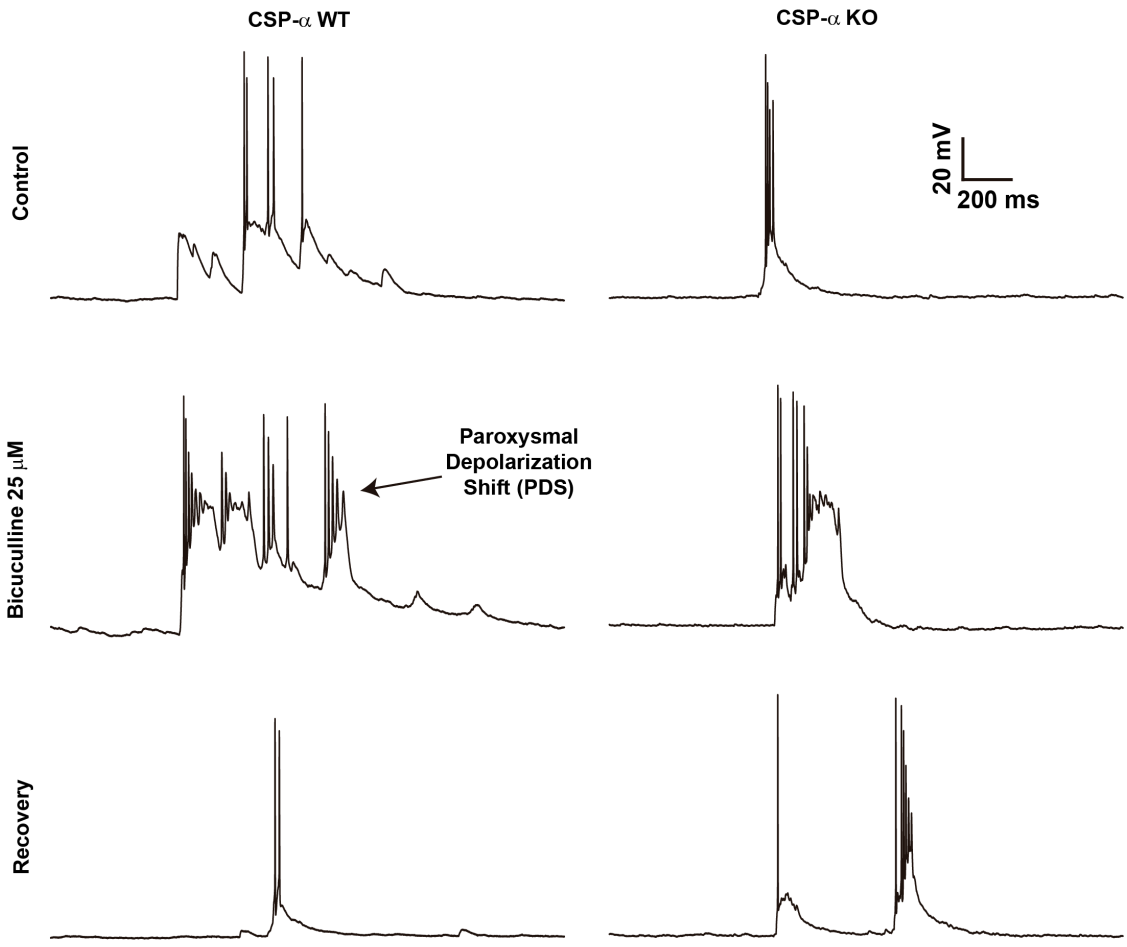

Figure 23: Excitatory/inhibitory imbalance caused by blocking inhibitory synapses with the $GABA_A$ antagonist bicuculline lead to PDS and plateau potentials in hippocampal neurons

Whole-cell current clamp recordings of neuronal spontaneous activity of control and CSP-α KO hippocampal cultures show Paroxysmal Depolarization Shift in the presence of the $GABA_A$ antagonist bicuculline. After washing bicuculline, neurons recover their usual activity.

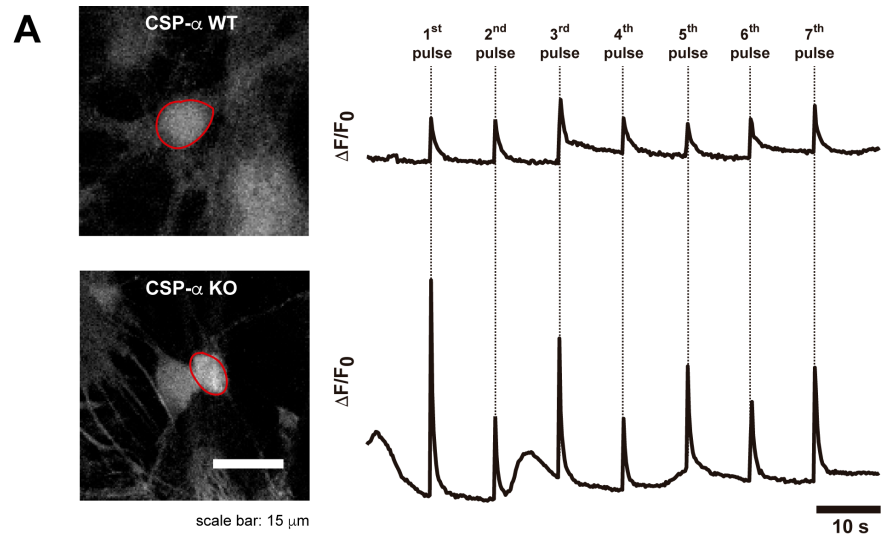
A
CSP-α WT
CSP-α KO
scale bar: 15 μm
1st pulse
2nd pulse
3rd pulse
4th pulse
5th pulse
6th pulse
7th pulse
ΔF/F0
ΔF/F0
10 s

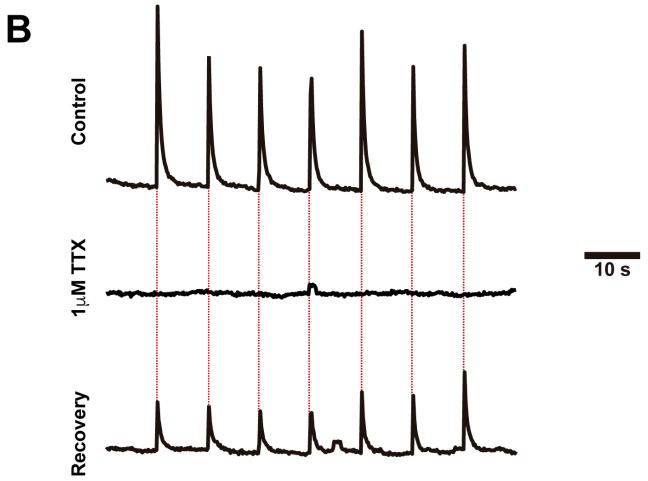
B
Control
1μM TTX
Recovery
10 s

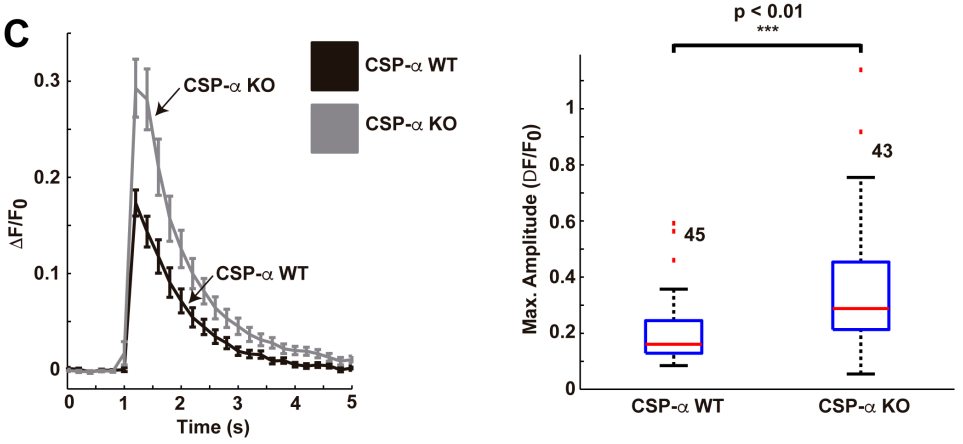
C
CSP-α WT
CSP-α KO
CSP-α KO
CSP-α WT
ΔF/F0
Time (s)
p < 0.01
***
Max. Amplitude (DF/F0)
45
43
CSP-α WT
CSP-α KO

Figure 24: Fluo4-AM fluorescence calcium spikes of neurons lacking CSP-α KO are higher than spikes from wild type neurons

A: Hippocampal neurons loaded with Fluo4-AM reveal calcium transients under electrical field stimulation (7 pulses separated by 10 s) in wild type and CSP-α KO neurons. Regions of interest (ROIs) were taken from the neuronal somata to represent the time course of calcium transients (red circles).

B: Hippocampal neurons loaded with Fluo4-AM do not show fluorescence changes in the presence of the Na^+ channel blocker TTX (1 mM) under electrical field stimulation (7 electrical pulses separated by 10 s) indicating that calcium signals are driven by action potentials. After TTX washing neurons recover fluorescence emission.

C: Fluorescence calcium signals of neurons lacking CSP-α are higher than spikes from wild type neurons. n=45 neurons for wild type neurons and n=43 neurons for CSP-α KO neurons at 17-31 DIV from at least three different cultures. Statistical significance was calculated using the Mann-Whitney U test.

calcium transient was calculated for each neuron. These experiments were carried out without blocking excitatory transmission. On the other hand, these evoked Fluo4-AM calcium spikes depend on action potential-mediated depolarization because hippocampal neurons loaded with Fluo4-AM do not show fluorescence changes in the presence of the Na^+ channel blocker TTX (1 μM) under electrical field stimulation (7 electrical pulses separated by 10 s) (Figure 24.B).

All representative neuronal wild type and CSP-α KO calcium spikes were averaged as we can see in figure 24.C, n=45 neurons for wild type and n=43 neurons for CSP-α KO cultures, revealing higher amplitude in CSP-α KO neurons. Values of maximum amplitudes are also represented as a whisker and box plot in figure 24.C. Amplitudes ($\Delta F/F_0$) shown as 1st quartile: 2nd quartile: 3rd quartile were 0.13:0.16:0.25 for wild type neurons and 0.21:0.29:0.45 for CSP-α KO neurons. Statistical significance was observed between amplitudes of wild type and CSP-α KO neurons using the Mann-Whitney U test. These results support electrophysiological recordings showed previously because higher calcium amplitudes in CSP-α KO neurons might be explained by higher hyperexcitability of mutant neurons due to a loss of inhibitory inputs.

4.3.3. Excitability of granule cells at the dentate gyrus of the hippocampus from mice lacking CSP-α

In this section we describe the intrinsic electrical properties of hippocampal granule cells of the dentate gyrus performing electrophyisiological recordings. Hippocampal granule cells are easily identified in acute brain slices and they represent a homogeneous population of neurons with similar electrical properties.

We first performed recordings in current-clamp configuration to know the spontaneous activity of hippocampal granule cells but we did not detect spontaneous action potentials neither in wild type nor CSP-α KO mutant brains but we do detect abundant local potentials (Figure 25.A). We calculated the resting membrane potential of granule cells from postnatal 10-13 days mice (P10-P13) and postnatal 24-31 days mice (P24-P31). In figure 25.B we can see the resting membrane potential at P10-P13. Indicating data sets as 1st quartile; 2nd quartile; 3rd quartile, the resting membrane potentials in mV were -85.9; -77.3; -67.9 for wild type cells (n=8 cells) and -82.2; -69.3; -67 for cells lacking CSP-α KO (n=10 cells). In figure 25.C we can see the resting membrane potentials of granule cells from P24-P31 mice. Quartiles of data sets were -81.4; -79; -76.4 for wild type (n=12 cells) and -72.7; -70.9; -66.6 for mutant cells (n=15 cells). Significant differences were found between wild type and mutant cells from P24-P31 mice (Student's t-test, $p<0.01$), indicating that cells lacking CSP-α are more depolarized. Furthermore, to know the intrinsic firing properties of granule cells we depolarized the cells under 10 pA steps of current injections for 500 ms to induce action potentials (Figure 25.D). In

Figure 25: Intrinsic firing properties of granule cells at the dentate gyrus of the hippocampus

A: Example whole-cell current clamp recordings of spontaneous activity in granule cells from wild type and CSP- α KO mice.

B and C: Box plot of resting membrane potentials of granule cells from P10-P13 mice (B) and P24-P31 mice (C). Significant differences between control and mutant were found at P24-P31 neurons (Student's t-test).

D: Example action potential traces from whole-cell current clamp recordings of control and CSP-α KO granule cells evoked by 500 ms depolarizing current steps.

E and F: Mean ± SEM number of action potentials in control and CSP-α KO neurons following injection of depolarizing current steps for P10-P13 granule cells (E) and P24-P31 granule cells (F). Significant differences were calculated by the Mann-Whitney U test.

G and H: Box plot of current necessary to reach at least one action potential in wild type and CSP-α KO neurons for P10-P13 granule cells (G) and P24-P31 granule cells (H).

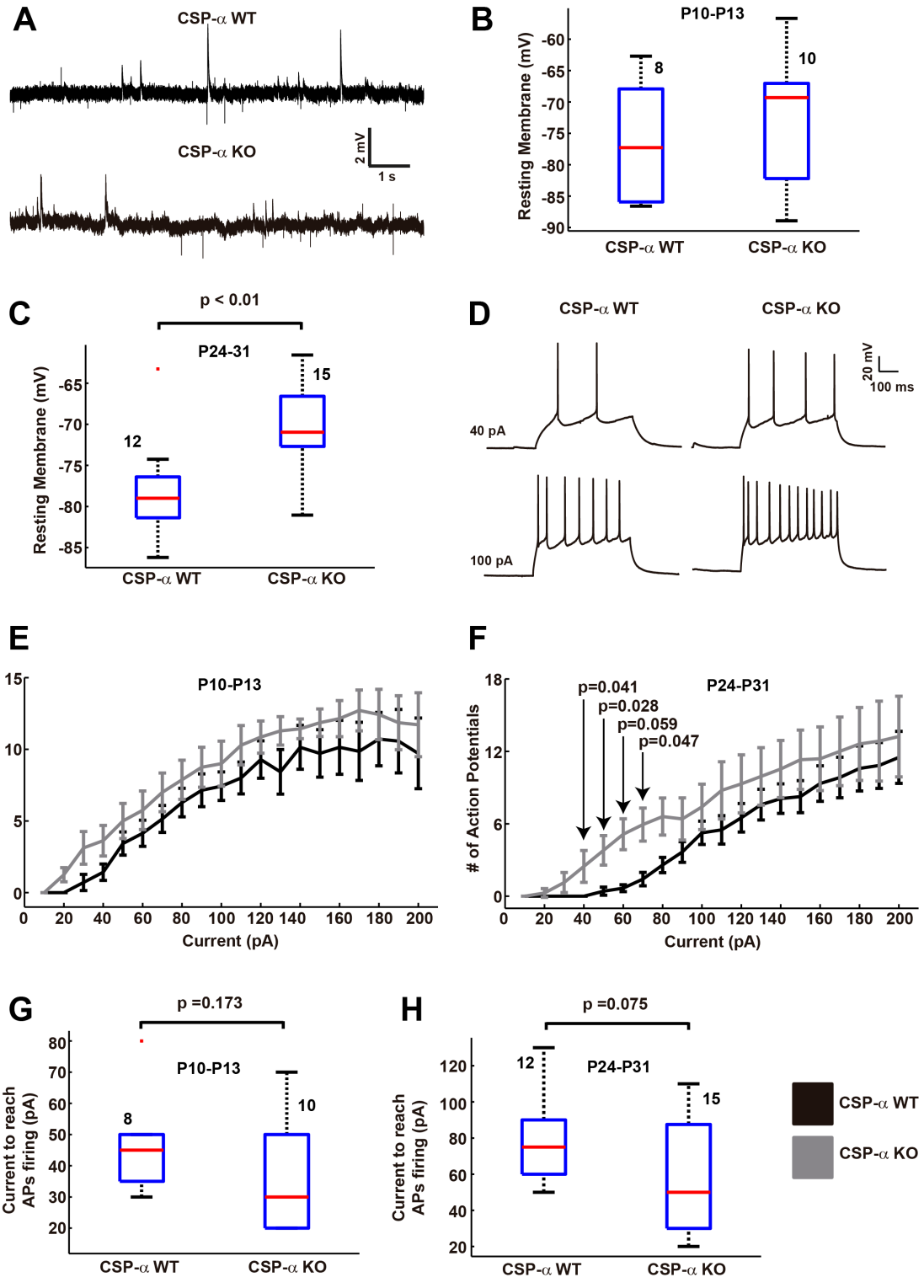
A
CSP-α WT
CSP-α KO
2 mV
1 s
B
P10-P13
Resting Membrane (mV)
-60
-65
-70
-75
-80
-85
-90
8
10
CSP-α WT
CSP-α KO
C
p < 0.01
P24-31
Resting Membrane (mV)
-65
-70
-75
-80
-85
12
15
CSP-α WT
CSP-α KO
D
CSP-α WT
CSP-α KO
20 mV
100 ms
40 pA
100 pA
E
P10-P13
# of Action Potentials
15
10
5
0
0 20 40 60 80 100 120 140 160 180 200
Current (pA)
F
p=0.041
p=0.028
p=0.059
p=0.047
P24-31
# of Action Potentials
18
12
6
0
0 20 40 60 80 100 120 140 160 180 200
Current (pA)
G
p =0.173
P10-P13
Current to reach APs firing (pA)
80
70
60
50
40
30
20
8
10
CSP-α WT
CSP-α KO
H
p =0.075
P24-31
Current to reach APs firing (pA)
120
100
80
60
40
20
12
15
CSP-α WT
CSP-α KO
CSP-α WT
CSP-α KO

figures 25.E and 25.F we represent numbers of action potentials under the different steps of current injections. In figure 25.F we can observe significant differences in the number of action potentials between wild type and mutant cells from P24-P31 mice at some steps of current injection (the Mann-Whitney U test), indicating that excitability is higher in neurons lacking CSP-α. Accordingly with higher depolarization and higher number of action potentials in granule cells lacking CSP-α, there is a decrease, although not significant, in the current necessary to reach at least one action potential in mutant neurons (Figure 25.G for P10-P13 mice and figure 25.H for P24-P31 mice). For P10-P13 neurons, quartiles of data sets in pA were 35; 45; 50 for wild type (n=8 cells) and 20; 30; 50 for mutant cells (n=12 cells) (Figure 25.G). For P24-P31 neurons, quartiles of data sets in pA were 60; 75; 90 for wild type (n=12 cells) and 30; 50; 87.5 for mutant cells (n=15 cells) (Figure 25.H). Higher excitability of mutant neurons is easily explained by the shifting in the resting membrane potential because these cells need less current to reach the threshold potential to fire action potentials. Furthermore, passive properties of granules cells were obtained. For each neuron, 10 steps of hyperpolarizing current injections (20 pA) were applied to calculate the time constant t using an exponential fit of the mean potential decay. Box plot of wild type and CSP-α KO neurons time constants t are represented at P10-P13 and P24-P31 (Figure 26.A). For P10-P13 neurons, quartiles of data sets in ms were 18.04; 20.77; 27.06 for wild type and 18.84; 25.08; 30.58 for CSP- KO neurons. For P24-P31 neurons, quartiles of data sets in ms were 10.2; 14.05; 17.83 for wild type and 8.87; 11.36; 15.97 for CSP-α KO neurons. In figure 26.B we can observe the input resistance of wild type and CSP-α KO neurons for these two age groups. 500 ms hyperpolarizing current injections of 10 pA steps (from 0 to -50 pA) were applied to calculate I-V plots for each neuron. The slope of a linear fit of each I-V plot gave us the input resistance according to Ohm's Law V=RI. Box plot of control and CSP-α KO neurons input resistances are represented at P10-P13 and P24-P31 in Figure 26.B. For P10-P13 neurons, quartiles of data sets in MW were 347; 429; 688 for wild type and 503; 623; 684 for CSP-α KO neurons. For P24-P31 neurons, quartiles of data sets in MW were 242; 280; 374 for wild type and 260; 333; 506 for CSP-α KO neurons. No significant differences were detected neither in time constants nor input resistances. Only we can observe a decrement with postnatal development in both, time constant and input resistance.

We have detected that CSP-α KO neurons are more depolarized, but however we have not seen differences in the passive properties between wild type and CSP-α KO neurons, ruling out that the depolarization of mutant neurons is an intrinsic defect of

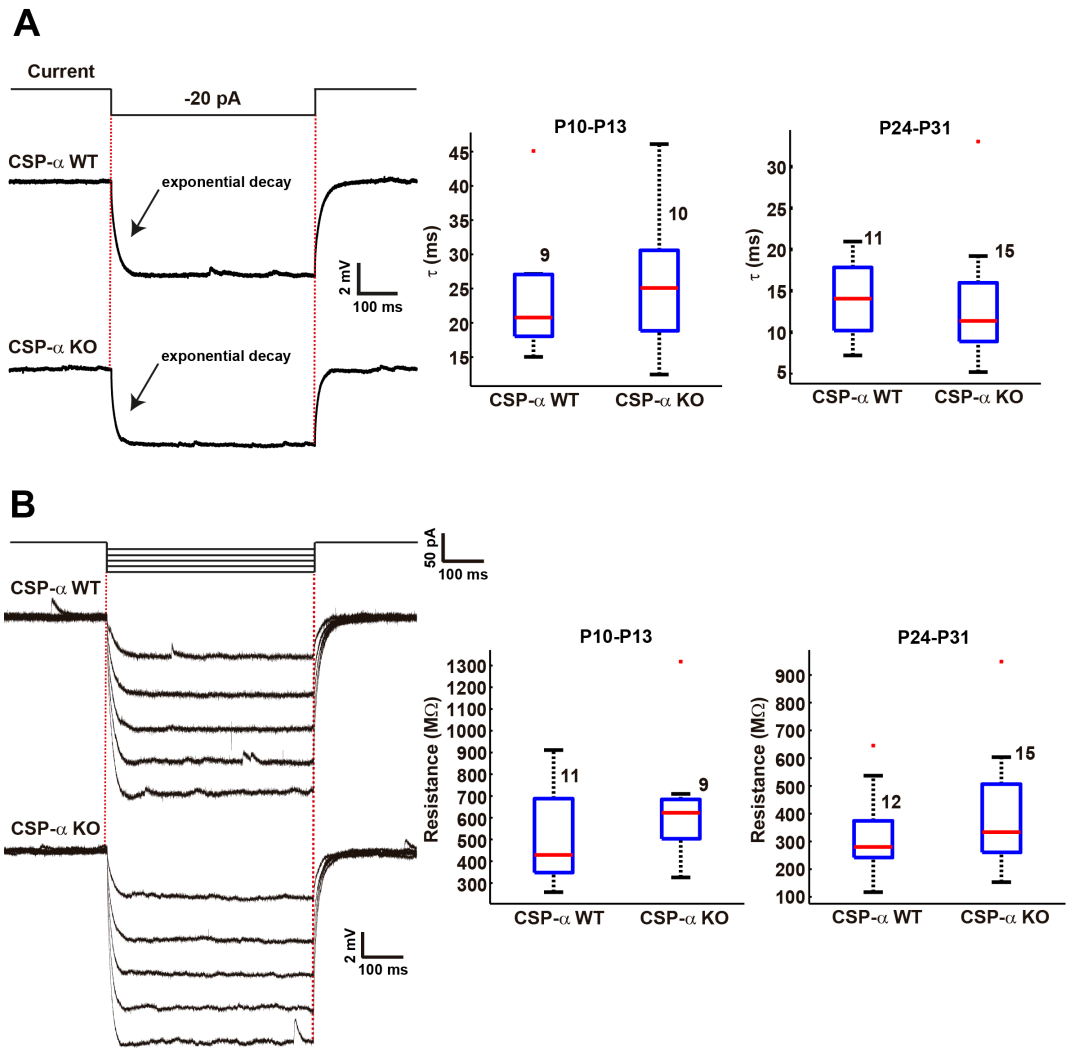

Figure 26: Passive properties of granule cells at the dentate gyrus of the hippocampus

A: For each neuron, 10 steps of hyperpolarizing current injections (20 pA) were applied to calculate the time constant t using an exponential fit of the mean potential decay. Box plot of control and CSP-a KO neurons time constants t are represented at P10-P13 and P24-P31.

B: 500 ms hyperpolarizing current injections of 10 pA steps (from 0 to -50 pA) were applied to calculate I-V plots for each neuron. The slope of a linear fit for each I-V plot give the input resistance of each neuron according to Ohm's Law V=RI. Box plot of control and CSP-a KO neurons input resistances are represented at P10-P13 and P24-P31 ages.

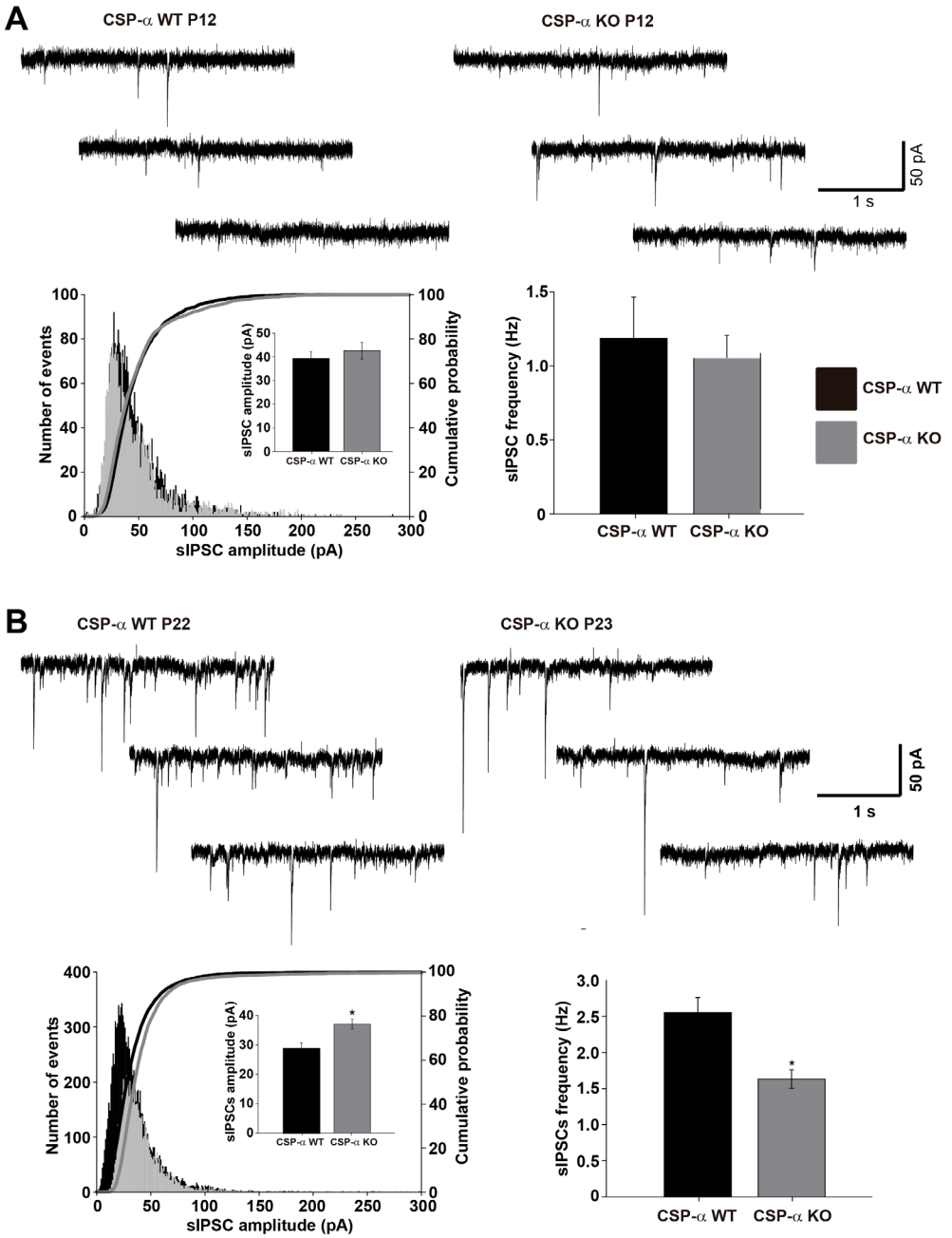

Figure 27: Imbalance of spontaneous inhibitory postsynaptic currents (sIPSCs) in CSP-a KO neurons

A and B: Histograms and cumulative probability of sIPSCs amplitudes from wild type and CSP-a KO neurons for P10 (A) and P20 granule cells (B). Inset: Mean ± SEM amplitudes. Bars representing sIPSCs frequency are also shown for P10 (A) and P20 (B) granule cells.

cells. Another explanation could be a defect in neuronal circuits such a loss of inhibitory inputs. To investigate this, we performed electrophysiological recordings of spontaneous inhibitory postsynaptic currents (sIPSCs) at hippocampal granule cells of the dentate gyrus (Figure 27). Histograms and cumulative probability of sIPSCs amplitudes from wild type and CSP-α KO neurons were calculated for P10 (Figure 27.A) and P20 granule cells (Figure 27.B). Insets represent Mean ± SEM amplitudes. Bars representing sIPSCs frequency are also shown for P10 (Figure 27.A) and P20 (Figure 27.B) granule cells. We cannot see differences neither in amplitude nor frequency between control and CSP-α KO neurons at P10, but however we can observe a significant decrease in sIPSCs frequencies and also a significant increase in sIPSCs amplitudes in P20 mutant neurons. The decrease in sIPSCs frequencies could be explained by a loss of inhibitory inputs and higher amplitude could indicate higher number of postsynaptic inhibitory receptors or even an increase in GABA release from synaptic vesicles. At any case, this imbalance in sIPSCs indicates a defect in inhibitory inputs of granule cells.

5. DISCUSSION

5.1. Normal exo- and endocytosis assessed by synaptopHluorin imaging in cultured hippocampal neurons lacking CSP-α

We have used the synaptic vesicle cycle reporter synaptopHluorin to investigate exo- and endocytosis in culture. As previously done in this type of cultures, we challenged the neurons at high frequency stimulation (20 Hz for 10 s) and found robust responses in both, wild type and CSP-α KO hippocampal cultures (Figure 6.A). We obtained the typical fluorescence responses characterized by a rising phase coincident with the stimulation train when exocytosis predominates (Kavalali and Jorgensen, 2014; Linares-Clemente et al., 2015). After stimulus cessation, the fluorescence started to decline to return to fluorescence basal levels. We quantified the peak amplitudes and the half-width durations and found no differences between control and CSP-α KO terminals (Figure 6.B-E). In addition we used ammonium chloride (NH_4Cl) to unmask the total pool of synaptopHluorin-expressing vesicles and used that parameter to normalize the peak amplitude. Again such a parameter did not show any differences between the two genotypes analyzed (Figure 7). We, therefore, concluded that, at least, using synaptopHluorin, the absence of CSP-α did not induce any change in exo- or endocytosis. These results turned out to be surprising for different reasons:

(1) A previous study from Fernández-Chacón laboratory has described a presynaptic degeneration in CSP-α KO hippocampal cultures restricted to GABAergic synapses formed by parvalbumin-positive (PV+) neurons (García-Junco-Clemente et al., 2010). Perhaps, in our experiments carried out at 17-24 DIV, if those synapses are already degenerated, or sufficiently altered to avoid the normal expression and/or synaptic targeting of synaptopHluorin, they will not be detected by functional imaging. On the other hand, as analyzed below, the lentiviral vectors with the human synapsin promoter preferentially transduces glutamatergic neurons, therefore our conclusions can be restricted to glutamatergic and not GABAergic synapses.

(2) Chandra's group (Zhang et al., 2012) has previously described that the number of synaptic vesicles is reduced in CSP-α hippocampal cultures, howewer, perhaps such a reduction which is around 20% might be detectable by electron microscopy but not by functional imaging. The same study describes that in the absence of CSP-α, the polymerization of dynamin 1 is impaired and the total levels of dynamin 1 are dramatically reduced. Such a molecular dysfunction should translate into a defect in endocytosis, however we cannot detect it with synaptopHluorin imaging. One possibility is that if dynamin 1 is reduced other dynamin isoforms can take over the role of dynamin

1 (Raimondi et al., 2011).

(3) Our previous study at the motoneurons of CSP-α KO mice detected a clear defect in endocytosis occurring during the stimulus (Rozas et al., 2012). This type of endocytosis has not been studied in CSP-α KO hippocampal cultures and we cannot rule out that the defect is also present in central synapses. Future experiments should investigate this aspect further.

5.2. Dynamics of presynaptic Ca^{2+} assessed by GCaMP3 in cultured hippocampal neurons lacking CSP-α

Temporal and spatial regulation of Ca^{2+} concentration at the presynaptic terminals is a major process to modulate neurotransmitter release and synaptic plasticity (Kaeser and Regehr, 2014). Calcium currents mediated through voltage-dependent Ca^{2+} channels is a key step to trigger fast changes in presynaptic Ca^{2+} concentration. Direct measurements of Ca^{2+} currents using the patch-clamp technique is, however, limited to synapses with big synaptic terminals such as the Calyx of Held synapse (Schneggenburger and Forsythe, 2006). Hippocampal terminals have a very small size that prevent direct electrophysiological terminals but are, however, suitable for imaging.

5.2.1. SyGCaMP3 localizes at glutamatergic but not at GABAergic synapses

We have used the calcium reporter GCaMP3 fused to the synaptic vesicle synaptophysin (syGCaMP3) to monitor Ca^{2+} changes associated to presynaptic depolarization. We cloned syGCaMP3 into a lentiviral vector (Lenlox Syn-WPRE-Syn-GFP-WPRE) to express the protein under the human synapsin promoter that allows specific expression in neurons but not in astrocytes (Gascon et al., 2008). In order to confirm the synaptic targeting of syGCaMP3, we demonstrated, using immunofluorescence, that the majority of spots positive for syGCaMP3 co-localized with the synaptic vesicle protein synaptobrevin 2 (Figure 8.D). In any case, syGCaMP3 expression seemed to be restricted to a subpopulation of synapses because many spots positive for synaptobrevin 2 turned out to be negative for syGCaMP3 (Figure 8.D). Further experiments to investigate the origin of such a restricted expression of syGCaMP3 (Figure 9) uncovered that the syGCaMP3 co-localized with the glutamatergic marker VGLUT1 but not with the GABAergic marker VGAT, indicating a preferential restricted expression to glutamatergic synapses. In order to have and additional test to confirm the exclusion of syGCaMP3 from GABAergic synapses we used a fluorescently labeled antibody against the luminal region of the vesicular GABA transporter VGAT (Martens et al.,

2008). Consistently with our initial observations, the GABAergic active synapses that internalized the luminal VGAT antibodies did not express syGCaMP3 (Figure 10). In summary, we observed that the expression mediated by the human synapsin 1 promoter through lentiviral infection translated in robust protein expression in glutamatergic but not in GABAergic neurons. Additional observations in our laboratory confirmed similar results for different proteins such as soluble GFP that turned out to be excluded from PV+ interneurons but not from glutamatergic neurons (data not shown). The lentiviral vector based on the human synapsin promoter that we have used has been reported to be useful for both neocortical and hippocampal cultures (Gascon et al., 2008), however, this study did not specifically analyzed GABAergic neurons. One factor to have into account is the title of viral particles used to infect the cultures. Likely increasing the viral title we might force the infection of GABAergic neurons. On the other hand, consistently with our results in culture, it has been reported that lentiviral infection *in vivo* drives expression under the human synapsin promoter also in a restricted manner (Nathanson et al., 2009). In comparison with adeno-associate virus (AAV), that transduce both cortical and inhibitory neurons at the mouse somatosensory cortex, the lentiviral vector at high viral titers principally labels cortical neurons. This study indicates that the endogenous different tropism of adeno-associated compared to lentivirus might be the reason for the preferential expression in different neuronal types (Nathanson et al., 2009). In contrast to what we initially thought, our observation is not surprising. Indeed we could not find publications specifically demonstrating successful and robust lentiviral transduction of GABAergic neurons in hippocampal cultures in contrast to the well established procedure based on neocortical cultures (Maximov et al., 2007).

For us, in any case, independently of the reason underlying the cell type specificity, it has been very important to confirm that our procedures consistently label glutamatergic neurons. This is advantageous because, in face of the heterogenous hippocampal neuronal populations, we can focus our study specifically in excitatory presynaptic terminals.

5.2.2. Advantages and limitations of syGCaMP3 to monitor presynaptic Ca^{2+} dynamics

The genetically encoded calcium indicator GCaMP3 is a convenient indicator to monitor neural activity because it is a single-wavelength indicator, it has a wide dynamic range and high affinity for Ca^{2+} (Tian et al., 2009). Both, GCaMP2 and GCaMP3 have been used to monitor presynaptic Ca^{2+} dynamics by targeting them to the synaptic vesicle by fusion to synaptophysin and named syGCaMP2 and syGCaMP3 respectively (Dreosti

et al., 2009; Li et al., 2011). Within this context, it has been shown that syGCaMP3 is useful for imaging calcium dynamics during prolonged electrical stimulation and, importantly, it does not affect the synaptic vesicle cycling (Li et al., 2011). The K_d for Ca^{2+} binding of GCaMP3 has been estimated to be between 540 and 660 nM (Lin and Schnitzer, 2016; Tian et al., 2009). Those are convenient values sensitive enough to monitor changes in presynaptic Ca^{2+} concentration because upon the arrival of an action potential to the presynaptic terminal terminal, the Ca^{2+} concentration increases from 0.1 μM up to 30–100 μM (Neher and Sakaba, 2008; Sakaba, 2008; Schneggenburger and Neher, 2000) at least at the location where the Ca^{2+} sensor for exocytosis resides. On the other hand, a potential disadvantage could be a low dynamic range in case of saturation of all the reporter molecules under high Ca^{2+} levels conditions. Such a limitation should be somehow overcome if the expression level of syGCaMP3 is substantially high. A previous study (Li et al., 2011) has shown that the expression levels of syGCaMP3 obtained by transfection provide a wide dynamic range suitable to investigate Ca^{2+} changes induced by high frequency stimulation (40 Hz for 30 s, 1200 action potentials) in hippocampal cultures. Indeed, that study demonstrates that the fluorescence levels achieved under high frequency stimulation are well below the maximum fluorescence levels obtained in the presence of the ionophore ionomycin in 2 mM external of Ca^{2+} concentration, which were 6.5 fold higher than the fluorescence levels recorded in 0 mM of Ca^{2+} concentration (Li et al., 2011). In any case, although syGCaMP3 Ca^{2+}-induced fluorescence is not a quantitative measure of cytosolic Ca^{2+}, it can be useful for comparative studies such the investigation of cytosolic Ca^{2+} dynamics in CSP-α KO hippocampal terminals compared to controls.

5.2.3. Different types of presynaptic Ca^{2+}-dependent fluorescence responses evoked by action potential trains

We used long trains of action potentials (20 Hz for 10 s) to evoke robust syGCaMP3 fluorescence increases that generally lasted during the train and were always reversibly blocked by the Na^+ channel blocker TTX (Figure 11). Interestingly we observed that the time-course of fluorescence during the stimulation displayed the following different patterns: (1) Long Duration Responses (LDRs) were high amplitude responses maintained during the train, (2) Short Duration Responses (SDRs) presented an initial high amplitude phase of short duration followed by a lower amplitude response that lasted until the end of the train and (3) Intermediate Responses characterized by high amplitude but fluctuating responses maintained along the whole train. The three type of responses appeared in WT and CSP-α KO cultures.

Consistently, LDRs did not maintain a constant plateau level, in contrast the fluorescence level decayed during the stimulation train. The same feature has been previously observed (Hendel et al., 2008; Li et al., 2011) and the explanation for such decay is not yet clear. That is a feature that likely depends on the properties of GCaMP dyes and it appears at rather high Ca^{2+} levels. Hendel et al. showed that the same stimulation pattern (160 Hz for 2 s) translated into a stable fluorescence plateau when using the organic Ca^{2+} dye Oregon-Green-BAPTA (OGB-1) but not when using GCaMP1.6 or GCaMP2 (Hendel et al., 2008). Li et al. stimulating at 40 Hz for 20 s obtained a stable plateau of fluorescence upon reducing Ca^{2+} influx in the presence of the calcium channel blockers omega-agatoxin and omega-conotoxin (Li et al., 2011).

In contrast to LDRs, that have been previously described (Li et al., 2011; Zhao et al., 2011), there are not previous reports of SDRs. The initial fast fluorescence transient observed in SDRs likely corresponds with a short train of action potentials that for unknown reasons cannot be maintained along the whole train or it induces calcium-channel inactivation. Following the fast transient, a much lower amplitude plateau shoulder-like signal lasted until the train stopped.

On the other hand, no significant differences were detected in amplitude and duration of presynaptic calcium signals between wild type and CSP-α KO neurons (Figure 13) in spite of biochemical interactions between CSP-α and presynaptic VGCC described previously (Leveque et al., 1998; Magga et al., 2000; Miller et al., 2003). Furthermore, mutant hippocampal cultures show higher number of synaptic spots with spontaneous activity than wild type recorded within a 40 s interval following the stimulation trains (Figure 14), that might indicate a propensity of mutant synapses to have uncontrolled calcium influx after sustained electrical activity perhaps produced by spontaneous action potentials.

5.2.3.1. Spatial segregation of LDRs and SDRs suggest they have an extrasynaptic origin

We applied correlation analysis to investigate the spatial relationships between the regions of interests (ROIs) that displayed different type of responses. We found that the ROIs, likely synaptic puncta, could be readily separated accordingly to the type of fluorescence response (Figure 15). The majority of ROIs displayed LDRs in control and CSP-α KO cultures. Interestingly, a visual inspection of the spatial distribution of every type of ROI type seemed to indicate that LDRs and SDRs occurred in spots that followed a rather continuous and/or linear organization. The most parsimonious explanation is

that those clusters correspond to en passant synapses residing within the same axon, that would be compatible with the separation distance (3.7 ± 0.6 microns) between this type of varicosities that has been previously described (Shepherd et al., 2002). We reasoned that if that were the case then LDRs and SDRs might be reflecting properties of action potential trains along distinct axons rather than special properties of different synapses. In order to test that hypothesis we infected the cultures with GCaMP3 that, in contrast to syGCaMP3, is soluble and get distributed through the neuronal cytoplasm. We found that, indeed, responses very similar to LDRs and SDRs existed in neurites at extrasynaptic locations indicating that the responses likely reflected a non-synaptic phenomena (Figure 17).

We were interested to check the consistency along the time of LDRs and SDRs measured with syGCaMP3. In order to investigate that we examined the same ROIs after a second stimulation train applied 10 minutes after the first train (Figure 16.A). To analyze the results, we plotted the duration (half width) of the responses during the first train versus the duration during the second train. Data scattered in several groups roughly clustered in the four arms of a square (Figure 16.B) as follows:

Group 1 or the LDR-to-LDR group. This is the most consistent behaviour that we found and corresponded to the data clustered in the upper right corner of the square. These points corresponded to LDRs recorded during the first train that were again evoked as LDRs during the second train.

Group 2 or the LDR shortening group. This group included ROIs with LDRs during the first train but presented a shorter duration response during the second stimulation train. These data are clustered within the right vertical arm of the plot (Figure 16.B). The LDRs temporal shortening, detected as lower duration half-widths, appeared as scattered values including durations just below 10 s up to approximately 4 s. In a few cases, the LDRs were not evoked during the second train and these cases were considered failures.

Group 3 or the SDR shortening group. This group included ROIs with rather short duration responses which appeared with even shorter durations during the second train. These data are clustered within the lower horizontal arm of the plot (Figure 16.B).

Group 4 or the SDR lengthening group. This group included ROIs with rather short duration responses which appeared with longer or similar durations during the second train. These results were very scattered and they are somehow clustered within the left vertical arm of the plot (Figure 16.B).

Group 5 or the SDR-to-LDR group. This group included ROIs with rather short duration responses which appeared converted to LDRs (10 s duration) during the second train. These data were clustered within the upper horizontal arm of the plot (Figure 16.B).

In contrast to the existence of Group 1, formed by robust LDRs that were consistently recorded as LDRs during the second train, we did not identify a consistent compact cluster of SDRs that keep the same very short duration during the second train. Modulation or fluctuations in action potential propagation might be subjacent to the variations in LDRs and SDRs along the time.

5.2.3.2. The nature of LDRs and SDRs

The protocol that we have used to depolarize neurons for Ca^{2+} imaging experiments is based in electrical field stimulation having in the bath blockers of glutamatergic synaptic transmission. The stimulation would therefore convey only electrical and not synaptic depolarization affecting the axonal and the somatodendritic compartments. We assumed that the action potentials generated at the initial axonal segment are the leading depolarizing signal to open voltage-dependent Ca^{2+} channels. We expect that backpropagation of action potentials open Ca^{2+}-channels at the somatodendritic compartment that contributes to the global increase in the cytosolic Ca^{2+} concentration (Stuart et al., 1997). In addition, under such a global electrical stimulation, we would expect to trigger dendritic action potentials able to open Ca^{2+} channels too. Alone by themselves, dendritic action potentials mediated by Na^{+} and Ca^{2+} channels (Golding et al., 1999), would be insufficient to trigger axonal action potentials, however, in the context of global depolarization they would also contribute to overcome the threshold to open Na^{+} channels at the axonal initial segment (Stuart et al., 1997). The Ca^{2+} signals at the somatodendritic compartment induced by back-propagating trains of action potentials are mediated by high-voltage activated (HVA) L-type and N-type channels located in pyramidal cell somata and proximal dendrites (Christie et al., 1995). In contrast, in more distal regions from the soma at the apical dendrites, Ca^{2+} influx is mediated by HVA R-type and low-voltage activated (LVA) T-type channels (Christie et al., 1995; Kavalali et al., 1997; Magee et al., 1995).

LDRs that we have observed are likely produced as a consequence of calcium influx through voltaged activated calcium channels upon the arrival of action potentials as it has been previously shown in studies based on the use of organic fluorescent Ca^{2+}-indicators in hippocampal cultures (Mackenzie et al., 1996), brain slices (Koester and Sakmann, 1998, 2000; Smetters et al., 1999) and *in vivo* (Stosiek et al., 2003). The

calcium synaptic signals measured with syGCaMP3 will likely have a major component mediated by typical high-voltage activated synaptic calcium channels such as N or P/Q type channels (Grienberger and Konnerth, 2012; Koester and Sakmann, 2000; Li et al., 2011; Mackenzie et al., 1996). On the other hand, the nature of the more infrequent SDRs is less straightforward to explain. We have considered two main possibilities to explain what could be causing SDRs:

(1) SDRs are the consequence of a failure in action potential propagation (Debanne, 2004, 2011).

(2) SDRs occur by a calcium-dependent inactivation of neuronal calcium channels (Budde et al., 2002).

5.2.3.2.1. SDRs as a consequence of action potential propagation failures

The importance of subthreshold variations in the presynaptic membrane potential and action potential propagation failures in neuronal signaling cannot be overstimated. Those are crucial events to secure or to block communication between the pre- and the postsynaptic terminals (Debanne et al., 2013). As discussed below, the mechanisms of action potential failures have been studied in axons from vertebrates and invertebrates using electrophysiological approaches. Our imaging study bears, within this context, important potential to investigate the mechanisms underlying action potential failure in neuronal cultures and, in perspective, in the brain *in vivo*. In vertebrates, several mechanisms have been proposed in cortical and hippocampal axons to explain action potential propagation failures:

(1) Failures due to geometrical factor such as axonal branching. In axons with collaterals, action potentials propagating through the parent axon might either continue or stop propagation upon the arrival to a branching point. This has been proposed to occur at the hippocampus (Debanne et al., 1997) and at the thalamic and cortical axons (Deschenes and Landry, 1980). It has been proposed that the relationship between the total longitudinal current produced by the arriving action potential and the input impedance of the branching collaterals is key for the success or the failure of the action potential propagation. Indeed, the relationship between the diameters of mother and daughter branch are useful parameters to predict the fate of the action potential propagation (Goldstein and Rall, 1974). Another geometrical contribution to propagation failure seems to be the axonal swelling at the en passant boutons. This factor has been studied in the neurohypophysis (Bourque, 1990) but not in hippocampal axons yet.

(2) Propagation failures of high frequency action potential trains. It has been proposed that axon conducting action potentials at high frequencies undergoes membrane potential changes that induce propagation failures. The changes could be in both directions: membrane depolarization and membrane hyperpolarization. During high frequency axonal activation, the accumulation of extracellular potassium in the peri-axonal space would be responsible for membrane depolarizations high enough to cause inactivation of sodium channels (Meeks et al., 2005; Meeks and Mennerick, 2004; Poolos et al., 1987). In parallel, the axon would accumulate sodium at faster rate in thin branches compared to thick branches due to the higher surface-to-volume ratio in the cylindrical axons with smaller diameters (Debanne, 2011). Therefore, the sodium accumulation will promote the Na^+/K^+ pump activation and the lowering of potassium ions more efficiently around the thin branches facilitating the action potential propagation (Grossman et al., 1979a, b).

The failure of action potential propagation has been also proposed as an important factor underlying short-term synaptic plasticity in hippocampal cultures. That could occur as a result of an increase in the probability of action potential conduction failure along axonal branches (Brody and Yue, 2000) or as a consequence of sodium-channel inactivation (He et al., 2002). Interestingly, sodium-channel inactivation could act as a modulatory step suitable to be modified with small tonic depolarizations under physiologically normal or abnormal levels of activity (He et al., 2002).

(3) Changes due to membrane hyperpolarization. It has been proposed that under high-activity conditions the axon might become hyperpolarized as a consequence of the Na^+/K^+-ATPase activation that would occur upon increases of intracellular Na^+ concentration. In addition, the opening of calcium activated-potassium channels could also contribute to activity-dependent axonal hyperpolarization (Bielefeldt and Jackson, 1993; Debanne, 2011; Ritchie and Straub, 1956, 1957). On the other hand, it has been proposed that activity-dependent hyperpolarization of Schaffer collateral axons could be reverted by the activation of the cationic current I_h (Soleng et al., 2003). Interestingly, the hyperpolarization-induced activation of I_h is required for long-term facilitation in invertebrate motorneurons (Beaumont et al., 2002). Another mechanism of hyperpolarization, not necessarily associated with high frequency stimulation, has been described at the presynaptic level in axon collaterals of CA3 pyramidal neurons in slice cultures: the activation of presynaptic A-type K^+ current that would transiently block the propagation of action potentials (Debanne et al., 1997). Although A-type K^+ channels are normally inactivated at the resting membrane potential, they recover from

inactivation after a transient hyperpolarization that could be, for example originated by an inhibitory postsynaptic potential (IPSP) (Debanne et al., 1997; Debanne et al., 1999). In addition to, or instead of, failure in axonal propagation, action potentials could also undergo a decline in amplitude during propagation (Brody and Yue, 2000) or changes in duration that could modify calcium influx through voltage-dependent Ca^{2+} channels (Boudkkazi et al., 2011; Geiger and Jonas, 2000; Hawkins et al., 1983).

In summary, if we take into account that modifications in action potential propagation through the axon is a major factor in the genesis of SDRs we can provide two interpretations to our findings:

(1) Modulation or fluctuations in action potential propagation might be subjacent to the variations in LDRs and SDRs along the time as observed in figure 16.

(2) Since the properties and relative percentages of LDRs and SDRs detected with the syGCaMP3 reporter are the same in CSP-α WT and CSP-α KO cultures, the reliability of action potential propagation is likely not altered in the absence of CSP-α in glutamatergic neurons in culture.

5.2.3.2.2. SDRs as a consequence of calcium-dependent inactivation of neuronal calcium channels

Calcium channels play an important role in controlling Ca^{2+}-dependent short-term depression and short term facilitation. Interestingly, P/Q-type Ca^{2+} synaptic currents facilitate in response to pairs or short trains of depolarizations and inactivate in response to prolonged trains. Both phenomena are Ca^{2+}-dependent mechanisms that take place through the direct binding of the channels to Ca^{2+}-activated CaM. It has been proposed that CaM plays a dual role by binding to the C-terminus of calcium channels. Increases in local Ca^{2+} triggers the binding of CaM C-terminus to the channel at the so called IM domain and leads to facilitation by increasing Ca^{2+} currents. In contrast, higher increases of global Ca^{2+} leads to the binding of CaM N-terminus at the CaM-binding domain (CBD) of the channel causing Ca^{2+}-induced inactivation (Budde et al., 2002; Catterall et al., 2013; Christel and Lee, 2012). Importantly, L-type calcium channels in hippocampal neurons also undergo calcium-dependent inactivation (Beck et al., 1999; Nagerl and Mody, 1998). The calcium binding protein calbindin disrupts calcium-dependent inactivation in L-type calcium channels (Nagerl et al., 2000). This is interesting because hippocampal granule cells from epileptic patients with reduced levels of calbindin present a reduced Ca^{2+} influx (Nagerl et al., 2000) which could be a protective mechanism for

neurons in epilepsy.

According to that we can not completely exclude that the SDRs could be caused by calcium-dependent inactivation. Within that scenario, the action potentials mediated by voltage-dependent Na^+ channels would be occurring normally but would be non-detectable with our assay that only detect electrical activity indirectly when there are changes in cytosolic Ca^{2+}. In order to further investigate this situation it would extremelly useful to image electrical activity with voltage-dependent sensitive dyes (Antic et al., 2016). Simultaneous high-rate acquisition imaging using syGCaMP3, to monitor presynaptic calcium and a voltage-sensitive indicator to monitor action potentials would be necessary to investigate the role of sodium channels in presynaptic depression. This would be possible using the new generation of genetically encoded voltage indicators based on microbial rhodopsin to image action potentials, such as Archaerhodopsin 3 (Kralj et al., 2012) or QuasAr1 and QuasAr2 (Hochbaum et al., 2014). These genetically encoded voltage indicators have been used to study the waveform of presynaptic action potentials (Hoppa et al., 2014).

5.2.3.2.3 SDRs as a consequence of a GABAergic inhibition

Hippocampal cultures are constituted by a heterogenous population of neurons reflecting the neuronal diversity of the hippocampus in vivo that includes glutamatergic and GABAergic neurons (Klausberger and Somogyi, 2008). Several types of interneurons such as fast-spiking parvalbumin-positive, regular-spiking cholecystokinin-positive basket cells and axo-axonic chandelier cells contribute to feedback inhibition at hippocampal circuits (Kullmann, 2011). In our experiments we imaged neurons in the presence of pharmacological blockers of glutamatergic synaptic transmission while the GABAergic transmission was not inhibited. Under these conditions, the excitation of interneurons mediated by a glutamatergic synapse would not be possible and we could remotely explain such a feedback if the excitation were driven by GABA within a multisynaptic neuronal circuit (Khazipov, 2016). On the other hand, if SDRs were induced by GABAergic inputs we should detect changes in the frequency or duration of SDRs in CSP-α KO cultures that suffer from a deficit of GABAergic inputs (García-Junco-Clemente et al., 2010). Since that is not the case we consider that likely SDRs are not caused by a GABAergic-dependent network mechanism.

We also explored the possibility of SDRs being caused by a GABAergic modulation of glutamatergic terminals mediated by metabotropic $GABA_B$ receptors at presynaptic terminals activated by the chemical messenger GABA that can inhibit VGCCs

(Gassmann and Bettler, 2012). In this thesis we have reported that under inhibition of $GABA_B$ receptors using CGP-55845 antagonist, hippocampal synapses exhibit SDRs indicating that this depression mechanism is not mediated by presynaptic metabotropic $GABA_B$ receptors (Figure 19). These findings are in concordance with previous results suggesting that SDRs are produced by an extra-synaptic mechanism.

5.2.4. Calcium waves detected with GCaMP3 in neuronal cultures

We used the genetically encoded indicator GCaMP3 that in contrast to syGCaMP3, does not have a restricted presynaptic localization. GCaMP3 is a soluble protein that, as expected, appeared distributed through the somatodendritic compartment. We observed that in some cases upon electrical stimulation the calcium signal reported by GCaMP3 appeared not as a static and homogeneous signal but, instead, as a calcium wave that originated in the neuronal soma and became spread through the somatodendritic compartment (Figure 18). It has been previously reported that neuronal calcium waves originate from both intracellular calcium stores and calcium influx through voltage-activated calcium channels (Ross, 2012). Calcium dependent inactivation (CDI) is a mechanism that inactivate VGCCs under elevation of intracellular calcium where in some cells, VGCCs are inactivated by calcium release from intracellular calcium stores, in a process known as calcium induced calcium release (CICR) (Budde et al., 2002). Calcium waves, such as we have described in cultured neurons expressing GCaMP3 (Figure 18) are produce by CICR, where elevated cytoplasmatic calcium induces further calcium releases from endoplasmic reticulum through a nonlinear cooperative process that involved either reticular IP_3 receptors (IP_3Rs) or reticular Ryanodine receptors (RyRs) (Ross, 2012). Neuronal IP_3Rs calcium waves needs IP_3 and calcium to open. After opening, the calcium is released from the receptor acting on the same IP_3Rs or other IP_3Rs, so calcium release is propagated as far as IP_3 is available (Ross, 2012). Calcium waves and therefore CICR are proposed as mechanism that transmit information from a synapse in the dendrites to the nucleus, where calcium activates genes or transcription factors involved in synaptic plasticity (Berridge, 1998). In this thesis, we show that dendrites exhibit calcium waves under sustain electrical field stimulation (20 Hz for 10 s). SDRs described in neurites (Figure 17) might be a form of CDI leading to speculate that intracellular calcium stores and CICR might be involved in the presynaptic depression underlying to SDRs. In any case, we do not have solid arguments to support that notion. Indeed we ignore if the Ca^{2+} waves observed in our experiments spread also along the axon and careful future experiments would be required to investigate that phenomenon. Indeed, the existence of CICR at presynaptic levels is very controversial and it has not been

convincingly demonstrated (Ross, 2012). Interestingly, it has been recently reported that the endoplasmic reticulum plays a role in the control of Ca^{2+} influx and neurotransmitter release (de Juan-Sanz et al., 2017). This study is based in the use of novel GCaMP-derive Ca^{2+} indicators properly modified to monitor Ca^{2+} dynamics within the ER. Remarkably that study demonstrates that upon neural activity the ER uptakes axonal Ca^{2+} uptake but not release, just the opposite to what has been hypothesized in previous work (Bouchard et al., 2003; Emptage et al., 2001; Liang et al., 2002; Nizami et al., 2010; Verkhratsky, 2005; Zhang et al., 2009). Therefore the possibility of presynaptic syGCaMP3 SDRs being produced by a mechanism dependent of Ca^{2+} release from presynaptic ER is rather a remote possibility. In any case, as we have discussed before, simultaneous high-rate acquisition imaging of calcium and voltage membrane and pharmacological inhibition of RyR and IP_3R would be useful to elucidate whether the mechanism underlying to SDRs is mediated by firing patterns of action potentials or by a mechanism of CDI that involve intracellular calcium stores.

5.2.5. Normal presynaptic calcium dynamic in the absence of CSP-α

Overall and specially our experiments using syGCaMP3 indicate that there are no differences in calcium dynamics between terminals lacking CSP-α and control terminals. Our results are relevant for the proposed role of SNAP-25 as a regulator of synaptic calcium channels, specially in glutamatergic synapses (Condliffe et al., 2010). Matteoli's group has shown an increased in calcium currents in SNAP-25 heterozygous mice. Since SNAP-25 is reduced in CSP-α KO mice would not be surprising to detect increases in presynaptic calcium signals in CSP-α KO mice. Since we do not detect that it is possible that either our assay is less sensitive than electrophysiological measurements or that the levels of SNAP-25 are not sufficiently reduced to trigger the effect on calcium channels.

5.3. The absence of CSP-α leads to neuronal hyperexcitability

In a previous study we have seen that the absence of CSP-α leads to presynaptic degeneration of parvalbumin-positive neurons. That phenotype has been observed in culture and in brain slices. Interestingly, in CSP-α KO hippocampal cultures, as a secondary consequence of presynaptic degeneration, the glutamatergic synaptic transmission scales down. These changes are considered to be caused by a downregulation in the number of postsynaptic AMPA receptors, a well described mechanism in homeostatic plasticity (Turrigiano, 2012). This kind of plasticity allows the homeostatic maintenance of the global network activity within physiological levels keeping. At the same time, homeostatic plasticity keeps the relative individual differences in synaptic strength

between distinct synapses (Turrigiano, 2012). In any case, we did not know if the homeostatic plasticity changes described in CSP-α KO cultures were strong enough to completely bring excitability at normal levels.

5.3.1. Paroxismal depolarization shifts in neuronal cultures of CSP-α KO mice

We carried out current-clamp measurements to monitor spontaneous action potentials in hippocampal cultures and found that neurons in CSP-α cultures trigger action potentials at a higher frequency (Figures 20 and 21). Interestingly, we observed, in CSP-α KO cultures, events characterized by a progressive depolarization that lead to supra-threshold membrane potentials levels high enough to trigger a continuous train of action potentials (Figure 22 A). We did not see this kind of events in control cultures. The spontaneous bursts of action potentials recorded in control cultures were different and lacked the characteristic depolarizing fast slope observed in the mutants (Figure 22 A). In addition we found that, within bursts, the action potentials were significantly triggered at higher frequencies in the mutants compared with the controls (Figure 22) supporting the notion of higher excitability in mutant neural networks. The characteristic hyperexcitability events that we observed likely correspond with paroxismal depolarization shift (PDS) that were originally observed by intracellular recordings in an epileptic focus in cat cortical neurons *in vivo* (Matsumoto et al., 1969). In that experimental model, the epileptic focus was created by the topical application of a $GABA_A$ receptor antagonist (penicillin) and the PDS usually coincided with a paroxysm in the electrocorticogram, the interictal discharges that appeared between epileptic seizures (Matsumoto et al., 1969). PDS have also been studied in brain slices in which, as *in vivo*, are induced by the epileptogenic effect of penicillin (Dingledine and Gjerstad, 1980; Schwartzkroin and Prince, 1978). Hippocampal neurons trigger bursts of action potentials that reflect the endogenous activity of the neuron. These bursts can happen either spontaneously or in response to the injection of a depolarizing current (Kandel and Spencer, 1961). On the other hand the bursts observed induced by convulsants such as penicillin in hippocampal neurons occurred as a sudden depolarization of membrane potential that triggered a train of action potentials (Dichter and Spencer, 1969a, b). These convulsant-induced bursts were proposed to be of synaptic nature and generated by recurrent excitatory circuitry (Dichter and Spencer, 1969a; Lebovitz et al., 1971; MacVicar and Dudek, 1979).

Later studies, carried out in hippocampal slices, confirmed that view by showing that bursts induced by the convulsant agents were not endogenous but network-driven bursts coincident with the synchronous activity of a neuronal population (Johnston and

Brown, 1984). PDS are considered network-driven bursts originated by large amplitude synaptic potentials. There are four evidences that support that notion (Johnston and Brown, 1984): (1) the probability of its occurrence is independent of membrane potential; (2) its amplitude depends on the membrane potential according to changes on the synaptic driving force; (3) the amplitude reverses in polarity when the membrane potential is brought beyond the synaptic potential equilibrium; (4) in voltage-conditions synaptic currents are detected in synchrony with the interictal discharge of the neuronal population and the amplitude of synaptic conductances underlying a PDS are between five to ten times larger than the currents associated with a regular EPSP. Although we did not investigate those details in our cultures, we think that, likely, the events that we have defined as PDS and the increased frequency of the action potential bursts in CSP-α cultures are likely a secondary effect of the synaptic GABAergic degeneration that we have previously described (García-Junco-Clemente et al., 2010). Indeed, the blocking of GABAergic synaptic transmission with bicuculline in control cultures evoked responses similar to the PDS observed in mutant cultures, an approach used to study the molecular basis of PDS in neuronal cultures (Stiglbauer et al., 2017). According to our observations, the homeostatic downscaling of glutamatergic (García-Junco-Clemente et al., 2010) transmission seems to be insufficient to completely bring back neuronal excitability at physiological levels. In addition, our results together with other recent study (Stiglbauer et al., 2017) show that neuronal phenomena associated to epilepsy such as PDS, previously described *in vivo* and in brain slices, are also measurable in hippocampal cultures, a circumstance that open new possibilities to investigate mechanisms in a rather simple system suitable for pharmacological screenings.

On the other hand, calcium imaging is an alternative technique to measure activity in neurons. As we have shown in this dissertation, genetically encoded calcium indicators do not drive the expression to all cell types. For this reason we used the calcium dye Fluo4-AM to measure calcium activity in neuronal cultures and obtained results which could be compatible with increased hyperexcitability observed in electrophysiological experiments. Furthermore, this dye provides a dissociation constant of 335 nM, lower than GCaMP3, being more sensitive to calcium changes. In these experiments with Fluo4-AM we did not use synaptic blockers to study the properties of the neural networks. We found that fluorescence spikes of mutant neurons loaded with the calcium dye Fluo4-AM show higher amplitude than wild type neurons (Figure 24). Larger calcium transients in mutant neurons can be explained by the high frequency firing patterns of mutant neurons supporting our results (Figure 22).

5.3.2. Hyperexcitability in hippocampal slices from knock-out mice lacking CSP-α due to presynaptic GABAergic deficit

In order to go deeper in our study we extended our investigations of neuronal excitability in hippocampal slices. In comparison with hippocampal cultures, the original circuitry organization is preserved in brain slices and allows the investigation of specific neuronal types. Since we had special interest in investigating the effects of GABAergic inhibition we focused our analysis on the granule cells at the dentate gyrus. The granule cell layer is prominently inervated by PV+ interneurons that suffer from presynaptic degeneration in CSP-α KO mice (García-Junco-Clemente et al. 2010). We investigated the properties of granule cells using current-clamp. We studied neurons at two postnatal ages (P10-P13 and P24-P31) and found significant changes only at the most advanced ages. At postnatal age P24-P31, granule cells from CSP-α KO mice were more depolarized and were more excitable than control neurons. CSP-α KO neurons easily triggered bursts of action potentials upon injecting lower current levels compared to control neurons (Figure 25). We studied if that could be a consequence of different membrane properties between the two different neuronal types but ruled out that possibility because the passive membrane properties were the same (Figure 26). Next we quantified the strength of GABAergic input by measuring the frequency of miniature inhibitory postsynaptic currents. Although we could not see any changes at early ages (P10) we detected that older mice (P22-P23) presented a lower frequency of minis that, in addition, had higher amplitude. We interpret those findings as signs of presynaptic GABAergic degeneration. A lower number of functional terminals would lead at a lower frequency assuming that the release properties of every terminal are similar and they maintain a constant rate of spontaneous GABA release. The increase in mini size is intriguing and could be reflecting a compensatory response to the presynaptic deficit expressed by either changes in the number or in the type of postsynaptic GABAergic receptors.

We did not detect PDS in granule cells in comparison with hippocampal cultures. We know that in culture conditions the presynaptic degeneration induced by the absence of CSP-α is faster that in the brain natural niche (García-Junco-Clemente et al. 2010). Because of that it is possible that, although the GABAergic input of granule cells is clearly reduced in hippocampal slices, it is not strong enough yet at P24-P31 to produce PDS events. On the other hand, it would be useful to investigate the excitability of pyramidal CA3 neurons in which typically PDS properties have been studied (Johnston and Brown, 1984). In any case, the granule cells at the dentate gyrus is considered to be the dentate

gate in limbic epileptogenesis that limitates the spread of excitation through the CA3 pyramidal neurons by filtering the excitatory signals coming from the entorhinal cortex (Goldberg and Coulter, 2013). Fast-spiking neurons, specially PV+ cells, form powerful synapses on the soma and the axonal initial segment of granule cells that control the action potential discharge on those cells (Hu et al., 2014). Within this context, knock-out mice lacking CSP-α would suffer from epileptic seizures. We, however, did not detect any obvious sign of seizures or convulsions just by visual inspection.

5.3.3. Increased susceptibility to epileptic seizures in CSP-α KO mice

In order to explore if indeed CSP-α KO mice had or not increased susceptibility to seizures we collaborated with Prof. Agnès Gruart and Prof. José María Delgado García at the Division of Neurosciences in Pablo de Olavide University (Seville, Spain). These unpublished results are very relevant for this thesis where electrophysiological recordings of the hippocampal pyramidal CA1 area in wild type and CSP-α KO alert behaving mice show that mutants manifest much higher propensity to convulsive seizures when animals are injected with the AMPA/kainate receptor agonist kainic acid (Figure 28).

Electrophysiological properties of the hippocampal CA3-CA1 synapses in wild type and mutant mice were analyzed and the responses of hippocampal pyramidal CA1 neurons to paired pulses (0.02-0.4 mA, 40 ms of inter-pulse interval) presented to the ipsilateral Schaffer collaterals were quantified in the two groups of mouse (n = 7 per group). As illustrated in the panel a of figure 28.A and in accordance with previous descriptions in alert behaving mice (Gruart et al., 2006), the two groups of mice presented a characteristic negative potential with a latency of approximately 4 ms. The amplitude of the field excitatory post-synaptic potentials (fEPSPs) evoked at the CA3-CA1 synapse in parallel with the increase intensity of the applied pulses (not illustrated).

Paired-pulse facilitation (PPF) was determined as PPF = [(amplitude of the 2nd pulse / amplitude of the 1st pulse) x 100]. As illustrated in the panel a of figure 28.A, no significant (P = 0.457) difference in PPF was observed between the two groups (n = 3 each) of mice. In addition, the two groups of mice presented fEPSPs of similar amplitude and profile following train stimulation (1 s; 10 Hz and 20 Hz) of the Schaffer collateral/ commissural pathway (Figure 28.A, panels b an c).

The spontaneous local field potentials (LFPs) present in the hippocampal CA1 area with the animal resting in a small box was recorded and analyzed (Figure 28.A, panel d) from the two groups of animal (n = 5 per group). As illustrated in the panel e of figure

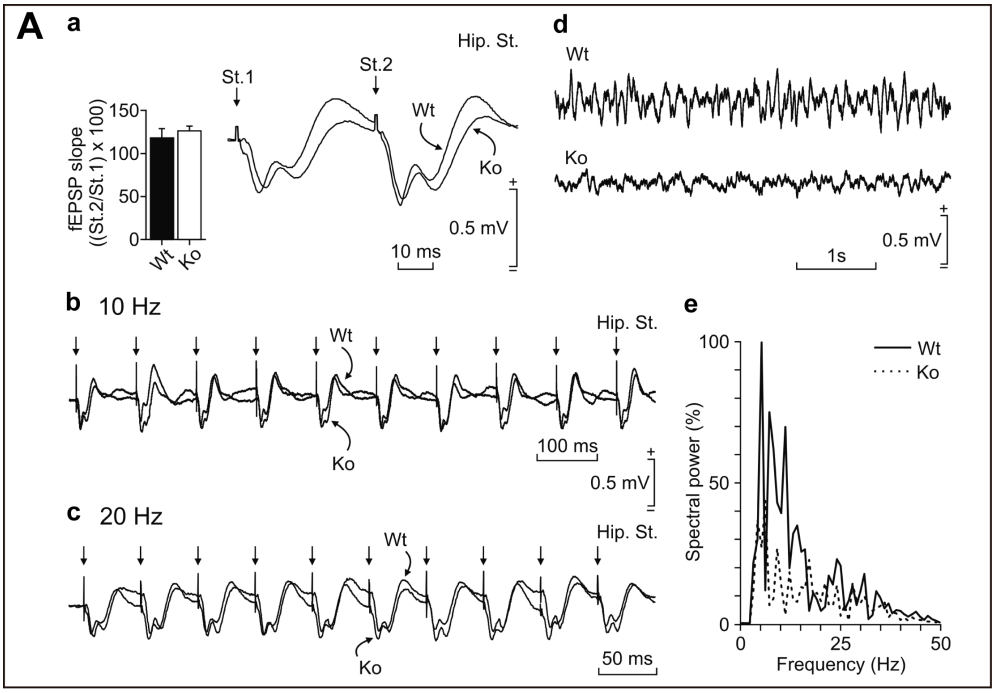
A
a
fEPSP slope ((St.2/St.1) x 100)
150
100
50
0
Wt
Ko
St.1
St.2
Hip. St.
Wt
Ko
0.5 mV
10 ms
d
Wt
Ko
1s
0.5 mV
b 10 Hz
Wt
Hip. St.
Ko
100 ms
0.5 mV
c 20 Hz
Wt
Hip. St.
Ko
50 ms
e
Wt
Ko
Spectral power (%)
100
50
0
0
25
50
Frequency (Hz)

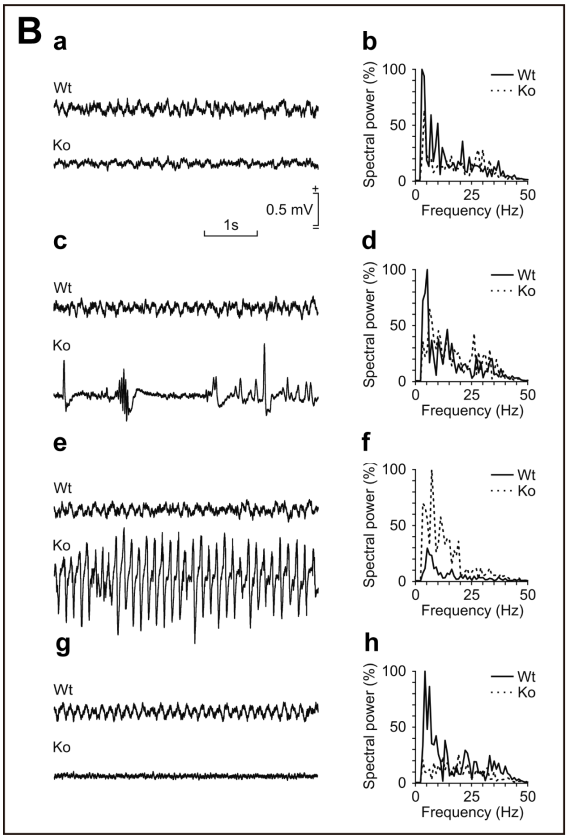
B
a
Wt
Ko
1s
0.5 mV
b
Spectral power (%)
100
50
0
Wt
Ko
0
25
50
Frequency (Hz)
c
Wt
Ko
d
Spectral power (%)
Wt
Ko
Frequency (Hz)
e
Wt
Ko
f
Spectral power (%)
Wt
Ko
Frequency (Hz)
g
Wt
Ko
h
Spectral power (%)
Wt
Ko
Frequency (Hz)

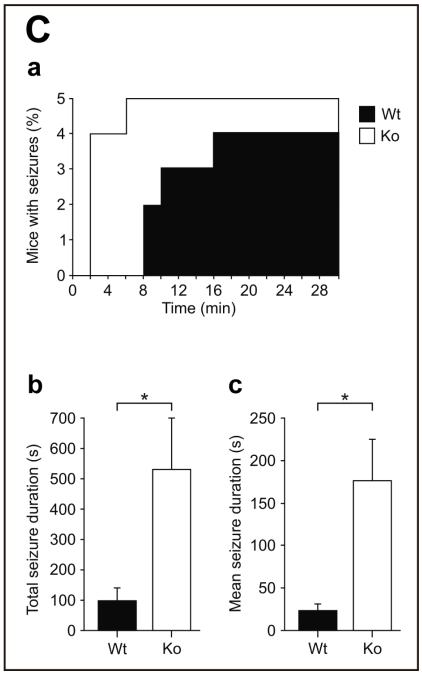
C
a
Mice with seizures (%)
5
4
3
2
1
0
Wt
Ko
0
4
8
12
16
20
24
28
Time (min)
b
Total seizure duration (s)
700
600
500
400
300
200
100
0
*
Wt
Ko
c
Mean seizure duration (s)
250
200
150
100
50
0
*
Wt
Ko

Figure 28: Electrophysiological recordings of behaving CSP-α KO mice

A: (a) Paired-pulse facilitation (PPF) of field excitatory post-synaptic potentials (fEPSPs) evoked at the CA3-CA1 synapse by pair of pulses of 40 ms of inter-pulse interval. Records collected from representative wild type and CSP-α KO mice mice are illustrated at the right. The left histograms illustrated the PPF evoked in WT (n = 3) and KO (n = 3) mice. PPF was calculated as follows: (amplitude of the 2nd pulse / amplitude of the 1st pulse) x 100. Note that no difference (P = 0.457) was observed between wild type and CSP-a KO mice. (b, c) Train (10 pulses) stimulation of the hippocampal CA3-CA1 synapse of representative wild type and CSP-α KO mice at 10 Hz (b) and 20 Hz (c). Amplitude calibration is for b and c. No differences were observed between wild type and CSP-α KO mice during train stimulation of the CA3-CA1 synapse. (d) LFPs recorded from representative wild type and CSP-α KO mice. Note the larger amplitude and better definition of the theta rhythm (approximately 7 Hz) recorded in the wild type animal. (e) Spectral power analysis of LFPs recorded from wild type and CSP-α KO mice. Note that the spectral power of wild type mice increased significantly ($P \leq 0.001$) at the theta band.

B: LFPs (a, c, g, e) recorded from wild type (top records) and CSP-α KO (bottom records) before (a) and after (c, e, g) kainic acid (8 mg/kg) injections (i.p.). Note the presence of a spontaneous seizure in the CSP-α KO mouse (e) preceded by the presence of some spontaneous spikes (c) and followed by a noticeable decrease in LFP amplitude (g). Calibrations in a are for all of the records. Spectral powers corresponding to the illustrated LFPs are shown in the left graphs (b, d, f, h). Spectral powers are represented as the percentage (%) of the maximal power.

C: (a) Percentage (%) presenting a seizure at the indicated times following the kainic acid injections. Note that CSP-α KO mice presented seizure activities in advance to wild type animals. In fact, a wild type mouse did not present any seizure-like activity during the whole (30 min) recording session. (b, c) Mean (b) and total (c) duration of seizures presented by both groups of animals during the recording period (30 min). *, $P < 0.01$.

28.A, the spectral analysis of recorded LFPs indicated a significantly ($P < 0.001$) larger spectral power in the control group as compared with KO mice, particularly in the theta (4-9) band.

The C57BL6J strain is seizure resistant in comparison to other mouse genetic backgrounds (McKhann et al., 2003; Rangel et al., 2009) and as already indicated (Fernández-Chacón et al., 2004), wild type and CSP-α KO mice were generated on a C57BL6J background. Also the susceptibility of the two of mice (n = 5 animals per group) to a single (8 mg/kg, i.p.) injection of kainic acid, an AMPA/kainite receptor agonist, was checked. As illustrated in figure 28.B, there were a noticeable variability in the latency, intensity and percentage of animals presenting spontaneous seizures. Thus, CSP-α KO mice presented a larger incidence of hippocampal seizures (100%), accompanied on

occasions (3 out of 5) of myoclonus. In contrast, wild type mice presented fewer signs of tonic, or clonic, seizures (Figure 28.B). Wild type mice presented a larger latency following kainic acid administration until the appearance of the first seizure (Figure 28.C, panel a). Even, a wild type mouse did not present any seizure during the whole test (Figure 28.C, panel a). In addition, their seizures were 85% shorter in duration (Figure 28.C, panel b), and the percentage of time with seizures during the recording period (30 min) was 80% shorter (Figure 28.C, panel c) than in CSP-α KO mice. These results show that CSP-α KO mice present a larger propensity to generate hippocampal seizures as compared with the wild type group.

Epileptic seizures can appear in dysfunctional neural networks dominated by excessive activity produced by fails in inhibitory inputs, such as in feed-forward inhibition and feed-back inhibition microcircuits, where parvalbumin interneurons are the inhibitory elements (Paz and Huguenard, 2015). On the other hand, CSP-α-Hsc70-SGT complex binds directly to SNAP-25 to impede its degradation (Sharma et al., 2011) and supporting our results, heterozygous SNAP-25 mice show higher susceptibility to kainate-induced seizures (Corradini et al., 2014) revealing that the reduction of the presynaptic protein SNAP-25, a similar phenotype found in CSP-α KO mice (Chandra et al., 2005), is involved in epileptic seizures. Furthermore, human autosomal-dominant adult-onset neuronal ceroid lipofuscinosis (ANCL) is a neurodegenerative disorder caused by mutations in CSP-α gene in which affected individuals show epileptic seizures (Noskova et al., 2011). These data demonstrate the role of CSP-α in epileptic seizures and the excitatory/inhibitory imbalance produce by loss of inhibition could be the main explanation, which is relevant to understant the neurological pathophysiology in ANCL patients.

6. CONCLUSIONS

1. Lentiviral transduction of genetically encoded fluorescent proteins under the specific human promoter synapsin can be used to preferentially target glutamatergic neurons. This circumstance is advantageous for studies focused on the presynaptic properties of glutamatargic synapses.

2. Imaging of synaptic exo- and endocytosis using synaptopHluorin shows that synapses, likely glutamatergic, from CSP-α KO mice present exo- and endocytosis responses similar to the responses found in hippocampal cultures from wild type littermates.

3. Evoked presynaptic calcium signals uncovered with the genetically encoded fluorescent calcium indicator syGCaMP3 identified two type of responses in glutamatergic synapses: long duration responses (LDRs) and short duration responses (SDRs). These responses are not synapse-specific responses but instead respond to the properties of individual neurons. The nature of SDRs is not a phenomenon that depends on classical feedback GABAergic inhibition and could depend on mechanisms regulating action potential firing or calcium influx through voltage depended calcium channels.

4. Activity correlation analysis is a very useful approach for the spatial separation of LDRs and SDRs.

5. LDRs and SDRs are similar in wild type and CSP-α KO hippocampal cultures indicating that, at least in glutamatergic synapses, CSP-α does not have an immediate direct or indirect major role in regulating presynaptic calcium dynamics.

6. In the absence of CSP-α, neuronal cultures become hyperexcitable and display typical neuronal features of epileptiform activity such as Paroximal Depolarization Shifts (PDS) and increased action potential frequency in spontaneous bursts.

7. Hippocampal granule cells from CSP-α KO mice progressively develop signs of hyperexcitability that are not due to changes in the intrinsic properties of the membrane but, instead, to the deficit of GABAergic input. These features predict increased susceptibility to seizures in the absence of CSP-α, which is relevant to understant the neurological pathophysiology in NCL-4 patients.

7. BIBLIOGRAPHY

Ahrendt, E., Kyle, B., Braun, A.P., and Braun, J.E. (2014). Cysteine string protein limits expression of the large conductance, calcium-activated K(+) (BK) channel. PloS one 9, e86586.

Álvarez de Toledo, G., Fernández-Chacón, R., and Fernández, J.M. (1993). Release of secretory products during transient vesicle fusion. Nature 363, 554-558.

Andersen, P., Morris, R., Amaral, D., Bliss, T., and O'Keefe, J. (2007). The Hippocampus Book (Oxford University Press).

Antic, S.D., Empson, R.M., and Knopfel, T. (2016). Voltage imaging to understand connections and functions of neuronal circuits. J Neurophysiol 116, 135-152.

Beaumont, V., Zhong, N., Froemke, R.C., Ball, R.W., and Zucker, R.S. (2002). Temporal synaptic tagging by I(h) activation and actin: involvement in long-term facilitation and cAMP-induced synaptic enhancement. Neuron 33, 601-613.

Beck, H., Steffens, R., Heinemann, U., and Elger, C.E. (1999). Ca(2+)-dependent inactivation of high-threshold Ca(2+) currents in hippocampal granule cells of patients with chronic temporal lobe epilepsy. Journal of neurophysiology 82, 946-954.

Benitez, B.A., Alvarado, D., Cai, Y., Mayo, K., Chakraverty, S., Norton, J., Morris, J.C., Sands, M.S., Goate, A., and Cruchaga, C. (2011). Exome-sequencing confirms DNAJC5 mutations as cause of adult neuronal ceroid-lipofuscinosis. PloS one 6, e26741.

Bennett, M.V., and Zukin, R.S. (2004). Electrical coupling and neuronal synchronization in the Mammalian brain. Neuron 41, 495-511.

Berridge, M.J. (1998). Neuronal calcium signaling. Neuron 21, 13-26.

Bielefeldt, K., and Jackson, M.B. (1993). A calcium-activated potassium channel causes frequency-dependent action-potential failures in a mammalian nerve terminal. J Neurophysiol 70, 284-298.

Bliss, T.V., and Lømo, T. (1973). Long-lasting potentiation of synaptic transmission in the dentate area of the anaesthetized rabbit following stimulation of the perforant path. The Journal of physiology 232, 331-356.

Bouchard, R., Pattarini, R., and Geiger, J.D. (2003). Presence and functional significance of presynaptic ryanodine receptors. Progress in neurobiology 69, 391-418.

Boudkkazi, S., Fronzaroli-Molinieres, L., and Debanne, D. (2011). Presynaptic action potential waveform determines cortical synaptic latency. The Journal of physiology 589, 1117-1131.

Bourque, C.W. (1990). Intraterminal recordings from the rat neurohypophysis in vitro. J Physiol 421, 247-262.

Braun, J.E., and Scheller, R.H. (1995). Cysteine string protein, a DnaJ family member, is present on diverse secretory vesicles. Neuropharmacology 34, 1361-1369.

Brodin, L., Low, P., and Shupliakov, O. (2000). Sequential steps in clathrin-mediated synaptic vesicle endocytosis. Current opinion in neurobiology 10, 312-320.

Brody, D.L., and Yue, D.T. (2000). Release-independent short-term synaptic depression in cultured hippocampal neurons. J Neurosci 20, 2480-2494.

Brown, H., Larsson, O., Branstrom, R., Yang, S.N., Leibiger, B., Leibiger, I., Fried, G., Moede, T., Deeney, J.T., Brown, G.R., et al. (1998). Cysteine string protein (CSP) is an insulin secretory granule-associated protein regulating beta-cell exocytosis. The EMBO journal 17, 5048-5058.

Buchner, E., and Gundersen, C.B. (1997). The DnaJ-like cysteine string protein and exocytotic neurotransmitter release. Trends in neurosciences 20, 223-227.

Budde, T., Meuth, S., and Pape, H.C. (2002). Calcium-dependent inactivation of neuronal calcium channels. Nature reviews Neuroscience 3, 873-883.

Caplan, A.J., Cyr, D.M., and Douglas, M.G. (1993). Eukaryotic homologues of Escherichia coli dnaJ: a diverse protein family that functions with hsp70 stress proteins. Molecular biology of the cell 4, 555-563.

Catterall, W.A., and Few, A.P. (2008). Calcium channel regulation and presynaptic plasticity. Neuron 59, 882-901.

Catterall, W.A., Leal, K., and Nanou, E. (2013). Calcium channels and short-term synaptic plasticity. The Journal of biological chemistry 288, 10742-10749.

Chamberlain, L.H., and Burgoyne, R.D. (1996). Identification of a novel cysteine string protein variant and expression of cysteine string proteins in non-neuronal cells. The Journal of biological chemistry 271, 7320-7323.

Chamberlain, L.H., and Burgoyne, R.D. (1998a). Cysteine string protein functions directly in regulated exocytosis. Molecular biology of the cell 9, 2259-2267.

Chamberlain, L.H., and Burgoyne, R.D. (1998b). The cysteine-string domain of the secretory vesicle cysteine-string protein is required for membrane targeting. The Biochemical journal 335 (Pt 2), 205-209.

Chamberlain, L.H., Henry, J., and Burgoyne, R.D. (1996). Cysteine string proteins are associated with chromaffin granules. The Journal of biological chemistry 271, 19514-19517.

Chandra, S., Gallardo, G., Fernández-Chacón, R., Schluter, O.M., and Südhof, T.C. (2005). Alpha-synuclein cooperates with CSPalpha in preventing neurodegeneration. Cell 123, 383-396.

Christel, C., and Lee, A. (2012). Ca2+-dependent modulation of voltage-gated Ca2+ channels. Biochim Biophys Acta 1820, 1243-1252.

Christie, B.R., Eliot, L.S., Ito, K., Miyakawa, H., and Johnston, D. (1995). Different Ca2+ channels in soma and dendrites of hippocampal pyramidal neurons mediate spike-induced Ca2+ influx. J Neurophysiol 73, 2553-2557.

Condliffe, S.B., Corradini, I., Pozzi, D., Verderio, C., and Matteoli, M. (2010). Endogenous SNAP-25 regulates native voltage-gated calcium channels in glutamatergic neurons. J Biol Chem 285, 24968-24976.

Condliffe, S.B., and Matteoli, M. (2011). Inactivation kinetics of voltage-gated calcium channels in glutamatergic neurons are influenced by SNAP-25. Channels 5, 304-307.

Corradini, I., Donzelli, A., Antonucci, F., Welzl, H., Loos, M., Martucci, R., De Astis, S., Pattini, L., Inverardi, F., Wolfer, D., et al. (2014). Epileptiform activity and cognitive deficits in SNAP-25(+/-) mice are normalized by antiepileptic drugs. Cereb Cortex 24, 364-376.

Cowan, W.M., Sūdhof, T.C., and Stevens, C.F. (2001). Synapses (U.S.A.: The Johns Hopkins University Press).

Dawson-Scully, K., Bronk, P., Atwood, H.L., and Zinsmaier, K.E. (2000). Cysteine-string protein increases the calcium sensitivity of neurotransmitter exocytosis in Drosophila. The Journal of neuroscience: the official journal of the Society for Neuroscience 20,

6039-6047.

de Juan-Sanz, J., Holt, G.T., Schreiter, E.R., de Juan, F., Kim, D.S., and Ryan, T.A. (2017). Axonal Endoplasmic Reticulum Ca2+ Content Controls Release Probability in CNS Nerve Terminals. Neuron 93, 867-881 e866.

Debanne, D. (2004). Information processing in the axon. Nat Rev Neurosci 5, 304-316.

Debanne, D. (2011). The nodal origin of intrinsic bursting. Neuron 71, 569-570.

Debanne, D., Bialowas, A., and Rama, S. (2013). What are the mechanisms for analogue and digital signalling in the brain? Nat Rev Neurosci 14, 63-69.

Debanne, D., Guerineau, N.C., Gahwiler, B.H., and Thompson, S.M. (1997). Action-potential propagation gated by an axonal I(A)-like K+ conductance in hippocampus. Nature 389, 286-289.

Debanne, D., Kopysova, I.L., Bras, H., and Ferrand, N. (1999). Gating of action potential propagation by an axonal A-like potassium conductance in the hippocampus: a new type of non-synaptic plasticity. J Physiol Paris 93, 285-296.

Deschenes, M., and Landry, P. (1980). Axonal branch diameter and spacing of nodes in the terminal arborization of identified thalamic and cortical neurons. Brain Res 191, 538-544.

Dichter, M., and Spencer, W.A. (1969a). Penicillin-induced interictal discharges from the cat hippocampus. I. Characteristics and topographical features. J Neurophysiol 32, 649-662.

Dichter, M., and Spencer, W.A. (1969b). Penicillin-induced interictal discharges from the cat hippocampus. II. Mechanisms underlying origin and restriction. J Neurophysiol 32, 663-687.

Dingledine, R., and Gjerstad, L. (1980). Reduced inhibition during epileptiform activity in the in vitro hippocampal slice. The Journal of physiology 305, 297-313.

Dreosti, E., Odermatt, B., Dorostkar, M.M., and Lagnado, L. (2009). A genetically encoded reporter of synaptic activity in vivo. Nature methods 6, 883-889.

Eberle, K.K., Zinsmaier, K.E., Buchner, S., Gruhn, M., Jenni, M., Arnold, C., Leibold, C., Reisch, D., Walter, N., Hafen, E., et al. (1998). Wide distribution of the cysteine

string proteins in Drosophila tissues revealed by targeted mutagenesis. Cell and tissue research 294, 203-217.

Emptage, N.J., Reid, C.A., and Fine, A. (2001). Calcium stores in hippocampal synaptic boutons mediate short-term plasticity, store-operated Ca2+ entry, and spontaneous transmitter release. Neuron 29, 197-208.

Evans, G.J., and Morgan, A. (2002). Phosphorylation-dependent interaction of the synaptic vesicle proteins cysteine string protein and synaptotagmin I. The Biochemical journal 364, 343-347.

Ferguson, S.M., and De Camilli, P. (2012). Dynamin, a membrane-remodelling GTPase. Nature reviews Molecular cell biology 13, 75-88.

Fernández-Chacón, R., Königstorfer, A., Gerber, S.H., García, J., Matos, M.F., Stevens, C.F., Brose, N., Rizo, J., Rosenmund, C., and Südhof, T.C. (2001). Synaptotagmin I functions as a calcium regulator of release probability. Nature 410, 41-49.

Fernández-Chacón, R., Wolfel, M., Nishimune, H., Tabares, L., Schmitz, F., Castellano-Muñoz, M., Rosenmund, C., Montesinos, M.L., Sanes, J.R., Schneggenburger, R., et al. (2004). The synaptic vesicle protein CSP alpha prevents presynaptic degeneration. Neuron 42, 237-251.

Fioravante, D., and Regehr, W.G. (2011). Short-term forms of presynaptic plasticity. Current opinion in neurobiology 21, 269-274.

Foster, M. (1897). A textbook of physiology (London: Macmillan).

Freund, T.F., and Buzsáki, G. (1996). Interneurons of the hippocampus. Hippocampus 6, 347-470.

García-Junco-Clemente, P., Cantero, G., Gómez-Sánchez, L., Linares-Clemente, P., Martínez-López, J.A., Luján, R., and Fernández-Chacón, R. (2010). Cysteine string protein-alpha prevents activity-dependent degeneration in GABAergic synapses. The Journal of neuroscience: the official journal of the Society for Neuroscience 30, 7377-7391.

Gascón, S., Paez-Gomez, J.A., Díaz-Guerra, M., Scheiffele, P., and Scholl, F.G. (2008). Dual-promoter lentiviral vectors for constitutive and regulated gene expression in neurons. Journal of neuroscience methods 168, 104-112.

Gassmann, M., and Bettler, B. (2012). Regulation of neuronal GABA(B) receptor func-

tions by subunit composition. Nature reviews Neuroscience 13, 380-394.

Geiger, J.R., and Jonas, P. (2000). Dynamic control of presynaptic Ca(2+) inflow by fast-inactivating K(+) channels in hippocampal mossy fiber boutons. Neuron 28, 927-939.

Gleave, T.L., Beechey, R.B., and Burgoyne, R.D. (2001). Cysteine string protein expression in mammary epithelial cells. Pflugers Archiv: European journal of physiology 441, 639-649.

Goldberg, E.M., and Coulter, D.A. (2013). Mechanisms of epileptogenesis: a convergence on neural circuit dysfunction. Nat Rev Neurosci 14, 337-349.

Golding, N.L., Jung, H.Y., Mickus, T., and Spruston, N. (1999). Dendritic calcium spike initiation and repolarization are controlled by distinct potassium channel subtypes in CA1 pyramidal neurons. J Neurosci 19, 8789-8798.

Goldstein, S.S., and Rall, W. (1974). Changes of action potential shape and velocity for changing core conductor geometry. Biophys J 14, 731-757.

Graham, M.E., and Burgoyne, R.D. (2000). Comparison of cysteine string protein (Csp) and mutant alpha-SNAP overexpression reveals a role for csp in late steps of membrane fusion in dense-core granule exocytosis in adrenal chromaffin cells. The Journal of neuroscience: the official journal of the Society for Neuroscience 20, 1281-1289.

Grienberger, C., and Konnerth, A. (2012). Imaging calcium in neurons. Neuron 73, 862-885.

Grossman, Y., Parnas, I., and Spira, M.E. (1979a). Differential conduction block in branches of a bifurcating axon. J Physiol 295, 283-305.

Grossman, Y., Parnas, I., and Spira, M.E. (1979b). Mechanisms involved in differential conduction of potentials at high frequency in a branching axon. J Physiol 295, 307-322.

Gruart, A., Muñoz, M.D., and Delgado-García, J.M. (2006). Involvement of the CA3-CA1 synapse in the acquisition of associative learning in behaving mice. The Journal of neuroscience: the official journal of the Society for Neuroscience 26, 1077-1087.

Gundersen, C.B., and Umbach, J.A. (1992). Suppression cloning of the cDNA for a candidate subunit of a presynaptic calcium channel. Neuron 9, 527-537.

Guzman, S.J., Schlögl, A., and Schmidt-Hieber, C. (2014). Stimfit: quantifying electrophysiological data with Python. Frontiers in neuroinformatics 8, 16.

Hartl, F.U., Bracher, A., and Hayer-Hartl, M. (2011). Molecular chaperones in protein folding and proteostasis. Nature 475, 324-332.

Hawkins, R.D., Abrams, T.W., Carew, T.J., and Kandel, E.R. (1983). A cellular mechanism of classical conditioning in Aplysia: activity-dependent amplification of presynaptic facilitation. Science 219, 400-405.

He, Y., Zorumski, C.F., and Mennerick, S. (2002). Contribution of presynaptic Na(+) channel inactivation to paired-pulse synaptic depression in cultured hippocampal neurons. J Neurophysiol 87, 925-936.

Hendel, T., Mank, M., Schnell, B., Griesbeck, O., Borst, A., and Reiff, D.F. (2008). Fluorescence changes of genetic calcium indicators and OGB-1 correlated with neural activity and calcium in vivo and in vitro. J Neurosci 28, 7399-7411.

Hochbaum, D.R., Zhao, Y., Farhi, S.L., Klapoetke, N., Werley, C.A., Kapoor, V., Zou, P., Kralj, J.M., Maclaurin, D., Smedemark-Margulies, N., et al. (2014). All-optical electrophysiology in mammalian neurons using engineered microbial rhodopsins. Nature methods 11, 825-833.

Hoppa, M.B., Gouzer, G., Armbruster, M., and Ryan, T.A. (2014). Control and plasticity of the presynaptic action potential waveform at small CNS nerve terminals. Neuron 84, 778-789.

Hu, H., Gan, J., and Jonas, P. (2014). Interneurons. Fast-spiking, parvalbumin(+) GABAergic interneurons: from cellular design to microcircuit function. Science 345, 1255263.

Inchauspe, C.G., Martini, F.J., Forsythe, I.D., and Uchitel, O.D. (2004). Functional compensation of P/Q by N-type channels blocks short-term plasticity at the calyx of Held presynaptic terminal. The Journal of neuroscience: the official journal of the Society for Neuroscience 24, 10379-10383.

Jackman, S.L., Turecek, J., Belinsky, J.E., and Regehr, W.G. (2016). The calcium sensor synaptotagmin 7 is required for synaptic facilitation. Nature 529, 88-91.

Jin, H., Wu, H., Osterhaus, G., Wei, J., Davis, K., Sha, D., Floor, E., Hsu, C.C., Kopke, R.D., and Wu, J.Y. (2003). Demonstration of functional coupling between gamma -am-

inobutyric acid (GABA) synthesis and vesicular GABA transport into synaptic vesicles. Proceedings of the National Academy of Sciences of the United States of America 100, 4293-4298.

Jinde, S., Zsiros, V., and Nakazawa, K. (2013). Hilar mossy cell circuitry controlling dentate granule cell excitability. Frontiers in neural circuits 7, 14.

Johnson, J.N., Ahrendt, E., and Braun, J.E. (2010). CSPalpha: the neuroprotective J protein. Biochemistry and cell biology. Biochimie et biologie cellulaire 88, 157-165.

Johnston, D., and Brown, T.H. (1981). Giant synaptic potential hypothesis for epileptiform activity. Science 211, 294-297.

Johnston, D., and Brown, T.H. (1984). The synaptic nature of the paroxysmal depolarizing shift in hippocampal neurons. Ann Neurol 16 Suppl, S65-71.

Junek, S., Chen, T.W., Alevra, M., and Schild, D. (2009). Activity correlation imaging: visualizing function and structure of neuronal populations. Biophysical journal 96, 3801-3809.

Kaeser, P.S., and Regehr, W.G. (2014). Molecular mechanisms for synchronous, asynchronous, and spontaneous neurotransmitter release. Annu Rev Physiol 76, 333-363.

Kandel, E.R., Schwartz, J.H., Jessell, T.M., Siegelbaum, S.A., and Hudspeth, A.J. (2013). Principles of neural science, Fifth Edition edn (U.S.A.: The McGraw-Hill Companies).

Kandel, E.R., and Spencer, W.A. (1961). Electrophysiology of hippocampal neurons. II. After-potentials and repetitive firing. J Neurophysiol 24, 243-259.

Katz, B. (1969). The release of neural transmitter substances (Liverpool: Liverpool Univ. Press).

Kavalali, E.T., and Jorgensen, E.M. (2014). Visualizing presynaptic function. Nat Neurosci 17, 10-16.

Kavalali, E.T., Zhuo, M., Bito, H., and Tsien, R.W. (1997). Dendritic Ca2+ channels characterized by recordings from isolated hippocampal dendritic segments. Neuron 18, 651-663.

Khazipov, R. (2016). GABAergic Synchronization in Epilepsy. Cold Spring Harb Perspect Med 6, a022764.

Klausberger, T., and Somogyi, P. (2008). Neuronal diversity and temporal dynamics: the unity of hippocampal circuit operations. Science 321, 53-57.

Koester, H.J., and Sakmann, B. (1998). Calcium dynamics in single spines during coincident pre- and postsynaptic activity depend on relative timing of back-propagating action potentials and subthreshold excitatory postsynaptic potentials. Proc Natl Acad Sci U S A 95, 9596-9601.

Koester, H.J., and Sakmann, B. (2000). Calcium dynamics associated with action potentials in single nerve terminals of pyramidal cells in layer 2/3 of the young rat neocortex. J Physiol 529 Pt 3, 625-646.

Kralj, J.M., Douglass, A.D., Hochbaum, D.R., Maclaurin, D., and Cohen, A.E. (2012). Optical recording of action potentials in mammalian neurons using a microbial rhodopsin. Nature methods 9, 90-95.

Kullmann, D.M. (2011). Interneuron networks in the hippocampus. Curr Opin Neurobiol 21, 709-716.

Kyle, B.D., Ahrendt, E., Braun, A.P., and Braun, J.E. (2013). The large conductance, calcium-activated K+ (BK) channel is regulated by cysteine string protein. Scientific reports 3, 2447.

Langley, J.N. (1921). The autonomic nervous system (Cambridge: Heffer).

Lebovitz, R.M., Dichter, M., and Spencer, W.A. (1971). Recurrent excitation in the CA3 region of cat hippocampus. Int J Neurosci 2, 99-107.

Leveque, C., Pupier, S., Marqueze, B., Geslin, L., Kataoka, M., Takahashi, M., De Waard, M., and Seagar, M. (1998). Interaction of cysteine string proteins with the alpha1A subunit of the P/Q-type calcium channel. The Journal of biological chemistry 273, 13488-13492.

Li, H., Foss, S.M., Dobryy, Y.L., Park, C.K., Hires, S.A., Shaner, N.C., Tsien, R.Y., Osborne, L.C., and Voglmaier, S.M. (2011). Concurrent imaging of synaptic vesicle recycling and calcium dynamics. Front Mol Neurosci 4, 34.

Liang, Y., Yuan, L.L., Johnston, D., and Gray, R. (2002). Calcium signaling at single mossy fiber presynaptic terminals in the rat hippocampus. Journal of neurophysiology 87, 1132-1137.

Lin, M.Z., and Schnitzer, M.J. (2016). Genetically encoded indicators of neuronal activity. Nat Neurosci 19, 1142-1153.

Linares-Clemente, P., Rozas, J.L., Mircheski, J., Garcia-Junco-Clemente, P., Martinez-Lopez, J.A., Nieto-Gonzalez, J.L., Vazquez, M.E., Pintado, C.O., and Fernandez-Chacon, R. (2015). Different dynamin blockers interfere with distinct phases of synaptic endocytosis during stimulation in motoneurones. J Physiol 593, 2867-2888.

Lorente de Nó, R. (1934). Studies on the structure of the cerebral cortex : Continuation of the study of the ammonic system (Leipzig: Johann Ambrosius Barth).

Mackenzie, P.J., Umemiya, M., and Murphy, T.H. (1996). Ca2+ imaging of CNS axons in culture indicates reliable coupling between single action potentials and distal functional release sites. Neuron 16, 783-795.

MacVicar, B.A., and Dudek, F.E. (1979). Intracellular recordings from hippocampal CA3 pyramidal cells during repetitive activation of the mossy fibers in vitro. Brain Res 168, 377-381.

Magee, J.C., Christofi, G., Miyakawa, H., Christie, B., Lasser-Ross, N., and Johnston, D. (1995). Subthreshold synaptic activation of voltage-gated Ca2+ channels mediates a localized Ca2+ influx into the dendrites of hippocampal pyramidal neurons. Journal of neurophysiology 74, 1335-1342.

Magga, J.M., Jarvis, S.E., Arnot, M.I., Zamponi, G.W., and Braun, J.E. (2000). Cysteine string protein regulates G protein modulation of N-type calcium channels. Neuron 28, 195-204.

Martens, H., Weston, M.C., Boulland, J.L., Grønborg, M., Grosche, J., Kacza, J., Hoffmann, A., Matteoli, M., Takamori, S., Harkany, T., et al. (2008). Unique luminal localization of VGAT-C terminus allows for selective labeling of active cortical GABAergic synapses. The Journal of neuroscience: the official journal of the Society for Neuroscience 28, 13125-13131.

Matsumoto, H., Ayala, G.F., and Gumnit, R.J. (1969). Neuronal behavior and triggering mechanism in cortical epileptic focus. J Neurophysiol 32, 688-703.

Maximov, A., Pang, Z.P., Tervo, D.G., and Sudhof, T.C. (2007). Monitoring synaptic transmission in primary neuronal cultures using local extracellular stimulation. Journal of neuroscience methods 161, 75-87.

McCombs, J.E., and Palmer, A.E. (2008). Measuring calcium dynamics in living cells with genetically encodable calcium indicators. Methods 46, 152-159.

McKhann, G.M., 2nd, Wenzel, H.J., Robbins, C.A., Sosunov, A.A., and Schwartzkroin, P.A. (2003). Mouse strain differences in kainic acid sensitivity, seizure behavior, mortality, and hippocampal pathology. Neuroscience 122, 551-561.

Meeks, J.P., Jiang, X., and Mennerick, S. (2005). Action potential fidelity during normal and epileptiform activity in paired soma-axon recordings from rat hippocampus. J Physiol 566, 425-441.

Meeks, J.P., and Mennerick, S. (2004). Selective effects of potassium elevations on glutamate signaling and action potential conduction in hippocampus. J Neurosci 24, 197-206.

Miesenbock, G., De Angelis, D.A., and Rothman, J.E. (1998). Visualizing secretion and synaptic transmission with pH-sensitive green fluorescent proteins. Nature 394, 192-195.

Miller, L.C., Swayne, L.A., Kay, J.G., Feng, Z.P., Jarvis, S.E., Zamponi, G.W., and Braun, J.E. (2003). Molecular determinants of cysteine string protein modulation of N-type calcium channels. Journal of cell science 116, 2967-2974.

Milner, B. (1958). Psychological defects produced by temporal lobe excision. Research publications - Association for Research in Nervous and Mental Disease 36, 244-257.

Mochida, S., Few, A.P., Scheuer, T., and Catterall, W.A. (2008). Regulation of presynaptic Ca(V)2.1 channels by Ca2+ sensor proteins mediates short-term synaptic plasticity. Neuron 57, 210-216.

Morales, M., Ferrus, A., and Martínez-Padrón, M. (1999). Presynaptic calcium-channel currents in normal and csp mutant Drosophila peptidergic terminals. The European journal of neuroscience 11, 1818-1826.

Muchowski, P.J., and Wacker, J.L. (2005). Modulation of neurodegeneration by molecular chaperones. Nature reviews Neuroscience 6, 11-22.

Nagerl, U.V., and Mody, I. (1998). Calcium-dependent inactivation of high-threshold calcium currents in human dentate gyrus granule cells. J Physiol 509 (Pt 1), 39-45.

Nagerl, U.V., Mody, I., Jeub, M., Lie, A.A., Elger, C.E., and Beck, H. (2000). Surviving

granule cells of the sclerotic human hippocampus have reduced Ca(2+) influx because of a loss of calbindin-D(28k) in temporal lobe epilepsy. J Neurosci 20, 1831-1836.

Nakai, J., Ohkura, M., and Imoto, K. (2001). A high signal-to-noise Ca(2+) probe composed of a single green fluorescent protein. Nature biotechnology 19, 137-141.

Nathanson, J.L., Yanagawa, Y., Obata, K., and Callaway, E.M. (2009). Preferential labeling of inhibitory and excitatory cortical neurons by endogenous tropism of adeno-associated virus and lentivirus vectors. Neuroscience 161, 441-450.

Neher, E. (1998). Vesicle pools and Ca2+ microdomains: new tools for understanding their roles in neurotransmitter release. Neuron 20, 389-399.

Neher, E., and Sakaba, T. (2008). Multiple roles of calcium ions in the regulation of neurotransmitter release. Neuron 59, 861-872.

Nie, Z., Ranjan, R., Wenniger, J.J., Hong, S.N., Bronk, P., and Zinsmaier, K.E. (1999). Overexpression of cysteine-string proteins in Drosophila reveals interactions with syntaxin. The Journal of neuroscience: the official journal of the Society for Neuroscience 19, 10270-10279.

Nizami, S., Lee, V.W., Davies, J., Long, P., Jovanovic, J.N., and Sihra, T.S. (2010). Presynaptic roles of intracellular Ca(2+) stores in signalling and exocytosis. Biochemical Society transactions 38, 529-535.

Noskova, L., Stranecky, V., Hartmannova, H., Pristoupilova, A., Baresova, V., Ivanek, R., Hulkova, H., Jahnova, H., van der Zee, J., Staropoli, J.F., et al. (2011). Mutations in DNAJC5, encoding cysteine-string protein alpha, cause autosomal-dominant adult-onset neuronal ceroid lipofuscinosis. American journal of human genetics 89, 241-252.

Paz, J.T., and Huguenard, J.R. (2015). Microcircuits and their interactions in epilepsy: is the focus out of focus? Nature neuroscience 18, 351-359.

Poolos, N.P., Mauk, M.D., and Kocsis, J.D. (1987). Activity-evoked increases in extracellular potassium modulate presynaptic excitability in the CA1 region of the hippocampus. J Neurophysiol 58, 404-416.

Poulin, J.F., Tasic, B., Hjerling-Leffler, J., Trimarchi, J.M., and Awatramani, R. (2016). Disentangling neural cell diversity using single-cell transcriptomics. Nature neuroscience 19, 1131-1141.

Raimondi, A., Ferguson, S.M., Lou, X., Armbruster, M., Paradise, S., Giovedi, S., Messa, M., Kono, N., Takasaki, J., Cappello, V., et al. (2011). Overlapping role of dynamin isoforms in synaptic vesicle endocytosis. Neuron 70, 1100-1114.

Ramón y Cajal, S. (1888). Estructura de los centros nerviosos de las aves. Rev Trim Histol Norm Pat.

Ramón y Cajal, S. (1911). Histologie du Système Nerveux de l'Homme et des Vertébrés (Madrid).

Ramón y Cajal, S. (1933). ¿Neuronismo o reticularismo? Las pruebas objetivas de la unidad anatómica de las células nerviosas (Madrid).

Rangel, A., Madroñal, N., Gruart, A., Gavin, R., Llorens, F., Sumoy, L., Torres, J.M., Delgado-García, J.M., and Del Rio, J.A. (2009). Regulation of GABA(A) and glutamate receptor expression, synaptic facilitation and long-term potentiation in the hippocampus of prion mutant mice. PloS one 4, e7592.

Ranjan, R., Bronk, P., and Zinsmaier, K.E. (1998). Cysteine string protein is required for calcium secretion coupling of evoked neurotransmission in drosophila but not for vesicle recycling. The Journal of neuroscience: the official journal of the Society for Neuroscience 18, 956-964.

Regehr, W.G. (2012). Short-term presynaptic plasticity. Cold Spring Harbor perspectives in biology 4, a005702.

Ritchie, J.M., and Straub, R.W. (1956). The after-effects of repetitive stimulation on mammalian non-medullated fibres. J Physiol 134, 698-711.

Ritchie, J.M., and Straub, R.W. (1957). The hyperpolarization which follows activity in mammalian non-medullated fibres. J Physiol 136, 80-97.

Rizzoli, S.O., and Betz, W.J. (2005). Synaptic vesicle pools. Nature reviews Neuroscience 6, 57-69.

Ross, W.N. (2012). Understanding calcium waves and sparks in central neurons. Nat Rev Neurosci 13, 157-168.

Rozas, J.L., Gómez-Sánchez, L., Mircheski, J., Linares-Clemente, P., Nieto-González, J.L., Vázquez, M.E., Luján, R., and Fernández-Chacón, R. (2012). Motorneurons require cysteine string protein-alpha to maintain the readily releasable vesicular pool and

synaptic vesicle recycling. Neuron 74, 151-165.

Saheki, Y., and De Camilli, P. (2012). Synaptic vesicle endocytosis. Cold Spring Harbor perspectives in biology 4, a005645.

Sakaba, T. (2008). Two Ca(2+)-dependent steps controlling synaptic vesicle fusion and replenishment at the cerebellar basket cell terminal. Neuron 57, 406-419.

Sankaranarayanan, S., De Angelis, D., Rothman, J.E., and Ryan, T.A. (2000). The use of pHluorins for optical measurements of presynaptic activity. Biophysical journal 79, 2199-2208.

Scharfman, H.E., and Myers, C.E. (2012). Hilar mossy cells of the dentate gyrus: a historical perspective. Frontiers in neural circuits 6, 106.

Schmitz, F., Tabares, L., Khimich, D., Strenzke, N., de la Villa-Polo, P., Castellano-Muñoz, M., Bulankina, A., Moser, T., Fernández-Chacón, R., and Südhof, T.C. (2006). CSPalpha-deficiency causes massive and rapid photoreceptor degeneration. Proceedings of the National Academy of Sciences of the United States of America 103, 2926-2931.

Schneggenburger, R., and Forsythe, I.D. (2006). The calyx of Held. Cell Tissue Res 326, 311-337.

Schneggenburger, R., and Neher, E. (2000). Intracellular calcium dependence of transmitter release rates at a fast central synapse. Nature 406, 889-893.

Schwartzkroin, P.A., and Prince, D.A. (1978). Cellular and field potential properties of epileptogenic hippocampal slices. Brain Res 147, 117-130.

Sharma, M., Burré, J., Bronk, P., Zhang, Y., Xu, W., and Südhof, T.C. (2012). CSPalpha knockout causes neurodegeneration by impairing SNAP-25 function. The EMBO journal 31, 829-841.

Sharma, M., Burré, J., and Südhof, T.C. (2011). CSPalpha promotes SNARE-complex assembly by chaperoning SNAP-25 during synaptic activity. Nature cell biology 13, 30-39.

Shepherd, G.M., Raastad, M., and Andersen, P. (2002). General and variable features of varicosity spacing along unmyelinated axons in the hippocampus and cerebellum. Proc Natl Acad Sci U S A 99, 6340-6345.

Silver, P.A., and Way, J.C. (1993). Eukaryotic DnaJ homologs and the specificity of Hsp70 activity. Cell 74, 5-6.

Smetters, D., Majewska, A., and Yuste, R. (1999). Detecting action potentials in neuronal populations with calcium imaging. Methods 18, 215-221.

Soleng, A.F., Chiu, K., and Raastad, M. (2003). Unmyelinated axons in the rat hippocampus hyperpolarize and activate an H current when spike frequency exceeds 1 Hz. J Physiol 552, 459-470.

Stiglbauer, V., Hotka, M., Ruiss, M., Hilber, K., Boehm, S., and Kubista, H. (2017). Cav 1.3 channels play a crucial role in the formation of paroxysmal depolarization shifts in cultured hippocampal neurons. Epilepsia 58, 858-871.

Stosiek, C., Garaschuk, O., Holthoff, K., and Konnerth, A. (2003). In vivo two-photon calcium imaging of neuronal networks. Proc Natl Acad Sci U S A 100, 7319-7324.

Stuart, G., Spruston, N., Sakmann, B., and Hausser, M. (1997). Action potential initiation and backpropagation in neurons of the mammalian CNS. Trends Neurosci 20, 125-131.

Südhof, T.C. (2004). The synaptic vesicle cycle. Annual review of neuroscience 27, 509-547.

Südhof, T.C. (2012). The presynaptic active zone. Neuron 75, 11-25.

Südhof, T.C. (2014). The molecular machinery of neurotransmitter release (Nobel lecture). Angewandte Chemie 53, 12696-12717.

Takamori, S., Holt, M., Stenius, K., Lemke, E.A., Grønborg, M., Riedel, D., Urlaub, H., Schenck, S., Brügger, B., Ringler, P., et al. (2006). Molecular anatomy of a trafficking organelle. Cell 127, 831-846.

Takamori, S., Riedel, D., and Jahn, R. (2000). Immunoisolation of GABA-specific synaptic vesicles defines a functionally distinct subset of synaptic vesicles. The Journal of neuroscience: the official journal of the Society for Neuroscience 20, 4904-4911.

Tian, L., Hires, S.A., Mao, T., Huber, D., Chiappe, M.E., Chalasani, S.H., Petreanu, L., Akerboom, J., McKinney, S.A., Schreiter, E.R., et al. (2009). Imaging neural activity in worms, flies and mice with improved GCaMP calcium indicators. Nat Methods 6, 875-881.

Tobaben, S., Thakur, P., Fernández-Chacón, R., Südhof, T.C., Rettig, J., and Stahl, B. (2001). A trimeric protein complex functions as a synaptic chaperone machine. Neuron 31, 987-999.

Turrigiano, G. (2012). Homeostatic synaptic plasticity: local and global mechanisms for stabilizing neuronal function. Cold Spring Harb Perspect Biol 4, a005736.

Umbach, J.A., and Gundersen, C.B. (1997). Evidence that cysteine string proteins regulate an early step in the Ca2+-dependent secretion of neurotransmitter at Drosophila neuromuscular junctions. The Journal of neuroscience: the official journal of the Society for Neuroscience 17, 7203-7209.

Verkhratsky, A. (2005). Physiology and pathophysiology of the calcium store in the endoplasmic reticulum of neurons. Physiological reviews 85, 201-279.

Watanabe, S., Rost, B.R., Camacho-Pérez, M., Davis, M.W., Söhl-Kielczynski, B., Rosenmund, C., and Jorgensen, E.M. (2013). Ultrafast endocytosis at mouse hippocampal synapses. Nature 504, 242-247.

Wilhelm, B.G., Mandad, S., Truckenbrodt, S., Kröhnert, K., Schäfer, C., Rammner, B., Koo, S.J., Classen, G.A., Krauss, M., Haucke, V., et al. (2014). Composition of isolated synaptic boutons reveals the amounts of vesicle trafficking proteins. Science 344, 1023-1028.

Xu, J., and Wu, L.G. (2005). The decrease in the presynaptic calcium current is a major cause of short-term depression at a calyx-type synapse. Neuron 46, 633-645.

Zeisel, A., Muñoz-Manchado, A.B., Codeluppi, S., Lonnerberg, P., La Manno, G., Jureus, A., Marques, S., Munguba, H., He, L., Betsholtz, C., et al. (2015). Brain structure. Cell types in the mouse cortex and hippocampus revealed by single-cell RNA-seq. Science 347, 1138-1142.

Zhang, C., Wu, B., Beglopoulos, V., Wines-Samuelson, M., Zhang, D., Dragatsis, I., Sudhof, T.C., and Shen, J. (2009). Presenilins are essential for regulating neurotransmitter release. Nature 460, 632-636.

Zhang, Y.Q., Henderson, M.X., Colangelo, C.M., Ginsberg, S.D., Bruce, C., Wu, T., and Chandra, S.S. (2012). Identification of CSPalpha clients reveals a role in dynamin 1 regulation. Neuron 74, 136-150.

Zhao, C., Dreosti, E., and Lagnado, L. (2011). Homeostatic synaptic plasticity through changes in presynaptic calcium influx. J Neurosci 31, 7492-7496.

Zinsmaier, K.E., Hofbauer, A., Heimbeck, G., Pflugfelder, G.O., Buchner, S., and Buchner, E. (1990). A cysteine-string protein is expressed in retina and brain of Drosophila. Journal of neurogenetics 7, 15-29.

Zucker, R.S., and Regehr, W.G. (2002). Short-term synaptic plasticity. Annual review of physiology 64, 355-405.